University of Arkansas, Fayetteville

ScholarWorks@UARK

Graduate Theses and Dissertations

7-2021

Tribological Studies of Thick Polytetrafluoroethylene Coatings Enhanced by Polydopamine and Nanoparticles

Sujan Kumar Ghosh
University of Arkansas, Fayetteville

Follow this and additional works at: https://scholarworks.uark.edu/etd

 Part of the Energy Systems Commons, Polymer and Organic Materials Commons, and the Tribology Commons

Citation

Ghosh, S. K. (2021). Tribological Studies of Thick Polytetrafluoroethylene Coatings Enhanced by Polydopamine and Nanoparticles. *Graduate Theses and Dissertations* Retrieved from https://scholarworks.uark.edu/etd/4129

This Dissertation is brought to you for free and open access by ScholarWorks@UARK. It has been accepted for inclusion in Graduate Theses and Dissertations by an authorized administrator of ScholarWorks@UARK. For more information, please contact scholar@uark.edu.

Tribological Studies of Thick Polytetrafluoroethylene Coatings Enhanced by Polydopamine and Nanoparticles

A dissertation submitted in partial fulfillment
of the requirements for the degree of
Doctor of Philosophy in Engineering

by

Sujan Kumar Ghosh
Khulna University of Engineering and Technology
Bachelor of Science in Mechanical Engineering, 2012
University of North Dakota
Master of Science in Mechanical Engineering, 2016

July 2021
University of Arkansas

This dissertation is approved for recommendation to the Graduate Council.

Min Zou, PhD
Committee Chair

Paul Millett, PhD
Committee Member

Xiangbo Meng, PhD
Committee Member

David Huitink, PhD
Committee Member

Jingyi Chen, PhD
Committee Member

Abstract

Polytetrafluoroethylene (PTFE) is a popular low friction solid lubricant with high chemical and thermal stability. Thick PTFE coatings have the potential for many tribological applications, such as replacing Tin-based Babbitt materials in journal bearings. However, the weak bonding strength to the substrate and the high wear rate of PTFE coatings are current limiting factors. The lack of understanding of their tribological properties and wear mechanisms in oil-lubricated conditions and how coating thickness affects the tribological performance further hindered the use of PTFE coatings. In this dissertation, polydopamine (PDA), a bio-inspired adhesive, is used as an underlayer for or as a constituent of PTFE coatings to improve the tribological properties of the resulting PDA/PTFE and PDA + PTFE composite coatings. The tribological properties and wear mechanisms of the coatings were studied in dry and oil-lubricated conditions. The wear mechanisms were investigated and correlated with their nanomechanical properties.

The durability of the PDA/PTFE coatings increased drastically when the thickness is over 34 μm due to the reduction in contact pressure. The 42 μm-thick PDA/PTFE coating was four times more durable in dry condition than the PTFE coating of similar thickness due to the better adherence to the substrate and higher load-carrying capacity. PDA mixed with PTFE helped prevent the detachment of PTFE coating from the substrate and improved the durability by 11 times. Hot compaction further increased the durability of the PDA+PTFE coating by 2.6 times by reducing the porosity and preventing delamination. In addition to better adhesion to the SS substrate and better load-carrying capacity, reduced porosity and roughness due to the hot-compaction prevented the local and global deformation of the compacted PDA+PTFE coating during wear tests, which in turn improved the durability of the coating.

Mixing PDA with PTFE increased Young's modulus of the PTFE coating from 0.61 to 0.97 GPa. Adding Cu nanoparticles (NPs) further increased Young's modulus of the PDA+PTFE coating and decreased the adhesion force between the AFM probe and coating surface. The PDA and PTFE particles cross-link themselves during the annealing process, and the presence of Cu NPs helps further cross-linking between the PDA and PTFE particles. The PDA+PTFE coating showed a 62.5% less COF in oil-lubricated conditions than in dry conditions. Moreover, the PDA+PTFE coating is five times more durable than PTFE coating in boundary oil-lubricated conditions. The delamination dominated the wear mechanism of the PDA+PTFE coating in the coating due to the presence of porous and non-annealed PDA+PTFE coating underneath the compacted top surface. The addition of 0.25 wt% of Cu NPs further improved the durability of PDA+PTFE coatings by 60% in boundary oil-lubricated conditions. The improved durability of the PDA+PTFE+0.25 wt% Cu NPs coating can be attributed to the lower adhesion force to the counterface, enhanced cross-linking between the PTFE and PDA in the presence of Cu NPs, better adherence to the substrate, and the better load-carrying capacity of these coatings. The addition of Cu NPs also improved the thermal conductivity of the PDA+PTFE coating by 12%. This research showed that the PDA can enhance the durability and adherence of the PTFE coatings to substrate, which open the avenue to investigate further the potential of the PDA+PTFE coatings in journal bearing applications.

Acknowledgment

I would like to thank Dr. Min Zou. Without her support, guidance, and vision, this dissertation would not come to fulfillment.

I want to thank my parents and siblings for their unconditional support throughout the process. A special thanks to my wife, Maia Ghosh, for her sacrifices, encouragement, and support. This journey was difficult, and without her, I wouldn't be able to complete this chapter of my life.

I want to thank the committee members for serving on my dissertation committee and guide me throughout this journey. Finally, I am thankful to my lab mates for their help for the last four years.

Contents

List of Papers

Chapter 2: Ghosh, S.K., Miller, C., Choudhury, D., Goss, J.A., and Zou M. (2020) "The Effects of PTFE Thickness on the Tribological Behavior of Thick PDA/PTFE Coatings." Tribology Transactions, 63, 575-584. DOI: 10.1080/10402004.2020.1728001

Chapter 3: Ghosh, S.K., Choudhury, D., Harris, N., Mahmoudi, N., Beckford, S., and Zou., M. (2021), "Improving the Tribological Performances of PDA+PTFE Nanocomposite Coatings by Hot Compaction." Tribology Transaction, DOI:10.1080/10402004.2021.1928351

Chapter 4: Ghosh, S.K., Perez, G., Goss, J.A., Beckford, S., and Zou, M. (2020) "Tribological Properties of PDA+PTFE Coating in Oil-lubricated Condition." Applied Surface Science. 534, 147627, DOI:10.1016/j.apsusc.2020.147627

Chapter 5: Ghosh, S.K., Miller, C., Carlton, H., Perez, G., Goss, J.A., Beckford, S., Huitink, D., and Zou, M. (2021) "Effect of Cu Nanoparticles on the Tribological Performance of PDA+PTFE Coatings in Oil-lubricated Condition" Applied Surface Science, 565, 150525, DOI: 10.1016/j.apsusc.2021.150525

Chapter 1

Introduction

1.1 Background and Motivation

Polytetrafluoroethylene (PTFE) is a linear fluoropolymer with strong covalent bonds between carbon (C) and Fluorine (F) [1]. Figure 1.1 shows the chemical structure of the PTFE. It can be seen that the backbone of the PTFE is C-C bonds, and the pendant of the PTFE is C-F bonds. The CF_2-CF_2 bonds repeat to form the fluoropolymer [2-4]. PTFE is a popular low friction solid lubricant with very high thermal and chemical stability [1]. However, when rubbed against a hard surface, PTFE is easily transferred to the counterface leading to a high wear rate [3-4]. Furthermore, PTFE coatings have low adhesion to metallic surfaces because of its non-stick properties [1], which leads to easy delamination under frictional loads. This further hindered the use of PTFE as coatings for tribological applications [1,5-7].

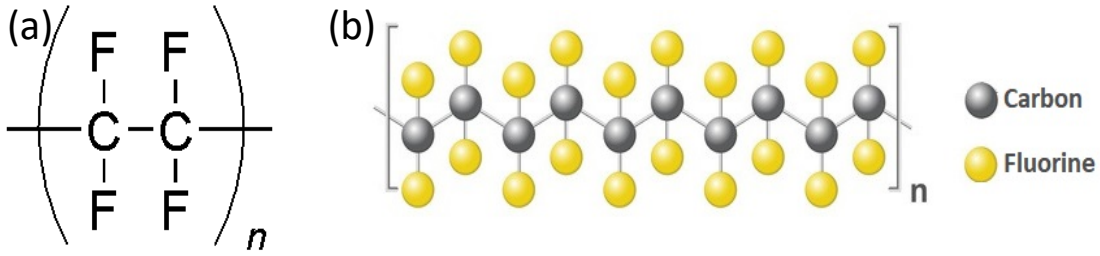

Fig 1.1: The chemical bonding and 3D chemical structure of the PTFE. (a) chemical bonding of PTFE and (b) 3D chemical structure of the PTFE [2].

Polydopamine (PDA) is a bio-inspired adhesive polymer formed by the oxidation of dopamine [8-12]. The PDA's chemical structure is still under discussion but possibly consists of covalently bonded dopamine, dihydroxy indole, and indoledione [12], as shown in Figure 1.2. Some researchers hypothesized that PDA is consists of a non-covalent arrangement among dopamine, dopamine-quinone, and 5,6-dihydroxyindole, but others hypothesized that PDA is a heteropolymer consist of catecholamine, quinone, and indole in repeating units [13]. Even though the chemical structure of PDA is still under study, it is widely accepted that DOPA ('3, 4 dihydroxy-L-phenylalanine') and 'lysine peptides' [8-11] are the main building blocks of PDA. The amine group of lysine peptides and DOPA can act as a binding agent to the inorganic substrate [8-11].

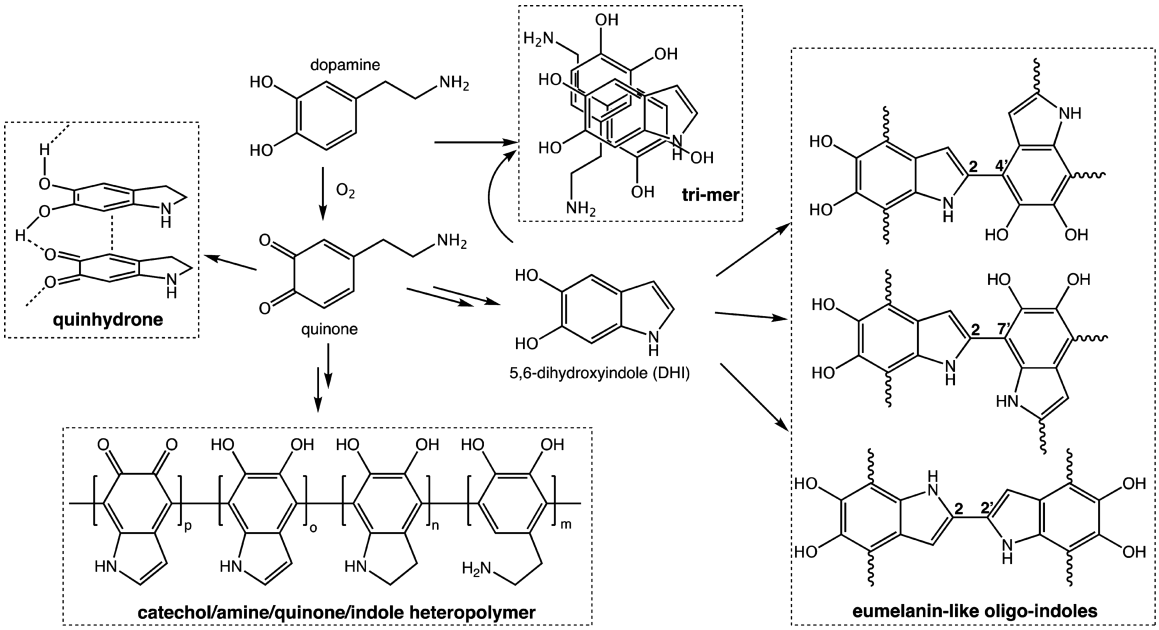

Fig. 1.2 The possible chemical structure of polydopamine and their formation by oxidation of dopamine in alkaline solution of controlled pH [12]. (Copyright 2013 American Chemical Society)

PDA has been used as an underlayer to improve the adhesion between the substrate and thin PTFE coatings and showed promising durability in dry contact conditions [13-23]. For many tribological applications, thick PTFE coatings are desirable [24-29]. For example, thick PTFE coatings can be used in journal bearings as an alternative to the Tin-based Babbitt to create environmentally safe lead-free bearings. The thickness of the PTFE coatings plays an important role in the tribological performance of the PDA/PTFE coatings. However, the effects of PTFE coating thickness on the durability of the PDA/PTFE coatings have not been systematically studied. In addition, PTFE coatings have not been extensively studied in oil-lubricated conditions, which is very critical for applying PTFE coatings to journal bearings. Furthermore, PDA can be added to PTFE to form PDA+PTFE composite coatings to enable more durable coatings.

In this dissertation research, the effects of the PTFE coating thickness on the tribological properties of thick PDA/PTFE coatings on stainless steel substrates were examined. The tribological performances of the PDA+PTFE nanocomposite coatings with the desired coating thickness on cast iron substrates in oil-lubricated conditions were then investigated for potential applications in journal bearings. Additionally, the effects of compacting and adding Cu nanoparticles (NPs) to the PDA+PTFE coatings on the nanomechanical properties (adhesion, modulus of elasticity, and hardness) of the coatings were studied and correlated to their tribological properties to understanding the wear mechanisms and tribological behavior of these coatings.

1.2 Literature Review

1.2.1 Tribological Properties of Thick PTFE Coatings

PTFE shows a low COF but has a high wear rate due to the weak Van der Waals interaction between the PTFE molecules [3-6]. The low COF of the PTFE can be attributed to the linear chain

molecules of PTFE, which can form a low shear film during sliding [3]. The continuous forming and breaking of the low shear films are responsible for the high wear rate of bulk PTFE during sliding [4-8, 30-40]. However, the high wear rate of PTFE thin coatings can also be attributed to the weak adhesion between the PTFE coatings and the substrates [13-23].

Much work has been carried out over the years to increase PTFE coatings' adhesion to metallic surfaces [7-12]. Using a primer coat of an acrylic-based polymer and roughening the surface with sandpaper are the most popular ways to increase adhesion between PTFE and a substrate surface [21]. Inspired by Lee et al. [8-11], Beckford et al. [13] had used an ultrathin polydopamine (PDA) underlayer to enhance the adhesion between the PTFE coating and a stainless steel (SS) substrate, and hence improved the durability of the PTFE coating dramatically in dry sliding contact conditions without the need of modifying the substrate surface.

The study of PDA/PTFE coatings has been limited to thin PTFE films of 500-1300 nm thickness [13-23] in dry sliding contact conditions with an ultrathin (40-50 nm) PDA underlayer. The tribological properties were evaluated in terms of COF and durability. The effect of the sintering temperature and time on the structure and tribological behavior of the PDA/PTFE coating has also been studied [14]. The mechanical properties of the PDA/PTFE thin films were studied by using the nanoindentation technique [21]. To further increase the durability of the PDA/PTFE coating, different NPs (graphite, Ag, Au, Cu, and PDA coated Cu) were added in the PTFE layer of the PDA/PTFE coating [16-23]. The exact effect of these NPs on the nanomechanical properties of nanocomposite PDA/PTFE coatings, however, is still unknown. It was hypothesized that, at certain load conditions, there would be an optimal thickness at which the coating will show a pronounced increase in wear life due to the soft coating increasing the contact area and thus reducing the contact pressure.

Thick PTFE coatings have a wide range of applications in the bearing, cookware, and insulation for different electric machinery [24-29]. They have been used for fabricating polymeric bearings due to their self-lubricity, low COF, and chemical stability [24-26]. Batzar et al. [28] used an alumina primer to adhere to a PTFE coating to a metal substrate to fabricate non-stick cookware. The researchers claimed that the desired thickness for this type of non-stick heat resistant coating is 32.5-45 μm. Woelki et al. [25] applied a 3-layer coating with a PTFE top layer of 50-100 μm thicknesses, depending on the loading condition and creep resistance needed for the desired journal bearings. Yagihashi et al. [29] found that an 80 μm-thick, porous PTFE tape with a non-porous PEEK coating on both sides of the tape can be used as an insulation tape in different electrical machinery. The thickness of the PEEK coating was 7 μm and was fabricated via melt extrusion. The porous PTFE coating was fabricated using a rolling process. PTFE coatings with various thicknesses have been investigated for many industrial applications, especially in roller bearings, air compressors, and cookware. However, the effect of the PTFE thickness on the tribological behavior of the PDA/PTFE coating has yet to be studied.

There are various methods in which the PTFE topcoat can be applied, such as melt extrusion [24-25], spray coating [29], and dip coating [13-23]. It is observed from the literature that the thickness of the PTFE coating played an important role in determining the wear resistance and application of the desired PTFE coating system. The coating thickness can vary from five to a few hundred microns, depending on the specific application. For this research, the thickness of the PTFE topcoat was varied from 3-45 μm. In addition to the tribology of the PDA/PTFE coatings, how the addition of PDA affects the coating thickness of the PTFE coating during fabrication also studied in this dissertation.

1.2.2 Tribological Properties of PTFE Composites

Much work has been carried out to improve the mechanical and tribological performance of bulk PTFE [30-48]. One popular method to improve the wear properties of PTFE is to introduce different filler materials in the PTFE matrix to form composite materials [30-39, 46]. Carbon-based nanofillers (graphite, diamond, carbon nanotubes (CNT)) and glass fibers have been used extensively to improve the wear and mechanical properties of PTFE composite materials [36-38]. Ceramic (SiO_2, ZrO_2, Al_2O_3) and Copper NPs powder have been used to enhance the wear properties of the PTFE matrix [30-37]. It was evident from the literature review that even a small percentage of the filler material can dramatically change the mechanical and tribological properties of the PTFE nanocomposite.

The size of the filler materials also plays an important role in determining the wear properties of the PTFE composites [32]. It was observed from the literature that PTFE composites with nanometer-sized alumina particles performed better tribologically than those with micron-sized alumina particles [32]. The composite contained NPs showed a more consistent tribological behavior due to the better dispersion of the NPs in the polymer matrix compared to the composite that contained micron-sized fillers.

It is important to note that most of the studies on PTFE nanocomposites have been performed on bulk PTFE. There are very few PTFE nanocomposites that have been tested for thin or thick PTFE coatings [13-23, 34, 48-54]. Rossi et al. [34] demonstrated that the addition of PTFE in the Ni-PTFE coating improved the wear properties of the coating due to the inherent self-lubricity of the PTFE and the toughness of Ni inner coating. Beckford et al. [16,19] found that a small percentage of graphite and Cu particles in the PTFE top layer of the PDA/PTFE coating can improve the durability of the PDA/PTFE+Cu and PDA/PTFE+graphite coating. Beckford et al.

used 0.01wt% Cu NPs in the PTFE layer to enhance the longevity of the PDA/PTFE thin films by two-fold [19]. The addition of these NPs has improved the mechanical properties, spread the films, and enhanced the transfer film formation during wear tests, thus leading to better durability of the coatings [16-19]. The NPs show an anchoring property to the substrate, which also helps to improve the adhesion between the coating and the substrate hence the improved durability [22].

It is well established from the literature that the addition of a small percentage of filler in the PTFE matrix can improve the tribological performance of the PTFE composite coatings. In this research, Cu NPs will be added to the PDA+PTFE coating to investigate the effect of the NPs on the nanomechanical and tribological behavior of thick PDA+PTFE+NP coatings.

1.2.3 PTFE Compaction

The studies by Beckford et al. [13,16-17] showed that thin PTFE coatings have porous structures. It is hypothesized that compacting the porous coatings might provide a better wear property for the PDA/PTFE coatings. Different compacting methods can be used to compact a polymer composite system. Cold compression [55-60], spark plasma compacting [61], roll compacting [72], and hot compression [62-71] have been used to achieve a compacted polymer composite system. Among them, hot compression is the most popular and widespread method to compact different nanocomposites. In hot compression, the composite system is heated up to the melting point of the polymer matrix, and pressure is applied simultaneously to compact the composite [62-65], whereas, in cold compression, the only pressure is applied without heating [55]. Hot compression is more efficient than cold compression to achieve a non-porous compacted surface. It is important to optimize the compacting time and pressure during hot compression to prevent the occurrence of creep and deformation [75]. It was observed from the literature that the

hot isostatic and hot hydraulic pressing helped to fabricate a denser PTFE composite in bulk form compared to the cold compression [70, 75]. PTFE coating fabricated by different melt extrusion procedures showed a lower porosity than other fabrication procedures [72-75]. In this research, a hot press was used to compact the PDA+PTFE coatings.

1.2.4 PTFE in Oil-lubricated Condition

PTFE coatings have been mostly studied in dry conditions. Although bulk PTFE has been studied in oil-lubricated conditions, not much progress has been made in the tribology of oil-lubricated PTFE coatings. Bulk PTFE and PTFE with different filler materials such as metal powder [76], the polymer [77], fiber and whisker [78], rare earth materials [79], metal sulfides and graphite [80], and lead [81] have been studied under different oil-lubricated conditions. Zhang et al. [81] found that the addition of Pb_3O_4 reduces the wear and COF of the PTFE+ Pb_3O_4 composites under liquid paraffin lubricant. They also found that graphite and metal sulfide-filled PTFE showed a reduction in both wear and COF under liquid paraffin lubricant [80]. Jia et al. [77] found that the addition of polyphenylene sulfide (PPS) and polyamide (PA) 66 into the PTFE matrix reduced the wear and COF under oil-lubricated conditions. Solid lubricant coatings such as Al_2O_3, PTFE, and MoS_2 are important because of their inherently low COF and the ability to reduce the COF and wear when used as a particle reinforcement in different composites. Liew et al. [82] found that both the COF and wear rate of Al_2O_3, Ni-P-PTFE, and MoS_2 coatings on aluminum alloy were reduced when tested under oil-lubricated conditions compared to under dry conditions. They observed that the self-lubricating properties of the filler materials helped to improve the wear performance of the PTFE composites.

It was observed from the literature [76-90] that the COF of PTFE was reduced when tested in oil compared to dry conditions. The wear properties of the PTFE also improved one order of magnitude or more when tested in oil-lubricated conditions compared to the dry conditions [76-80]. The addition of different particles in the PTFE matrix reduced the COF and improved the wear resistance of the PTFE composite compared to pristine PTFE. Although the PTFE composite showed better tribological properties in the oil-lubricated condition than in the dry condition, the tribological behavior of the PTFE coatings in the oil-lubricated condition is still not understood. Currently, all studies of the PDA/PTFE thin films have been carried out in dry sliding conditions, yielding the tribological performances of the PDA/PTFE and PDA+PTFE nanocomposite coatings in oil-lubricated conditions yet to be elucidated by the scientific community. Furthermore, how the addition of the NPs in the PTFE matrix impacts the wear behavior of the PTFE composite coatings needs to be understood.

It can be seen from the literature that to improve the wear properties of bulk PTFE composite in both dry and oil-lubricated conditions, different NPs have been added to improve the wear properties of the PTFE coatings. In this dissertation, Cu NPs were used in the PDA+PTFE matrix to investigate the effect of Cu NPs on the nanomechanical and tribological performance of PDA+PTFE coating in boundary oil-lubricated conditions.

1.2.5 Studying of the Nanomechanical Properties of Polymer Nanocomposites by PeakForce Quantitative Nanomechanical (PFQNM)

Nanomechanical properties such as adhesion, modulus of elasticity, and hardness play an important role in determining the tribological behavior of polymer nanocomposites. There are different methods of determining the nanomechanical properties of a polymer nanocomposite.

Recently, the PFQNM method by AFM has been used to determine the elastic modulus and adhesion of different materials [91-113]. In the PFQNM method, the AFM is used to image the surface topography and generate the nanomechanical property map of the nanocomposites. Abd et al. [112] measured the adhesion of bituminous binders using AFM and pull-off tests and found that the adhesion values obtained from both the test methods were very close. PFQNM by AFM has an advantage over the pull-off tests in that it can show the local topography and variations in the nanomechanical properties over the mapped area [91-93,112].

PFQNM method can be used to measure the nanomechanical properties of a wide range of materials depending on the AFM probe used [113]. It has been extensively used to study biological cells such as local cells [92], animal cells [93], marine diatom [94], HeLa cells [95], corneal cells [97], and collagen fibrils [98]. Rashid et al. [101-102] studied nanomechanical properties of asphalts using the PFQNM method. They studied the change in the nanomechanical properties when the ground tire was added to the asphalts [101]. They also studied the reclaimed asphalts with an incorporated binder [102]. The researchers correlated the higher performance grading temperature of the tire/asphalts composite to the higher stiffness of the composite [101-103].

Studies of the nanomechanical properties of a polymer or polymer composite are scarce [109-111]. Tian et al. [109] used the PFQNM to measure the nanomechanical properties of SiO_2/Rubber nanocomposites and to understand the double layer interphase and the better mechanical performance of these composite materials. Bulk PTFE has an elastic modulus of 0.4-2.5 GPa and a hardness of 60-70 MPa [21, 111]. The addition of the filler particles, in general, increased the elastic modulus of the PTFE-based composite materials [21]. Beckford et al. [16] reported that the elastic modulus and hardness of the PTFE thin films measured by nanoindentation are 1.6-2 GPa and 60-65 MPa, respectively. The researchers also found that the addition of graphite

decreases the elastic modulus of the thin PTFE films [16]. For polymer coating, adhesion between the coating and the substrate plays a very important role in the tribological properties of the coating [13-23]. Not much work was carried out to measure the adhesion of the PTFE top surface and the AFM probes to understand the effect of the filler materials on the adhesion properties of the PTFE composite coating. The elastic modulus of the nanocomposite also gives an indication of how the coating will behave under different loading conditions in tribological applications. It is important to study the nanomechanical properties of the PDA+PTFE nanocomposite and understand the change in the nanomechanical properties when different NPs are added to the PDA+PTFE coating. The nanomechanical properties of the PDA+PTFE nanocomposite coating can be correlated to the tribological properties of these coatings, which will be useful to design a polymeric coating in the future for various applications.

1.3 Research Objectives

The goal of this research is to understand the tribological behavior of thick PDA+PTFE nanocomposite coatings and their nanomechanical properties by a combination of tribological study, thorough characterization, and PFQNM. At the end of this study, a correlation among the nanomechanical properties, chemical bonding, and tribological behavior of the thick PDA+PTFE+NP coatings in oil-lubricated conditions is established, which will guide the future design of the PDA+PTFE nanocomposite coatings for different applications. The scopes of this research are shown in Figure 1.3.

The specific objectives of this dissertation are to investigate

1. how the PTFE coating thickness affects the tribological behavior of thick PDA/PTFE coatings in dry conditions, and to determine an optimum coating thickness for the remaining study,
2. how PDA affects the tribological behavior of PTFE coating when PDA is added as a constituent. How the tribological property of the PDA+PTFE coating changes when the porosity of the coating is reduced by hot compaction,
3. what is the wear mechanism of PTFE coating in oil-lubricated conditions, how the addition of PDA affects the tribological properties of PTFE coating in oil-lubricated condition, and how the nanomechanical and tribological properties of the PDA+PTFE coating is related to each other,
4. what are the effect of Cu NPs in the PDA+PTFE+ Cu NP coatings on the coating nanomechanical properties, and how the changes in nanomechanical properties affect the tribological performance of PDA+PTFE+Cu NPs coating in oil-lubricated conditions.

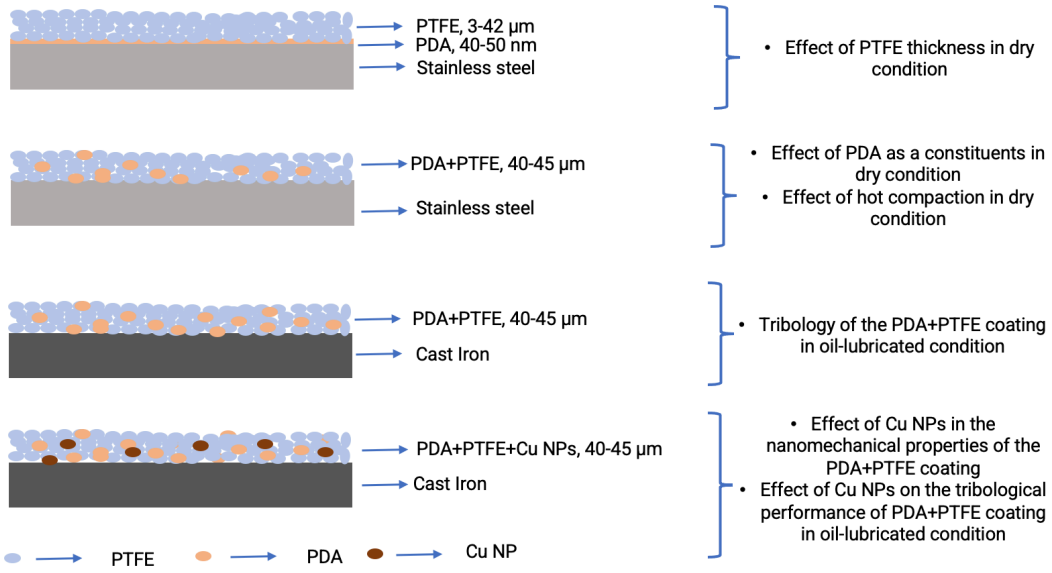

Fig 1.3: Schematic diagram of the different types of coating fabricated, (a) PDA/PTFE thick coating on SS substrate, (b) PDA+PTFE composite coating on cast iron substrate, and (c) PDA+PTFE+PP coatings on cast iron substrate.

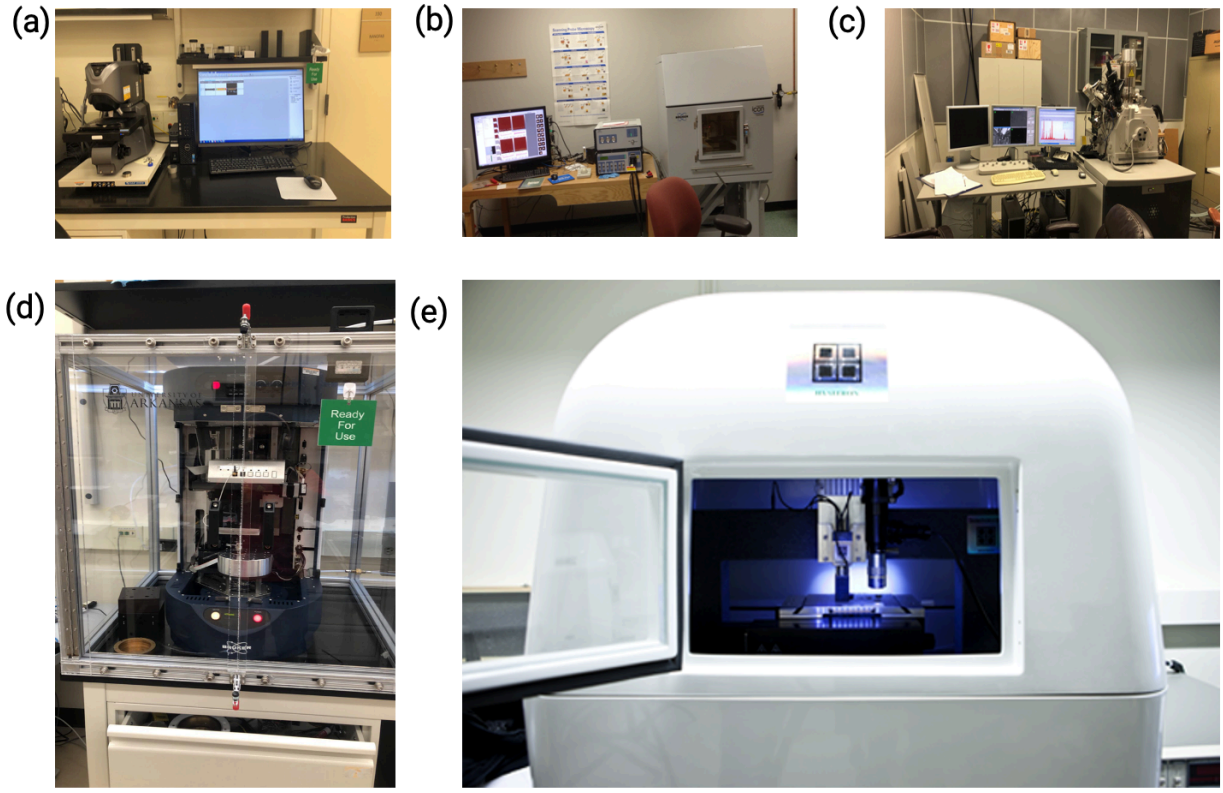

Fig 1.4: Instruments used to characterize the PDA/PTFE and PDA+PTFE coatings. (a) keyence optical microscopy, (b) AFM, (c) SEM, (d) UMT-2, and (e) nanoindenter.

1.4 Coating Characterization Instruments

The thickness of the coatings was measured using a stylus profilometer (Dektak 150, Bruker, USA). The topography of the coating surfaces was investigated by means of 3D laser scanning microscopy (VK X260K, Keyence Corporation, USA) (Figure 1.4 (a)), AFM (Dimension Icon, Bruker, USA) (Figure 1.4 (b)), and scanning electron microscopy (SEM) (XL-30, Phillips/FEI, Hillsboro, OR, USA) (Figure 1.4 (c)). A hot press was used to perform hot compaction. The optimized coating thickness from the thickness and compaction study was used for further studying the coatings. The PDA+PTFE coating was spray-coated using an in-house apparatus. The tribological performance was studied using a single 10N load in a ball-on-disc configuration using a universal mechanical tester (UMT-2, Bruker, USA) (Figure 1.4 (d)). X-ray

photoelectron spectroscopy was performed on the coatings to study the bonding structure of the coatings (XPS; PHI 5000 VersaProbe, ULVAC-PHI, Kanagawa, Japan). The PFQNM module of the AFM and nanoindentation (TI-900, Hysitron, USA) (Figure 1.4 (e)) were used to measure the nanomechanical properties (adhesion and elastic modulus) of the nanocomposite coating. The hardness of the coatings was measured using a nanoindenter. The nanomechanical properties of different nanocomposite coatings are correlated to their tribological behavior in oil-lubricated conditions.

References

1. Dhanumalayan, E., and Joshi, G.M. (2018), “Performance Properties and Applications of Polytetrafluoroethylene (PTFE)—a Review.” Advanced Composites and Hybrid Materials (1), pp 247–268

2. https://omnexus.specialchem.com/selection-guide/polytetrafluoroethylene-ptfe fluoropolymer, accessed October 27, 2020.

3. McKeen, L.W. (2013), “The effect of UV light and weather on plastics and elastomers,” Third edition.

4. Ebnesajjad, S. (2017), “Polytetrafluoroethylene: Properties and Structure,” Technology, Manufacturing and Application, pp 9-24

5. Burris, D. L., and Sawyer, W.G., (2006), “A Low Friction and Ultra Low Wear Rate PEEK/PTFE Composite.” Wear 261(3–4), pp 410–18

6. Unal, H., Mimaroglu, A., Kadıoglu, U., and Ekiz, H. (2004), "Sliding friction and wear behaviour of polytetrafluoroethylene and its composites under dry conditions," Materials & Design (25), pp 239

7. Eustathios, V. (1977), “Fluoropolymer primer having improved scratch resistance”, US Patent No. 4049863 A

8. Lee, H., Dellatore, S. M., Miller, W. M., and Messersmith P. B. (2007), "Mussel-inspired surface chemistry for multifunctional coatings," Science (318), pp426

9. Ye, Q., Zhou, F., and Liu, W. (2011), "Bioinspired catecholic chemistry for surface modification," Chemical Society Reviews (40), pp 4244

10. Lee, H., Lee, Y., Statz, A. R., Rho, J., Park, T. G., and Messersmith, P. B. (2008), "Substrate-independent layer-by-layer assembly by using mussel-adhesive-inspired polymers," Advanced Materials (20), pp1619

11. Lee, H., Rho, J., and Messersmith, P. B. (2009), "Facile conjugation of biomolecules onto surfaces via mussel adhesive protein inspired coatings," Advanced Materials (21), pp 431

12. Liebscher, J., Mrowczynski, R., Scheidt, H.A., Filip, C., Hadade, N.D., Turcu, R., Bende, A., and Beck, S. (2013), “Structure of Polydopamine: A Never-Ending Story,” Langmuir (29), pp 10539-10548

13. Beckford, S. and Zou, M. (2014), “Wear Resistant PTFE Thin Film Enabled by a Polydopamine Adhesive Layer,” Applied Surface Science (292), pp 350-356.

14. Jiang, Y., Choudhury, D., Brownell, M., Nair, A., Goss, J.A., and Zou, M. (2019), "The Effects of Annealing Conditions on the Wear of PDA/PTFE Coatings," Applied Surface Science (481), pp 723-735

15. Zhao, Y. and Zou, M. (2019), "Experimental Investigation of the Wear Mechanisms of Thin PDA/PTFE Coatings," Progress in Organic Coatings (137), pp 105341

16. Beckford, S., Cai, J., Fleming, R., and Zou, M. (2016), "The Effects of Graphite Filler on the Tribological Properties of Polydopamine/PTFE Coatings." TRIBOLOGY LETTERS (64), pp 1-10.

17. Beckford, S., Mathurin, L., Chen, J., Fleming, R., and Zou, M. (2016), "The Effects of Polydopamine Coated Cu Nanoparticles on the Tribological Properties of Polydopamine/PTFE Coatings." *Tribology International* (103), pp 87-94.

18. Choudhury, D., Niyonshuti, I., Chen, J., Goss, J., and Zou, M. (2020), "Tribological Performance of Polydopamine + Ag Nanoparticles/PTFE Thin films." *Tribology International* (144), pp 106097.

19. Beckford, S., Mathurin, L., Chen, J., and Zou, M. (2015), "The Influence of Cu Nanoparticles on the Tribological Properties of Polydopamine/PTFE + Cu Films." Tribology Letters (59).

20. Beckford, S., Cai, J., Chen, J., and Zou, M. (2014), "Use of Au Nanoparticle-Filled PTFE Films to Produce Low-Friction and Low-Wear Surface Coatings," Tribology Letters (56), pp 223-230

21. Miller, C., Choudhury, D., and Zou, M. (2019), "The Effects of Surface Roughness on the Durability of Polydopamine/PTFE Solid Lubricant Coatings on NiTiNOL 60," Tribology Transactions, 62(5), pp 919-929.

22. Kordshuli, F., Okyere, D., Chen, J., Miller, C., Harris, N., Mohajer, M., Ghosh, S., and Zou, M. (2021), "Tribological behavior of the PDA/PTFE+Cu-SiO_2 nanoparticle thin coating," Surface & Coating technology. 409.

23. Choudhury, D., Miller, C., Harris, N., and Zou, M. (2020), "The Effect of Coating Thickness on the Tribological Properties of Polydopamine/PTFE + Graphite Particle Coatings on 60NiTi," Surface Coatings and Technology, DOI:10.1016/j.surfcoat.2021.127320

24. Doll, G.L., Evans, R.D., and Ribaudo, C.R. (2006), "Coated Rolling Element Bearing Cages", US Patent No. 6994475 B2

25. Woelki, P., Petit, D., and Harig, F. (1999), "Self-Lubricating Bearing", US Patent No. 5971617 A.

26. Tevruz, T. (1998), “Tribological behaviours of Carbon Filled Polytetrafluoroethylene (PTFE) dry Journal Bearings”, Wear (221), pp 61-68.

27. Nunez, E.E., Yeo, S.M., Polychronopoulou, K., and Polycarpou, A.A. (2011), “Tribological study of high bearing blended polymer-based coatings for air-conditioning and refrigeration compressors”, Surface & Coatings Technology (205), pp 2994–3005

28. Batzar, K. (1993), “Cookware Coating Systems”, US Patent No. 5250356 A

29. Yagihashi, H. (1993), “Electrical insulation and articles thereof”, US patent US005393929A.

30. Yeob, L.J, and Lim, D.S. (2004), “Tribological Behavior of PTFE Film with Nanodiamond.” Surface and Coatings Technology 188–189 (1–3 SPEC.ISS.), pp 534–38

31. Lee, J.Y., and Lim, D.S. (2004), "Tribological behavior of PTFE film with nanodiamond," Surface and Coatings Technology (188), pp 534

32. Steven E.M., Blanchet, T. A., Schadler, L. S., and Sawyer, W. G. (2008), “Effect of Particle Size on the Wear Resistance of Alumina-Filled PTFE Micro- and Nanocomposites.” Tribology Transactions 51(3), pp 247–53

33. Hua, C.X, Xue, Y.J., and Xie, C.Y. (2002), “Friction and Wear of Rare-Earth Modified Glass-Fiber Filled PTFE Composites in Dry Reciprocating Sliding Motion with Impact Loads.” Wear 253(7–8), pp 869–77.

34. Rossi, S., Chini, F., Straffelini, G., Bonora, P.L., Moschini, R., and Stampali, A. (2003), “Corrosion protection properties of electroless Nickel/PTFE, Phosphate/MoS2 and Bronze/PTFE coatings applied to improve the wear resistance of carbon steel”, Surface and Coatings Technology (173), pp 235–242

35. Bahadur, S., and Tabor, D. (1984), "The wear of filled polytetrafluoroethylene," Wear (98), pp 1

36. McElwain, S. E., Blanchet, T. A., Schadler, L. S. and Sawyer, W. G. (2008), "Effect of particle size on the wear resistance of alumina-filled PTFE micro-and nanocomposites," Tribology Transactions (51), pp 247

37. Burris, D. L. (2007), “Effects of nanoparticles on the wear resistance of polytetrafluoroethylene.” A dissertation submitted to the University of Florida

38. Lim, D., Lee, J., Lim, D., Ahn, S., and Lyo, I. (2009), "Effect of reinforcement particle size on the tribological properties of nano-diamond filled polytetrafluoroethylene based coating." Journal of Nanoscience and Nanotechnology (9), pp 4197

39. Xiang, D., Li, K., Shu, W., and Xu, Z. (2007), "On the tribological properties of PTFE filled with alumina nanoparticles and graphite." Journal of Reinforced Plastics and Composites (26), pp 331

40. Sawyer, W. G., Freudenberg, K. D., Bhimaraj, P., and Schadler, L. S. (2003), "A study on the friction and wear behavior of PTFE filled with alumina nanoparticles." Wear (254), pp 573

41. Acheson. Product data sheet: Emralon 333, http://www.silitech.ch/upload/fiche_technique_D/343.PDF, accessed date 9/13/2015.

42. Chen, Y.C., Lin, H.C., and Lee, Y.D. (2003), "The effects of filler content and size on the properties of PTFE/SiO_2 composites." Journal of Polymer Research (10), pp 247
43. Joyce, J. A. and Joyce, P. J. (2004), "The fracture toughness of polytetrafluoroethylene." ECF15 Stockolm.

44. Yidong, Z., Guangbin, Y., and Pingyu, Z. Z. Z. (2010), "Friction reducing anti-wear and self-repairing properties of nano-Cu additive in lubricating oil." Journal of Mechanical Engineering (5), pp 014 .

45. Zhang, Y., Zhao, X. J., He, Q., Jun, Y., and Niu, Q. P. (2011), "Experimental study of nanoparticle as oil additives in Advanced Materials Research." Trans Tech Publ, (230), pp 288-292.

46. Jia, Z., Hao, C., and Yang, Y. (2014), "Tribological performance of hybrid PTFE/serpentine composites reinforced with nanoparticles." Tribology (8), pp 139

47. Yan, Y., Jia, Z., and Yang, Y. (2011), "Preparation and mechanical properties of PTFE/nano-EG composites reinforced with nanoparticles." Procedia Environmental Sciences (10), pp 929

48. Shi, M., Miyazawa, F., Tobe, S., and Stolarski, T. (2005), "The friction and wear properties of PTFE composite-thermal spray metallic binary coatings." Materials Transactions (46), pp 84

49. Blanchet, G.B. and Shah, S.I. (1993), "Deposition of polytetrafluoroethylene films by laser ablation," Applied Physics Letters (62), pp 1026

50. Norton, M.G., Jiang, W., Dickinson, J.T., and Hipps, K. (1996), "Pulsed laser ablation and deposition of fluorocarbon polymers." Applied Surface Science (96), pp 617

51. Holmberg, K., and Matthews, A. (2009), "Coatings tribology : properties, mechanisms, techniques and applications in surface engineering." Elservier, Amsterdam.

52. Nishimura, M., Watanabe, M., and Yoshimura, R. (1989), "Friction and wear of sputtered PTFE films," Proc. Symp. on Tribochemistry (Chinese Academy of Science, Lanzhou, P.R. China).

53. Zhao, Q., and Liu, G. (2002), “Graded Ni-P-PTFE coatings and their potential application.” Surface and Coatings tech. (155), pp 279-284.

54. Zhao, Q. and Liu, G. (2005), “Electroless Ni-Cu-P-PTFE composite coatings and their anticorrosion properties.”Surface and Coatings tech. (200), pp 2510-2514

55. Reilly, J. (1989), “Cold compaction of polyetheretherketone and nickel powders blends.” Polymer Engineering and Science, 29 (20), pp 1446-1455

56. Clark et al. (2005), “Method for making articles by cold compaction molding and molded articles prepared thereby.” US patent, US 6846869 B2

57. Canto, R.B., Schmitt, N. and Billardon, R. (2011), "Experimental identification of the deformation mechanism during sintering of cold compacted PTFE powders.” Polymer Engineering and Science, pp 2220-2235.

58. Azhdar, B. and Kari, L. (2008), "Polymer-nanofiller prepared by high energy ball milling and high velocity cold compaction.” polymer composites, pp 252-261.

59. Jayaraman, G. (1976), “Cold compaction molding and sintering of polystyrene.” Polymer Engineering and Science, 16 (8), pp 529-536

60. Truss, R. (1980), “Cold compaction and sintering of ultra-high molecular weight polyethylene.” Polymer Engineering and Science, 20 (11), pp 747-755

61. Li, J., Wang, L. and Jiang, W. (2010), “Super hydrophobic surface of bulk carbon nanotubes compacted by spark plasma sintering followed by modification with polytetrafluoroethylene.” Carbon (48), pp 2644-2673.

62. Hine, P.J., and Ward, I.M. (2005), “Hot compaction of woven nylon 6,6 multifilaments.” Wiley inter science, pp 991-998

63. Hine, P.J., and Ward, I.M. (2005), “Hot compaction of polyethylene napthalate”, Wiley inter science, pp 796-803.

64. Zhang, C., Ma, C. and Wang, P. (2005), “Temperature dependence of electrical resistivity for carbon black filled ultra-high molecular weight polyethylene composites prepared by hot compaction.” Carbon (43), pp 2544-2553

65. Hine, P.J., and Ward, I.M. (1977), “The hot compaction of spectra gel-spun polyethylene fibre.” Journal of Material science (32), pp 4821-4831

66. Jebawi, K.A., Sixou, B. and Vigier, G. (2006), “Hot compaction of polyoxymethylene, part 1: processing and mechanical evaluation.” Wiley inter science, pp 1274-1284

67. Hine, P.J., and Ward, I.M. (2008), “The use of interleaved films for optimizing the production and properties of hot compacted, self-reinforced polymer composites”, Composite science and technology 68 (6), pp 1413-1421

68. Dashevesky, A. and Bodmeier, R. (2004), “Compression of pellets with various aqueous polymer dispersions.” International journal of Pharmaceuticals (279), pp 19-26.

69. Pan, X., Han, K., Chen, B., and Wu, C. (2010), “Novel compaction techniques with pellet-containing granules.” European journal of pharmaceutics and biopharmaceutics (75), pp 436-442

70. Ghosh, S. K. (2016), “On the development of novel multifunctional max reinforced polymers (MRPS) matrix composites” Theses, University of North Dakota
71. Hine, P.J., and Ward, I.M. (1993), “The hot compaction of high modulus melt-spun polyethylene fibers.” Journals of materials science, (28), pp 316-324

72. Zhao, Z. H. (2011), “Preparation of single-PTFE composites by the processes of compression molding and free sintering.” Composites Part B, (42) pp 1306-1310

73. Khedkar, J. and Meletis, E. (2002), “Sliding behavior of PTFE composites.” Wear (252), pp 361-369

74. Knopp, W.V. (1981), “Roll compacting of polymer powders into fully dense products.” US Patent, US 4436682

75. Howard, E. G. (1993), “PTFE with improved creep resistance, and preparation thereof.” US patent, US005420191A

76. Zhang, Z.Z., Xue, Q.J., Liu,W., Shen., W. (1997), “Friction and wear of metal powder filled PTFE composites under oil lubricated conditions.” Wear (210-1), pp 151-156

77. Jia, B., Li, T., Liu, X. and Hong, P. (2007), " Tribological behaviors of several polymer-polymer sliding combinations under dry friction and oil-lubricated conditions." Wear (262-11), pp 1253-1359.

78. Xue, Q.J., and Zhang, Z.Z. (1997), "Friction and wear characteristics of fiber and whisker reinforced PTFE composites under oil lubricated conditions." Applied polymer science (69-7), pp 1393-1402

79. Bao, D., and Cheng, X. (2006), "Evaluation of tribological performances of PTFE composite filled with rare earths treated carbon fibers under water lubricated condition." Journal of Rare Eraths (24-5), pp 564-568.

80. Zhang, Z.Z., and Xue, Q.J. (1999), "Friction and wear characteristics of metal sulfides and graphite filled PTFE composites under dry and oil lubricated conditions." Applied polymer science (72-6), pp 751-761.

81. Zhang, Z.Z., and Xue, Q.J. (1998), "Friction and wear characteristics of lead and its compounds filled poly tetrafluoroethylene composites under oil lubricated conditions." Tribology International (31-7), pp 361-368

82. Liew, K.W., Chia, S.Y., Kok, C.K., and Low, K.O. (2013), "Evaluation on tribological design coatings of Al_2O_3, Ni-P-PTFE and MoS_2 on aluminum alloy 7075 under oil lubrication." Materials & Design (48), pp 77-84

83. Qian, S.Q. and Hua, C.X. (2006), "On the friction and wear behavior of PTFE filled with rare earths treated carbon fibers under oil-lubricated condition." Wear (260), pp 1243-1247

84. Zhang, Z.Z., and Xue, Q.J. (1997), "Friction and wear behaviors of several polymers under oil lubricated condition." Polymer science (68), pp 2175-2182

85. Dai, W., Kheireddin, B., Gao, H., and Liang, H. (2016), "Roles of nanoparticles in oil lubrication." Tribology international (102), pp 88-98

86. Li, J. and Su, Y.H. (2008), "The oxidation-treated interface on tribological properties of carbon fibers-reinforced PTFE composite under oil lubricated condition." Surface interface analysis (41), pp 333-337

87. Li, J. and Cheng, X.H. (2008), "Friction and wear properties of surface-treated carbon fiber-reinforced thermoplastic polyimide composites under oil lubricated condition." Materials chemistry and physics (108), pp 67-72

88. Golchin, A., Simmons, G.F., and Glavatskih, S.B. (2012), "Break-away friction of PTFE materials in lubricated conditions." Tribology international (48), pp 54-62

89. Xiong, D., Qin, Y., and Wan, Y. (2015), "Tribological properties of PTFE/laser surface textured stainless steel under starved oil lubrication." Tribology international (82), pp 305-310

90. Zhang, Z.Z., Xue, Q.J., and Liu, W.M. (2000), "Effects of various kinds of fillers on the tribological behavior of PTFE composites under dry and oil-lubricated conditions." Applied polymer science (80), pp 1891-1897

91. Xavier, P. and Bose, S. (2016), "Nanomechanical mapping, hierarchical polymer dynamics and miscibility in the presence of chain-end grafted nanoparticles." Macromolecules (49), pp 1036-1048

92. Coceano, G., Ndoye, F., and Ferrari, E. (1992), "Local cell mechanics investigation by AFM mapping and optical tweezers indentation", Thesis,

93. D. Alsteens, D.J. Muller, 2016, "Nanomechanical mapping of first binding steps of virus to animal cell", Nature nanotechnology.

94. Pletikapic, G. and Berquand, A. (2012), "Quantitative nanomechanical mapping of marine diatom in seawater using peak force tapping atomic force microscopy." J, phycol (48), pp 174-182

95. Abdelhady, H.G., Muller, A., and Effat, A.M. (2016), "Spatiotemporal PFQNM visualization of the effect of suicide dendriplexes on dividing HeLa cells." Nanomedicine (12), pp 2365-2371

96. Sause, M.G.R. (2017), "Experimental methods to validate modeling of fiber reinforced materials." 7th GACM on computational mechanics, Germany.

97. Seki, T.S., Takahashi, H., and Itoh, N. (2015), "AFM characterization of chemically treated corneal cells." Anal. bioanal. Chem. (407), pp 2631-2635

98. Papi, M., Geraghty, B., and Akhtar, R. (2014), "Nanoscale characterization of the biomechanical properties of collagen fibrils in the sclera." Applied physics letters (104), pp 104-109

99. Rashid, A.M.F. and Hossain, Z. (2016), "Morphological and nanomechanical analysis of ground tire rubber-modified asphalts." Imov. Infrastructure solution (136), pp 36-43

100. Chlanda, A., Wozniak, M.J., and Kurzydlowski, K.J. (2015), "Quantitative imaging of electrospun fibers by peakforce quantitative nanomechanics atomic force microscopy using etched scanning probes." Micron (72), pp 1-7

101. Hossain, Z., Rashid, A.M.F., and Rahman, M.Z. (2017), "Morphological and nanomechanical characterization of industrial and agricultural waste-modified asphalts binders." Int. Journal of geomech.17(3), pp 84-94

102. Rashid, A.M.F., Hossain, Z., and Bhasin, A. (2017), "Nano-mechanistic properties of reclaimed asphalt pavement modified binders using an atomic force microscopy." Int. Jour. Of pavement engineering.

103. Zeng, G., Dirscherl, K., and Garnaes, J. (2018), "Toward accurate quantitative elasticity mapping of rigid nanomaterials by atomic force microscopy: effect of acquisition frequency, loading force, and tip geometry." Nanomaterials (8), pp 615-626

104. Adineh, V.R., Liu, B., Rajan, R., and Fu, J. (2015), "Multidimensional characterization of biomechanical structures by combining atomic force microscopy and focused ion beam: A study of the rat whisker." Acta Biomaterialia (21), pp 132-141

105. Roy, S. and Hossain, Z. (2019), "Nanoscale quantification of moisture susceptibility of paving asphalts." MATEC web of conferences (271).

106. Heu, C., Berquand, A., Caille, C.E., and Nicod, L. (2012), "Glyphosate-induced stiffening of HaCaT keratinocytes, a peak force tapping study on living cells." Jouranla of structural biology (178), pp 1-7

107. Adamcik, J. and Berquand, A. (2011), “Single step direct measurement of amyloid fibrils stiffness by peak force quantitative nanomechanical atomic force microscopy.” Applied physics letters (98), pp 193701

108. Plaut, J.S. and Bottini M. (2019), “Quantitative atomic force microscopy provides new insight into matrix vesicle mineralization.” Archives of biochemistry and biophysics (667), pp 14-21

109. Tian, C., Chu, G., Feng, Y., and Tian, M. (2019), “Quantitatively identify and understand the interphase of SiO_2/rubber nanocomposites by using nanomechanical mapping techniques of AFM.” Composites science and technology (170), pp 1-6

110. Gallyamov, M.O., Vinokur, R.A., and Schaumburg, K. (2002), “High quality ultrathin polymer films obtained by deposition from supercritical carbon dioxide as imaged by atomic force microscopy.” Langmuir (18), pp 6928-6934

111. Pittenger, B., Erina, N. and Su, C. (2014), “Mechanical property mapping at the nanoscale using peakforce QNM scanning probe technique.” Solid mechanics and its application (203), pp 31-51.

112. Abd, D.M., Khalid H.A., and Akhtar, R. (2017), “Adhesion properties of warm-modified bituminous binders determined using pull-off tests and atomic force microscopy.” Road materials and pavement design (19), pp 1926-1939

113. https://www.bruker.com/products/surface-and-dimensional-analysis/

Chapter 2

The Effects of PTFE Thickness on the Tribological Behavior of Thick PDA/PTFE Coatings

2.1 Abstract

In this study, the effects of polytetrafluoroethylene (PTFE) thickness on the wear and friction properties of spin-coated PTFE and polydopamine (PDA)/PTFE coatings on stainless-steel (SS) substrates were investigated. The PTFE coating thickness was varied by controlling the number of PTFE spin-coating deposition cycles. The PDA/PTFE coatings showed 1.4 to 4.9 times the wear life of that of the PTFE coating deposited at the same number of PTFE spin-coating cycles. The coefficients of friction and water contact angles of the PDA/PTFE coatings were found to be slightly higher than those of the PTFE coatings due to higher surface roughness. The addition of PDA underlayer helped the PTFE to adhere more strongly to the SS substrate, which contributed to the coatings' improved durability. The durability of the PDA/PTFE coating increased sharply when the PTFE thickness exceeded 30 μm. Notably, a 42 μm-thick PDA/PTFE coating had 105 times the wear life of that of a 3 μm-thick PTFE coating. The enhanced transfer film on the counterface and the larger contact area for supporting the load were responsible for the extended durability of the thicker coatings.

Keywords: PTFE, coating thickness, durability, roughness, coefficient of friction.

2.2 Introduction

Polytetrafluoroethylene (PTFE) is an alluring polymer for industrial applications due to its self-lubrication properties, low coefficient of friction (COF), and thermal and chemical stability [1-2]. PTFE is also a popular non-stick material used for various coating applications. However,

PTFE's adhesion to metallic substrates is very poor, which causes delamination and premature failure of PTFE coatings.

There has been much work reported in the literature to increase the adhesion between metallic substrates and PTFE coatings. Two popular ways of doing this are roughening the surface with different polishing methods and using an acrylic primer coating on the metallic substrate [3-7]. Other research seeks to enhance the tribological properties of PTFE by incorporating different nanomaterials into the PTFE matrix in order to increase the mechanical strength of both bulk PTFE and PTFE coatings [8-12,15,16].

Inspired by Lee et al.'s discovery of the adhesive property of polydopamine (PDA) [13], Beckford et al. [14-16] used a thin underlayer of PDA to enhance the tribological performance of thin PTFE coatings. The two main building blocks of PDA are the DOPA ('3, 4 dihydroxy-L-phenylalanine') and 'lysine peptides' [13]. The amine group of lysine peptides along with DOPA provides many sites for adhesion between the substrate and PTFE coating. Beckford et al. [14-16] reported that a 40 nm-thick PDA layer deposited over a stainless-steel (SS) substrate improved the wear performance of PDA/PTFE coatings 500-fold without sacrificing the low COF of the PTFE coatings. The PDA/PTFE coatings wore very fast initially, but the interface between the PDA and PTFE was able to sustain most of the rubbing cycles. They concluded that the PDA underlayer is responsible for the increased adhesion between the SS substrate and the PTFE top layer, thereby the enhanced wear resistance of PDA/PTFE thin coatings. Beckford et al. compared the thin PDA/PTFE coating against a commercial low friction, high durability coating and found that the COF of the thin PDA/PTFE coating was 43% lower than that of the commercial coating [17]. More importantly, the thin (1.3 μm) PDA/PTFE coating demonstrated twice the wear life with only 5% of the thickness of the commercial coating (25 μm) [17]. Even though the PDA underlayer can

dramatically improve the wear performance of the PTFE coating, the thickness of the coating was limited to 0.5-1.3 μm and a more lenient loading condition (0.5 N) was used. Thicker PTFE coatings are expected to further improve the wear life of the PDA/PTFE coatings, but they have not been systematically investigated.

Thick PTFE coatings have many applications in commercial bearings [18-20], refrigerator compressors [21], and cookware [22]. Doll et al. [18] applied a three-layered PTFE coating to a rolling-element bearing for better self-lubricity. They found that a 5 μm-thick PTFE topcoat along with a 1 μm-thick amorphous carbon coating underneath can improve the self-lubricity of the rolling element bearing, even in the presence of abrasive third-body wear caused by the silver wear debris in the roller bearing. Woelki et al. [19] applied a 3-layer coating with a PTFE top-layer of 50-100 μm thicknesses, depending on the loading condition and creep resistance needed for the desired journal bearings. They found that the PTFE top-layer creates a self-lubricating bearing system with a better load-bearing capacity than that of the leading competitors. E. E. Nunez et al. [21] found that both 20 - 40 μm-thick PEEK and PTFE blend, and PTFE and MoS_2 composite coatings showed better wear resistance and lower friction than pristine PTFE coating in refrigerator compressors undergoing starved lubrication condition. K. Batzar et al. [22] used an alumina primer to better adhere a PTFE coating to a metal substrate to fabricate non-stick cookware. The researchers found that the desired thickness for this type of non-stick heat-resistant coating was 32.5 - 45 μm. The porous PTFE coating was fabricated using a rolling process. Lastly, thick PTFE coatings have also been used to protect carbon steel from corrosion [23].

The thicknesses of the PTFE topcoat played an important role in imparting self-lubricity in different PTFE coating applications. The desired thickness for the thick PTFE coating varied from five micrometers to several hundred micrometers depending on the applications. The wide range

of applications for thick PTFE coatings provides salient support for finding the thickness at which the tribological performance of the PDA/PTFE coating is maximized.

In this study, the effects of the PTFE topcoat thickness and the PDA underlayer on the tribological behavior of thick PDA/PTFE coating (3-42 μm) are reported. The surface topography, water contact angle (WCA), COF, durability, and wear mechanisms of the coating were investigated to characterize the thick PDA/PTFE coatings.

2.3 Methodology

2.3.1 Sample Preparation

Mirror-finished 0.762 mm-thick 316 SS sheets cut into 1.25”-diameter round samples were used as the substrate. The average roughness Ra of the SS substrate, measured over a 5000 μm^2 area using an optical microscope, was 26 ± 2 nm. The SS substrates were first cleaned using deionized (DI) water for 10 minutes, then soaked in an acetone bath for 15 minutes. After acetone cleaning, the SS samples were further cleaned in isopropanol alcohol (IPA) for 10 minutes in an ultrasonic bath and then rinsed with DI water. The SS substrates were finally dried by blowing nitrogen gas. The PDA underlayer deposition for the PDA/PTFE coating was achieved by a rocking shaker method [24]. Briefly, the SS samples were submerged in a container placed on a rocking shaker at 60°C and 25 Hz rocking frequency. The container has 700 mL of water solution with 0.848 g of Trizma base and 1.4 g of dopamine hydrochloride. The pH of the solution was maintained at ~8.5 for the entire duration of the PDA deposition process. After 45 minutes, the substrates were removed from the rocking shaker and washed in DI water before drying them using nitrogen gas. The substrates were then coated with PTFE using a standard spin coating process at a speed of 600-rpm for 30 seconds. As received DISP 30 PTFE dispersion containing 60 wt.% of

PTFE particles was used to coat eight sets of samples with 8 different thicknesses by varying the number of PTFE spin coating deposition cycles. After each PTFE spin-coating cycle, the samples were heat treated at 120°C for 3 minutes to remove the water and then at 270°C for 4 minutes to remove the surfactant from the aqueous dispersion. The coatings were then annealed at 372°C for 4 minutes to sinter the PTFE particles. Eight sets of PTFE control samples with the same PTFE spin-coating deposition cycles on SS were also fabricated.

2.3.2 Coating Characterization

The thicknesses of the coatings were measured using a stylus profilometer with a diamond tip of 12.5 μm-radius over a 9000 μm-length at a speed of 300 μm/second. A copper bar was first used to remove part of the PTFE coating to expose the SS substrate (Copper is softer than SS and did not wear into the SS substrate). The PTFE thickness was then determined from the height difference between the exposed SS substrate and the top of the PTFE coating from the stylus profilometry measurement. An atomic force microscope (AFM) was used to evaluate the surface topography and roughness of each sample. The water contact angle was measured using a water contact angle goniometer.

Nanoindentation tests were performed to measure the elastic modulus and the hardness of both PTFE and PDA/PTFE coatings. The indents were made using a spheroconical diamond probe with a 1-μm tip radius and a 60° cone angle. The indentation load was 50 μN and the loading and unloading rates were 10 μN/s with a 5-second holding time. The maximum indentation depths were controlled at 200-300 nm, which were less than 30% of the coating thickness to avoid the effects of the substrate. Each coating was indented 5 times and the average and standard deviation values of modulus of elasticity and hardness were determined.

2.3.3 Tribological Study

To evaluate the tribological properties of thick PDA/PTFE coatings on SS, samples with 8 different PDA/PTFE coating thicknesses, ranging from 3 μm to 42 μm, were tested using a tribometer. PTFE coatings were also tested for comparison against PDA/PTFE coatings of similar thickness. Linear reciprocating wear tests were performed with an applied normal load of 10 N, a stroke length of 5 mm, and a sliding speed of 10 mm/s with a 0.1-second delay between each testing cycle. The wear tests were performed in a ball-on-disc configuration (Figure 2.1).

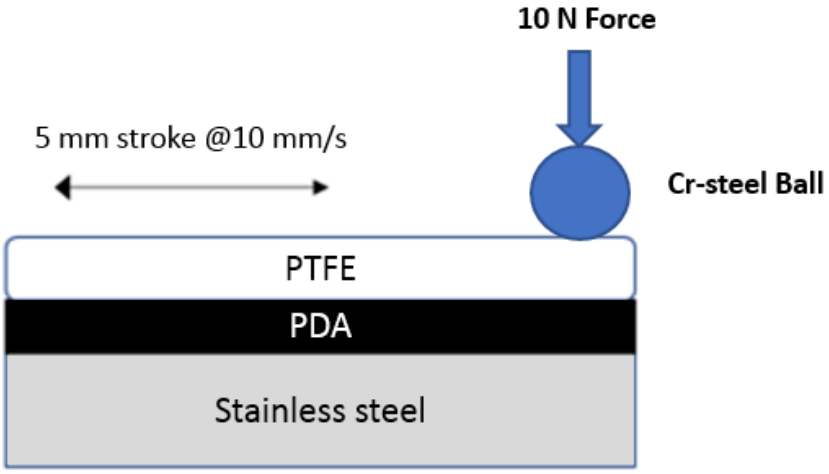

Fig. 2.1 The schematic of the PDA/PTFE coating tribological test setup.

A chrome steel ball with 6.35 mm diameter was used as the counterface surface after thorough cleaning. Test was programmed to stop once the friction force surpassed 3.0 N, before which point a sharp increase in COF was always observed, indicating a coating failure. To determine coating durability, three sets of tests were performed at every coating thickness. To study the coating adhesion to substrate, scratch tests were performed by linearly varying the load from 0.5 to 18 N over a 100-s time span at 0.1 mm/s speed. Again, chrome steel balls of 6.35 mm diameter were used as the counterface for the scratch tests. The scratch length was 10 mm for all

the scratch tests performed. The wear track and the chrome steel counterface used for tribological and scratch tests were evaluated using a 3D laser scanning confocal microscope.

To estimate contact pressure, PDA/PTFE coatings with 8 different thicknesses were tribologically tested for 100 cycles (below the number of cycles needed to cause failure of the thin PTFE and PDA/PTFE coatings) using the same test routine for durability testing. The area deformed under this loading condition was measured using a confocal 3D laser scanning confocal microscope. Since the coating was permanently deformed under the applied normal load, the average contact pressure between the PDA/PTFE coating and chrome steel ball was estimated by dividing the normal load of 10 N by the measured plastically deformed area.

2.4 Results and Discussion

2.4.1 Coating Thickness and Topography

Table 2.1 shows all samples fabricated in this study along with the measured coating thickness and surface roughness. The thickness of the PDA underlayer was 45-50 nm. Figure 2.2 shows the PTFE coating thickness as a function of the PTFE spin-coating deposition cycles. It can be observed that the thicknesses of the PTFE and PDA/PTFE coatings increased linearly with the PTFE deposition cycles. At the same number of PTFE deposition cycles, the PDA/PTFE coating had a higher coating thickness compare to the PTFE coating.

AFM images of the PTFE and PDA/PTFE coatings deposited for 1 and 8 spin coating cycles are shown in Figure 2.3. It can be seen that both PTFE and PDA/PTFE coatings have a needle-like structure. Both the PDA/PTFE coatings deposited at 1 (3 μm) and 8 (42 μm) cycles have a rougher surface topography than the PTFE coatings deposited at the same number of cycles. The AFM image of the PDA underlayer (not shown here) showed some PDA aggregates, which

were responsible for the observed large waviness of the PDA/PTFE coating after the first cycle of PTFE deposition. The average roughness (Ra) and the skewness of the PDA underlayer were 32.2 ± 2.1 nm and 3.43 ± 0.22, respectively. The positive skewness number of the PDA underlayer indicate that the PDA coating was peak dominated.

Table 2.1. Coating thickness and surface roughness of the samples

Sample Name	PTFE deposition cycle	Coating thickness and standard deviation (μm)	Average roughness, Ra, and standard deviation (nm)
PTFE -1	1	3.0±0.2	14.6±2.1
PTFE -2	2	7.5±0.8	19.8±1.2
PTFE -3	3	12.8±0.9	19.8±1.4
PTFE -4	4	18.3±1.3	19.9±1.7
PTFE -5	5	22.1±1.6	20.7±2.2
PTFE -6	6	27.4±0.7	21.2±1.9
PTFE -7	7	31.2±1.5	28.2±3.4
PTFE -8	8	36.3±2.2	36.4±3.8
PDA/PTFE -1	1	3.0±0.3	39.2±3.4
PDA/PTFE -2	2	10.5±1.2	66.3±2.8
PDA/PTFE -3	3	15.7±0.9	63.4±3.5
PDA/PTFE -4	4	22.3±1.8	68.8±2.9
PDA/PTFE -5	5	28.2±1.1	67.2±3.9
PDA/PTFE -6	6	34.2±1.4	71.2±4.2
PDA/PTFE -7	7	38.6±1.5	69.8±3.8
PDA/PTFE -8	8	42.2±2.8	67.4±4.5

Figure 2.4 shows the average roughness, Ra, root mean square roughness, Rq, and skewness of the PTFE and PDA/PTFE coatings deposited at different numbers of cycles. It was observed from Figures 2.4(a) and (b) that, in general, the roughness of the PTFE coating increased gradually as a function of the PTFE coating deposition cycle. However, for PDA/PTFE coatings, the roughness of the coating increased sharply after the first PTFE deposition cycle. After which, the roughness remained somewhat similar after each deposition cycles.

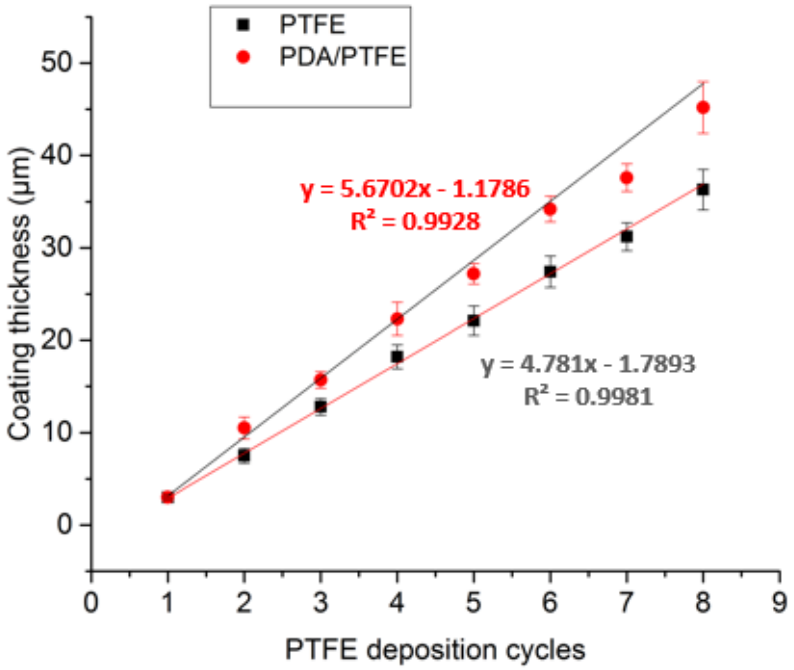

Fig. 2.2 Coating thickness as a function of the PTFE spin coating deposition cycles for the PTFE and PDA/PTFE coatings.

It was also observed that the PDA/PTFE coating had a much higher roughness than the PTFE coatings after all deposition cycles. The average roughness of the PTFE coating was 14.67 nm and 36.42 nm for coatings deposited at 1 (3 µm) and 8 (42 µm) cycles, respectively, whereas the average roughness of the PDA/PTFE coatings was 39.2 nm and 67.49 nm, respectively. From

Figures 2.4(a) and 4(b), it can be concluded that the addition of PDA had a large impact on the roughness of the PDA/PTFE coating. The higher adhesion of the PDA underlayer was responsible for rougher PDA/PTFE coating compared to the PTFE coating at the 1st cycle (3 µm) of PTFE deposition. From Figure 2.4(c), it can be seen that the skewness values of the PTFE coatings were negative up to 6 cycles (27 µm) of the PTFE deposition, whereas the skewness values of the PDA/PTFE coatings were all positive. The negative skewness values indicate that the PTFE coatings were mostly valley-dominant, but the PDA/PTFE coatings were peak-dominant.

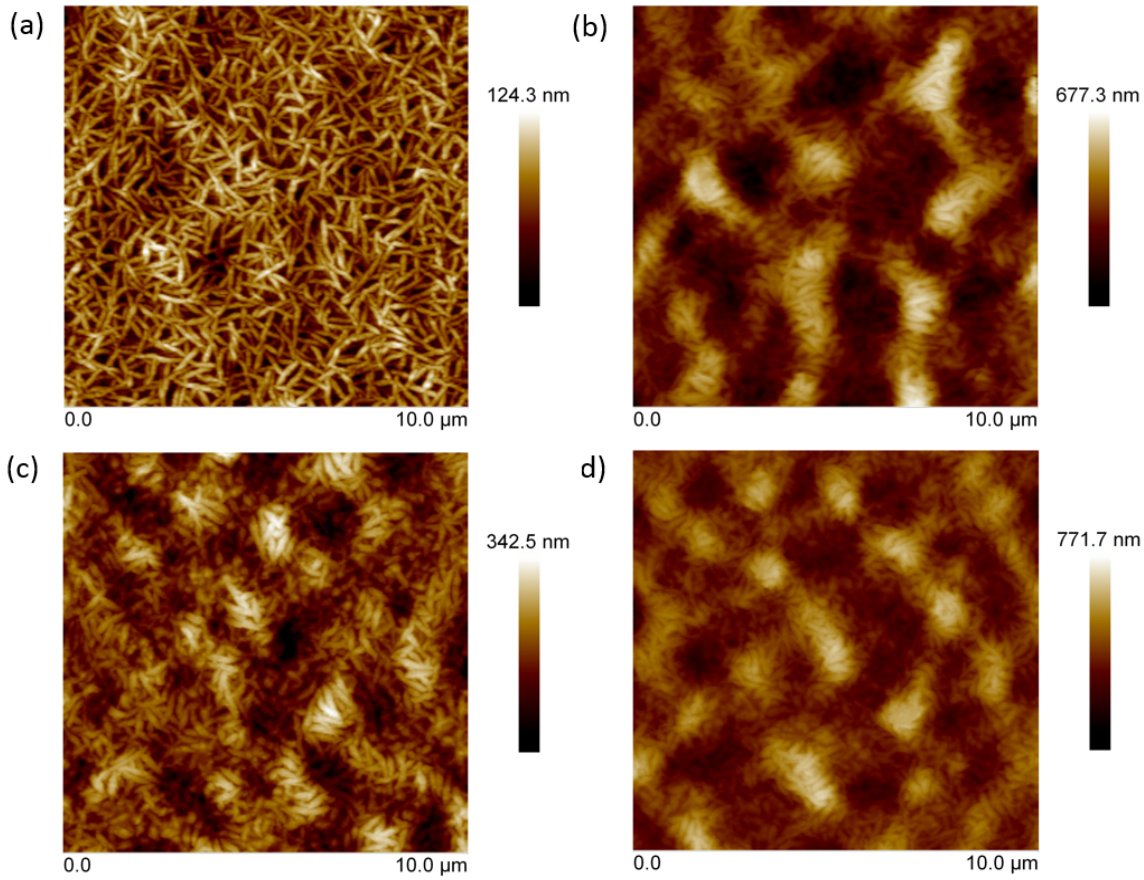

Fig. 2.3 AFM topography images of (a) PTFE and (b) PDA/PTFE coatings deposited at 1 spin-coating cycle, and (c) PTFE and (d) PDA/PTFE coatings deposited at 8 spin-coating cycle.

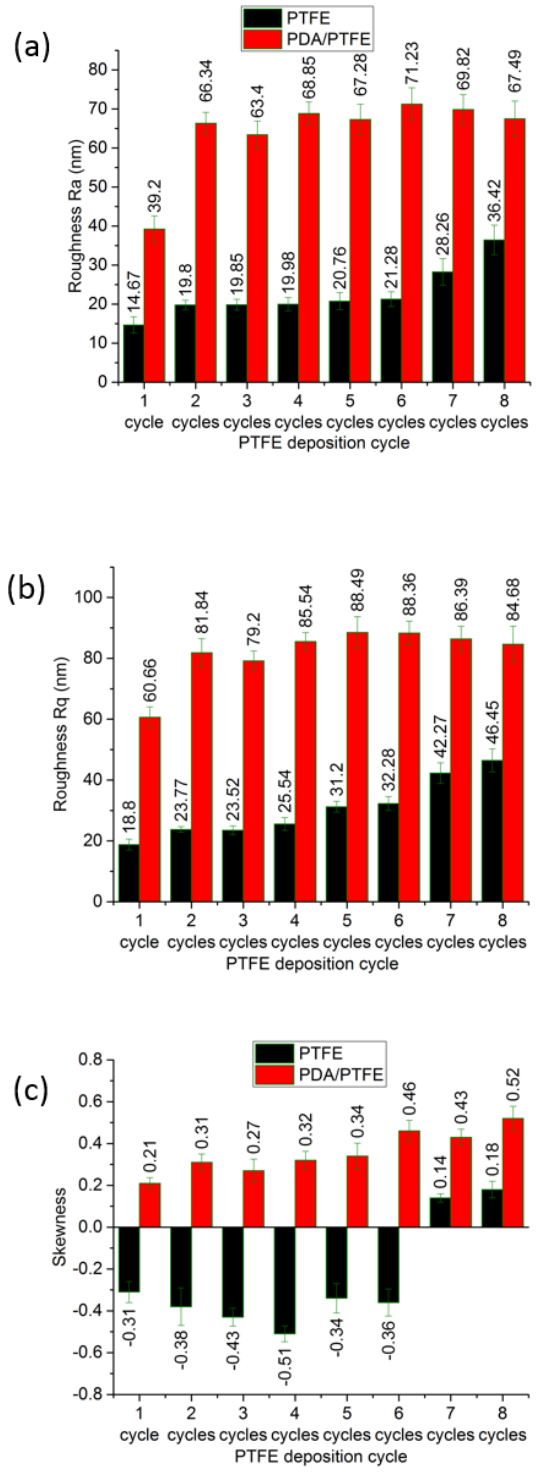

Fig. 2.4 The roughness of the PTFE and PDA/PTFE coatings for different deposition cycles: (a) The average roughness, R_a, (b) root mean square roughness, R_q, and (c) the skewness, R_{sk}.

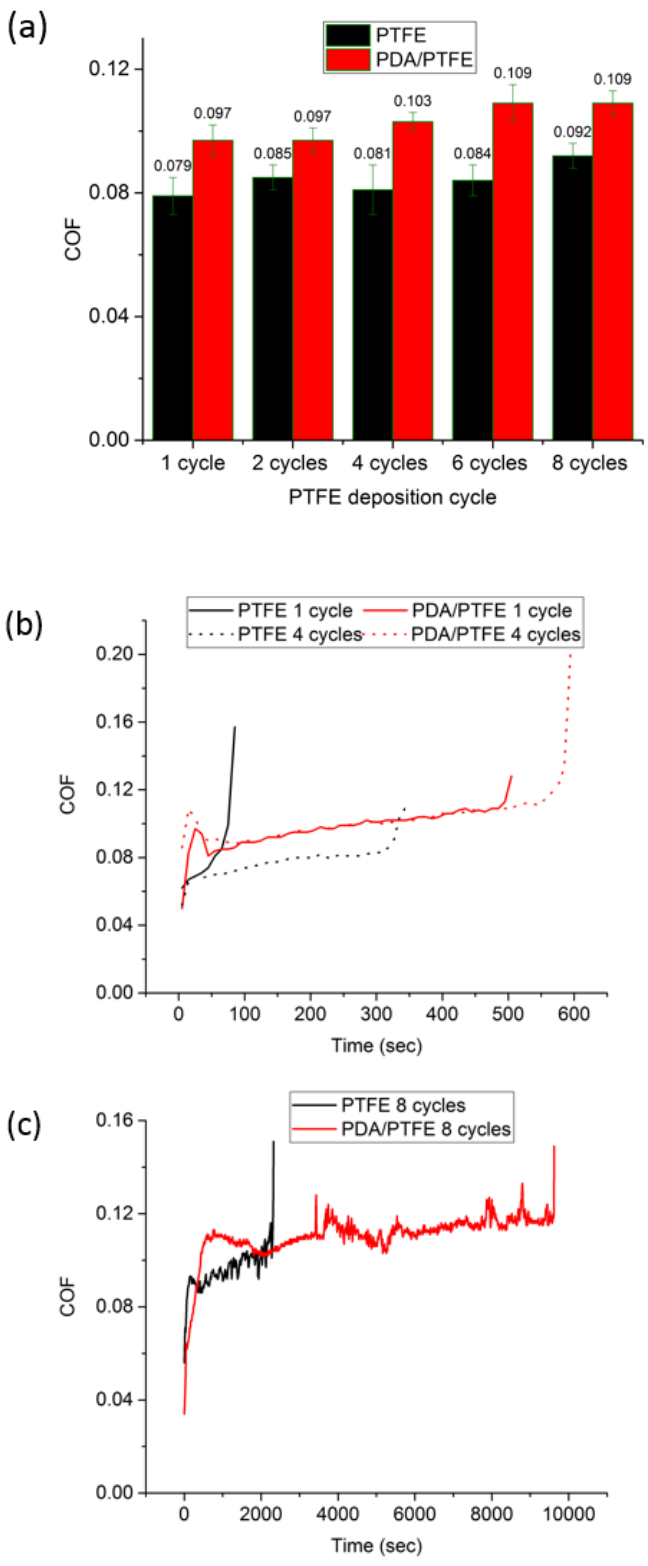

Fig. 2.5 The COFs of the PTFE and PDA/PTFE coatings: (a) average COF at different deposition cycles, (b) the COF profile during the test period for the PTFE and PDA/PTFE coatings deposited at 1 and 4 cycles, and (c) the COF profile during the test period for the PTFE and PDA/PTFE coatings deposited at 8 cycles.

It was also observed that the skewness number of the PDA/PTFE coatings increased with the deposition cycles. The increasing number of brighter, high spots in the AFM images of the PDA/PTFE coatings in Figure 2.3(d) compared to 2.3(b) also support this conclusion. From Figures 2.2-2.4, it can be concluded that higher roughness helped to attain a thicker coating with subsequent PTFE deposition cycles.

The average roughness of the coatings also had an impact on the COF of the coatings. Figure 2.5(a) shows the average COF of PTFE and PDA/PTFE coatings deposited at different numbers of cycles, measured from the entire tests excluding the data points where an abrupt increase in the COF was observed. It can be seen that as the number of deposition cycles increased, the average COF of the coating also increased slightly for the PDA/PTFE coating, while the average COF of the PTFE coatings is more or less the same up to 6 cycles (34 μm). Figure 2.5(a) also shows that PDA/PTFE coatings have higher COFs than PTFE coatings due to the higher surface roughness as shown in Table 2.1 and Figure 2.4. Figure 2.5(b)and 2.5(c) shows the COF of the PTFE and PDA/PTFE coatings over the testing time span before the coating failure. It was observed that the COF increased gradually over time for all coatings before a sharp increase at the end of the testing, indicating coating failure.

2.4.2 Water Contact Angle

The WCAs and water droplet images on the PTFE and PDA/PTFE coatings deposited at 1 and 8 cycles are shown in Figure 2.6. It can be seen that both the PTFE and the PDA/PTFE coatings demonstrated hydrophobic behavior. The 1- and 8-cycle PTFE coatings showed very similar hydrophobicity with WCAs of 109.8º and 108.7º, respectively. The PDA/PTFE showed slightly higher hydrophobic behavior than the PTFE coating with WCAs of 112.0º and 118.2º for the 1-

and 8-cycle coatings, respectively. According to Wenzel's model [25], a higher surface roughness will lead to a higher water contact angle of a hydrophobic surface. Although both the PTFE and the PDA/PTFE coating have similar needle-like structures, the higher surface roughness of the PDA/PTFE coatings resulted in higher water contact angles than the PTFE coatings.

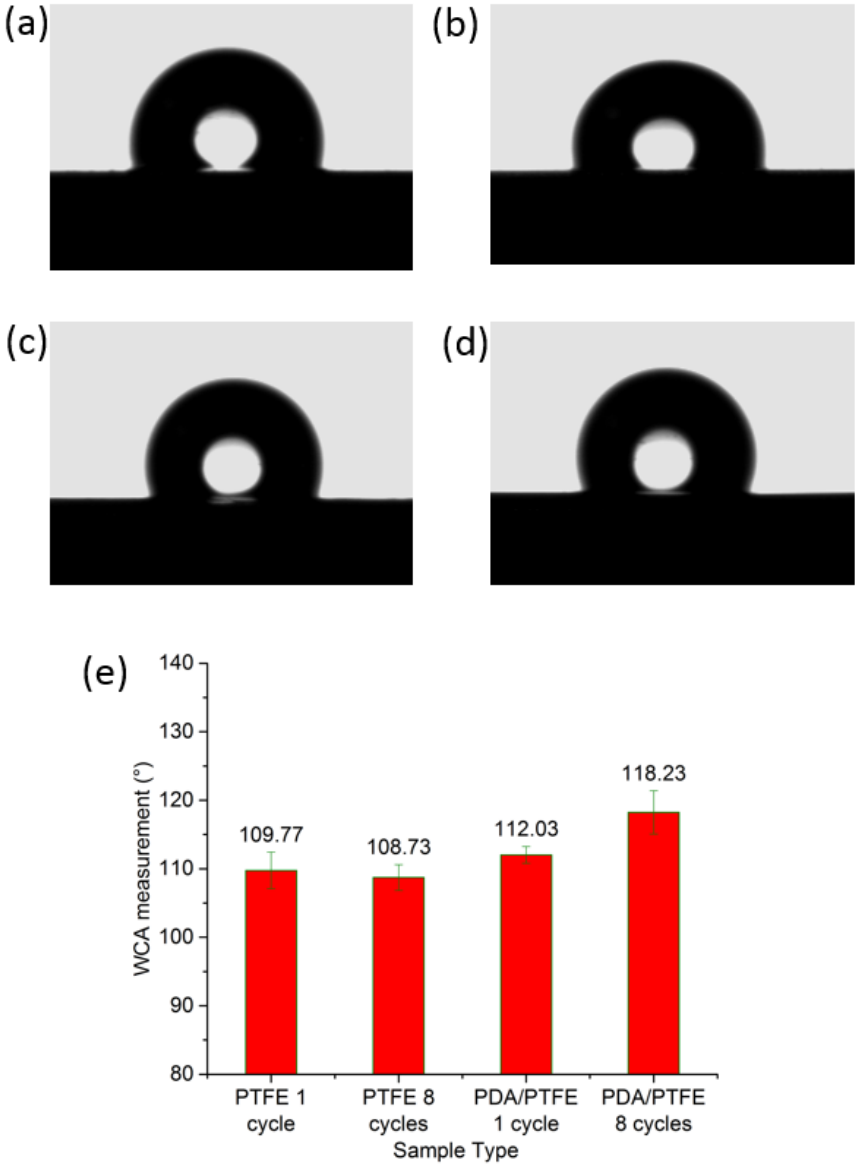

Fig. 2.6 Water contact angle images of the (a) PTFE coating deposited at 1 cycle, (b) PTFE coating deposited at 8 cycles, (c) PDA/PTFE coating deposited at 1 cycle, (d) PDA/PTFE coating deposited at 8 cycles, and (e) the comparison of WCAs of the PTFE and PDA/PTFE coatings deposited at 1 and 8 cycles.

2.4.3 Mechanical Properties

The hardness and modulus of elasticity of the coatings measured from the nanoindentation tests are plotted in Figure 2.7. Each value represents the average of 5 indents. The average hardness for the 1-cycle PTFE (3 µm), 8-cycle PTFE (36 µm), 1-cycle PDA/PTFE (3 µm), and 8-cycle PDA/PTFE (42 µm) coatings were 75.1, 60.2, 65.3, and 69.1 MPa, respectively. The average modulus of elasticity of the 1-cycle PTFE (3 µm), 8-cycle PTFE (36 µm), 1-cycle PDA/PTFE (3 µm), and 8-cycle PDA/PTFE (42 µm) coatings was 0.94, 0.75, 0.77, and 0.76 GPa, respectively.

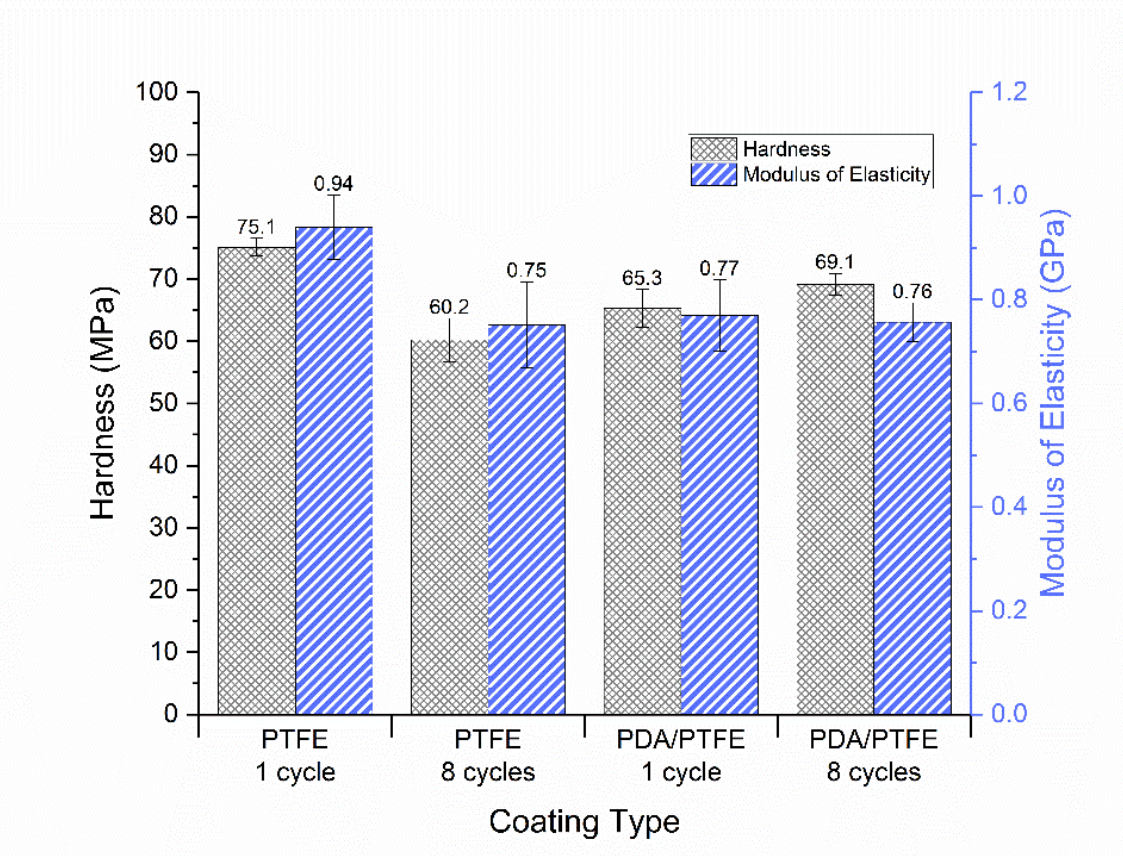

Fig. 2.7 Comparison of the hardness and modulus of elasticity of PTFE and PDA/PTFE coatings at 1 and 8 deposition cycles.

The marginally higher hardness and elastic modulus for the 1-cycle PTFE (3 µm) coating was most likely due to the larger contact area that resulted from its lower surface roughness. However, there was no substantial difference in these values among the 8-cycle PTFE (36 µm)

and 1(3 μm)- and 8 (42 μm)-cycle PDA/PTFE coatings. Furthermore, the inclusion of the PDA adhesive underlayer did not create a noticeable trend in this data.

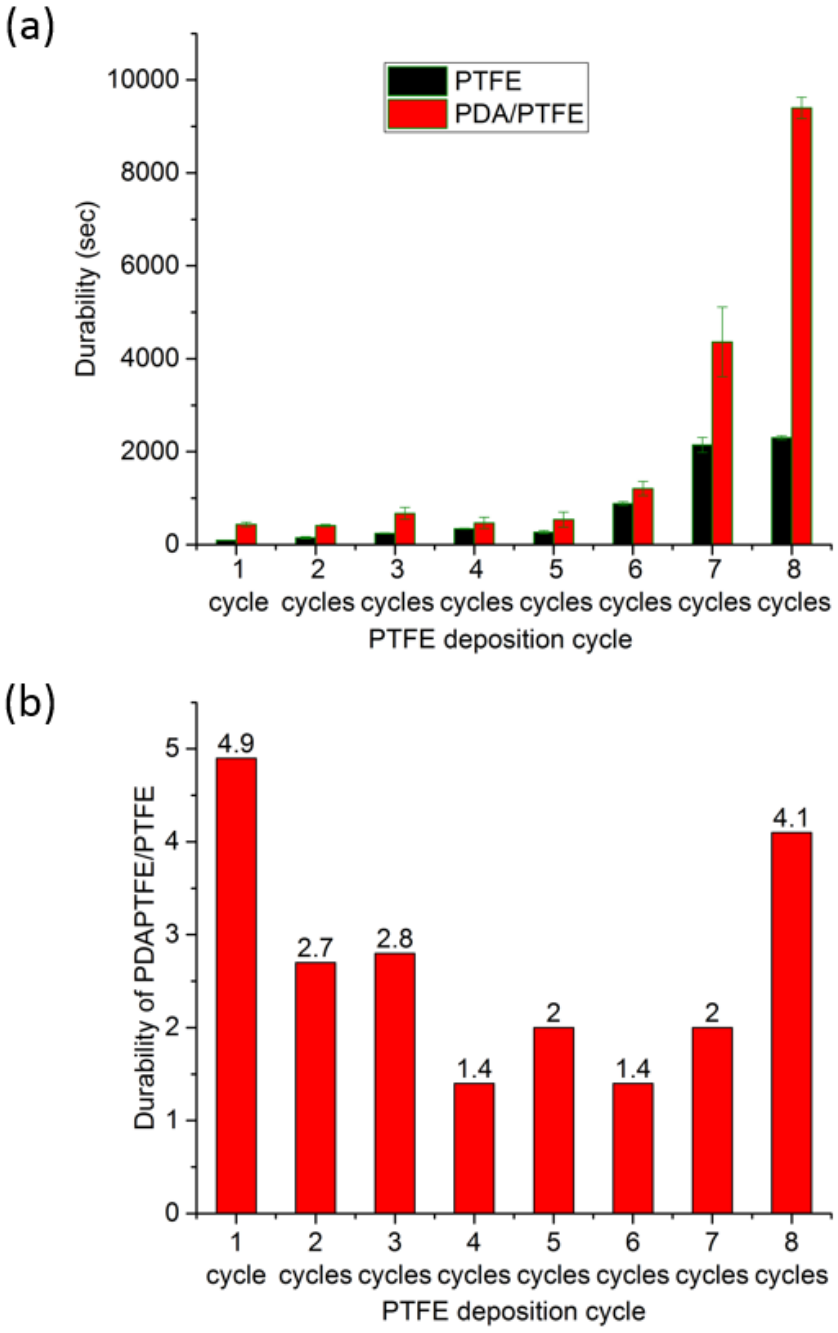

Fig. 2.8 Comparisons of (a) the durability of the PTFE and PDA/PTFE coatings and (b) the durability ratio of the PDA/PTFE and the PTFE coatings at different deposition cycles.

2.4.4 Durability

The durability comparison between the PTFE and PDA/PTFE coatings at different coating deposition cycles is given in Figure 2.8(a). It was observed that the PDA/PTFE coatings show higher durability than the PTFE coatings at all deposition cycles. The PDA/PTFE coating deposited at 8 cycles (42 μm) lasted 9,400 cycles before failure, whereas the PTFE coating at the same number of deposition cycles lasted only about 2,300 cycles. Figure 2.8(b) shows how the durability of the PDA/PTFE coatings compared to PTFE coatings at the same number of deposition cycles. The PDA/PTFE coatings performed 1.4 - 4.9 times better than the PTFE coatings, depending on the number of deposition cycles and the thickness of the coatings. Notably, the highest durability gain is at the thinnest and the thickest coatings, at 4.9 and 4.1 times, respectively. For the thinnest coating, the addition of the PDA underlayer helped to make the PDA/PTFE coating more durable because the PDA provides strong adhesion to both the PTFE and the substrate. For the thickest coating, the reason is different and will be analyzed later with the wear track data.

Interestingly, the PTFE film durability remained relatively constant for 1-5 (3-22 μm) deposition cycles. After 6 PTFE deposition cycles (27 μm), the durability showed clear improvement from 268 to 883 cycles. The PTFE coating durability increased sharply to 2,144 and 2,300 cycles, respectively, at 7 (31 μm) and 8 (36 μm) deposition cycles. Similar to the PTFE coating, the PDA/PTFE coating showed similar durability up to 5 (28 μm) PTFE deposition cycles. Starting at 6 PTFE deposition cycles (34 μm), the PDA/PTFE coating showed significantly enhanced durability. For the PDA/PTFE coating, the durability improvement is more pronounced at 7 (38 μm) and 8 (42 μm) deposition cycles, with improvements from 1,207 to 4,360 cycles and from 4,360 to 9,400 cycles, respectively. From Figure 2.8(a) and Table 2.1, it can be seen that only the coatings thicker than about 30 μm had a significant impact on the durability of the coatings.

This could be attributed to the rapid reduction in contact pressure when the thickness of the coating was increased over 30 μm.

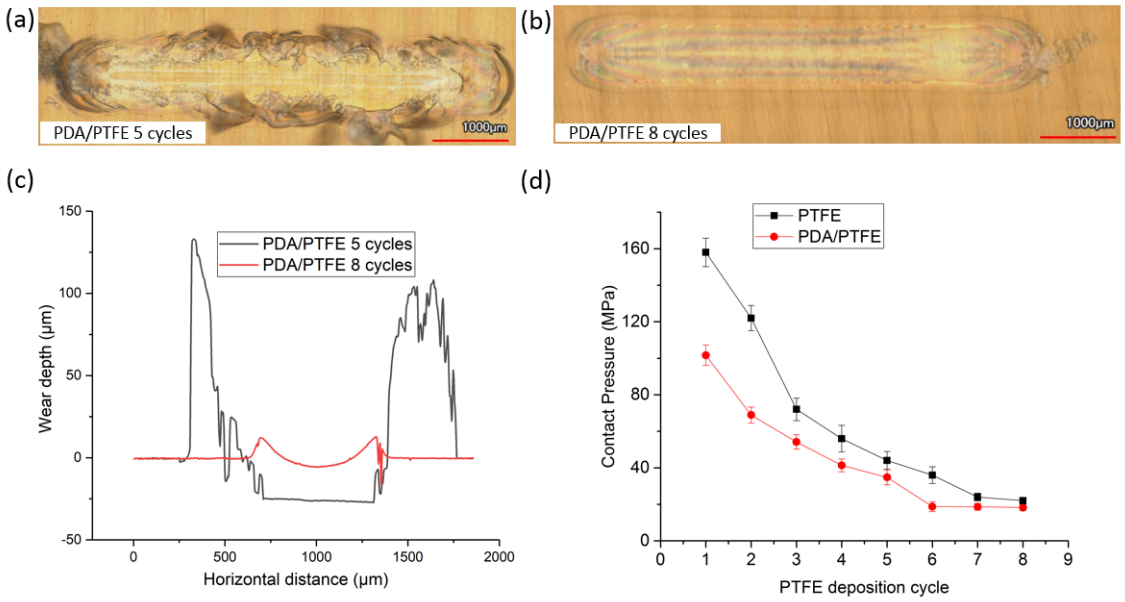

Fig. 2.9 Optical microscopy of the wear track of the PDA/PTFE coating deposited at (a) 5 and (b) 8 deposition cycles (27 μm and 42 μm thick) after tribological testing for 100 cycles, (c) wear profiles of the PDA/PTFE coating deposited at 5 and 8 deposition cycles after tribological testing for 100 cycles, and (c) the estimated contact pressure at the interface as a function of the coating deposition cycle.

Figure 2.9(a) and 2.9(b) show the wear tracks of the PDA/PTFE coatings deposited at 5 and 8 cycles, respectively (with thicknesses of 27 μm and 42 μm, respectively), after tribological testing under 10 N normal load for 100 cycles. It can be seen that the 27-μm PDA/PTFE coating was almost worn out from global delamination, which was evident by the large pileups at the two sides and two ends of the wear track (Figures 2.9(a) and (c)). However, the 42-μm PDA/PTFE coating did not experience this global delamination and still showed a smooth wear track that indicated a more gradual wear (Figures 2.9(b) and (c)).

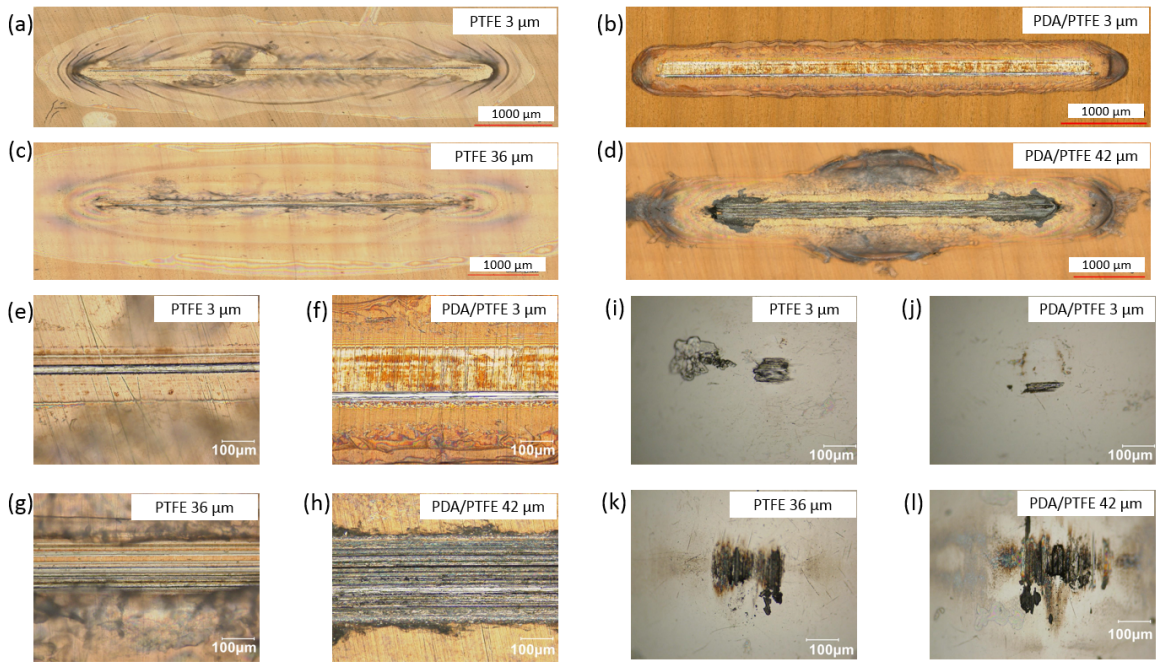

Fig. 2.10 Optical microscopy images of the wear tracks of the thin and thick PTFE and PDA/PTFE coatings corresponding to the test in Figure 5b: (a-d) Low magnification images of the full wear track, (e-h) higher magnification images of each wear track center, and (i-l) the optical microscopy images of the counterface surfaces after failure for the thin and thick PTFE and PDA/PTFE coatings.

Figure 2.9(d) shows the estimated average contact pressures calculated by dividing the applied normal load by the approximate contact area between the coating and the counterface ball, assuming the contact area is circular with a diameter that is the same as the wear track width after the 100-cycle tribological testing. The two ends of the wear track can be fitted perfectly with a circle, indicating the contact area was indeed circular. It was observed from figure 2.9(d) that the contact pressure decreased when the coating deposition cycle (or thickness) increased for both the PTFE and the PDA/PTFE coatings. The contact pressure of the PDA/PTFE coating deposited at 5 cycles (27 µm thick) was around 34.80 MPa, while the contact pressure of the PDA/PTFE coating deposited at 6 cycles (34 µm) showed a remarkable decrease down to 18.76 MPa. For thicknesses larger than 34 µm, the contact pressure remained more or less constant, between 18-19 MPa.

Similarly, for the PTFE coating, a rapid decrease in contact pressure was observed after the 7th (31 μm) and 8th (36 μm) cycle of the PTFE deposition. Therefore, the reduction in the average contact pressure due to the increased coating thickness was responsible for the higher durability of the thicker PDA/PTFE and PTFE coatings. However, because the PDA in the PDA/PTFE coatings can prevent global delamination, the coating life continued to increase after the 6th (34 μm) deposition cycle, while the PTFE coating life did not change after the 7th (31 μm) deposition cycle (Figure 2.8(a)).

Figure 2.10 shows the optical microscopy images of the wear tracks of the thin and thick PTFE and PDA/PTFE coatings (deposited at 1 and 8 cycles, respectively) tested at 10 N normal load, 10 mm/s speed, and 5 mm stroke length, and their counterface images after the tribological tests. The counterface images of the thin (3 μm) PTFE and PDA/PTFE coatings showed some wear debris and a small amount of transfer films (Figures 2.10(i) and (j)). However, the counterface images of the thick PTFE and PDA/PTFE coatings showed an enhanced and larger area film formation (Figures 2.10(k) and (l)). It was also observed from the wear track images that the thin PTFE and PDA/PTFE showed a failure caused by a line scratch (Figures 2.10(e) and (f)), whereas the thick coating showed a failure caused by many line scratches (Figures 2.10(g) and (h)). The enhanced transfer film helped to prevent the metal-on-metal interaction during the tribological testing of the thick PTFE and PDA/PTFE coatings, which prevented the coating failure at an early stage.

It was observed from the wear tracks that the deformation in PTFE coatings at all thicknesses occurred in a much larger area than the thin PDA/PTFE coatings of similar thicknesses (Figures 2.10(a)-(d)). The PTFE coatings also showed large area detachment from the substrate under the current testing condition.

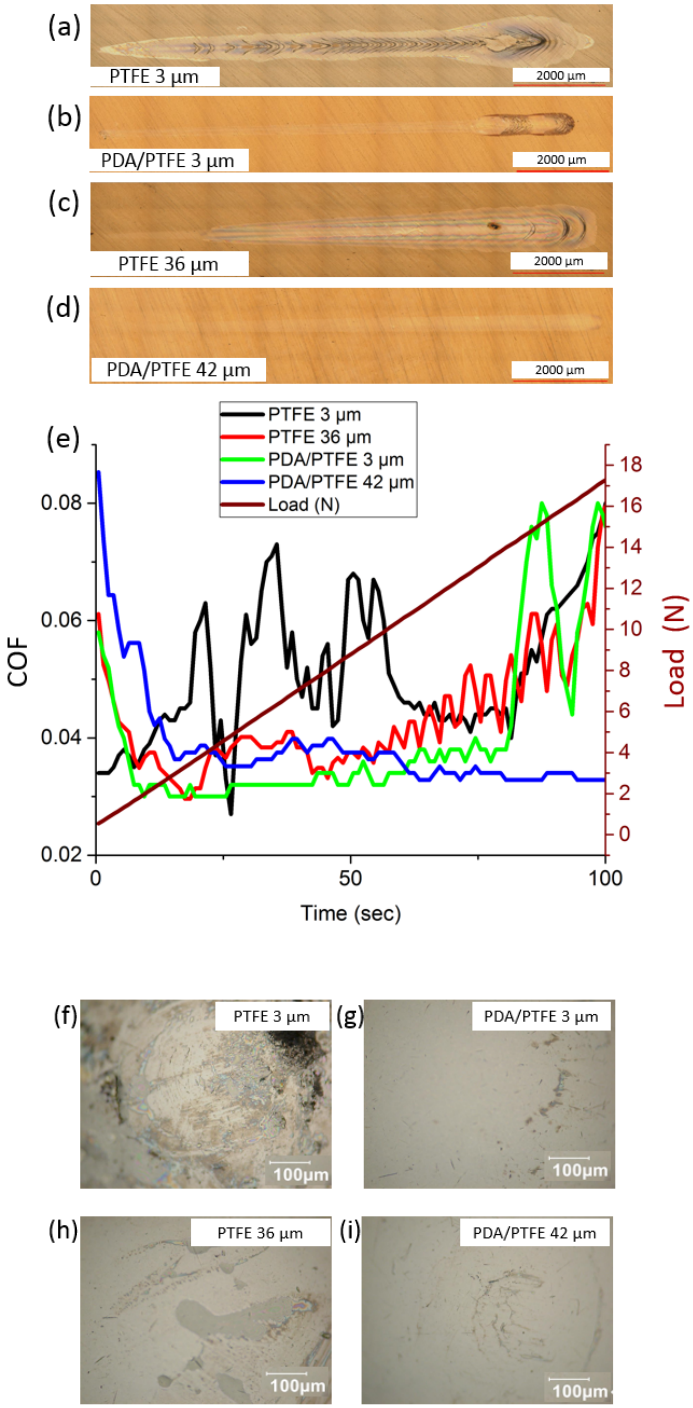

Fig. 2.11 Wear tracks after scratch test of (a-d) thin and thick PTFE and PDA/PTFE coatings, (e) COF profile of the scratch test for different coatings, and (f-i) the counterface images after the scratch tests.

It was hypothesized that the PDA underlayer improved the PDA/PTFE substrate adhesion and thus provided a higher load carrying capacity. Scratch tests were performed on thin and thick PTFE and PDA/PTFE coatings to confirm this hypothesis and further study the failure mechanisms of the PDA/PTFE thick coatings.

2.4.5 Scratch Tests

The wear tracks of the coatings generated by scratch tests with linearly increasing normal load and the counterface images are shown in Figure 2.11. It was observed from Figure 2.11(a) that the thin PTFE coating was deformed at the very beginning of the scratch test. Initial wrinkling (delamination) of the coating started when 3 N normal load was applied, whereas the PDA/PTFE thin coating didn't show any sign of delamination until the application of 14 N of normal load (Figure 2.11(b)). This can also be confirmed from the COF plot of the scratch test shown in Figure 2.11(e). A sharp increase was observed in the COF profile of the thin PTFE coating at around 3 N normal load. Whereas, tor thin PDA/PTFE coating, a peak in COF was observed at 14 N load. On the other hand, the thick PTFE showed some sign of delamination at about 4 N normal load (Figure 2.11(c)), while the thick PDA/PTFE coating didn't show any form of wrinkle caused by delamination, even at the highest normal load, and the wear track was very smooth with much less deformation (Figure 2.11(d)). The COF profile also showed consistently low values over the entire period of scratch tests (Figure 2.11(e)).

The images of the counterfaces after scratching are shown in Figure 2.11(f)-(i). The counterfaces of the PTFE coatings after the scratch test had a lot of transferred materials due to the coating delamination, whereas only a small amount of transferred materials on the counterfaces for the PDA/PTFE coatings. In summary, the scratch test results support the hypothesis that the

PDA underlayer gives the PDA/PTFE coating a better adhesion and load bearing capacity. The higher adhesive force between the PTFE topcoat and the PDA underlayer, which was strongly adhered to the SS substrate, made it harder for the PDA/PTFE coating to delaminate, deform, and tear.

2.5 Conclusions

The effects of PTFE thickness on the tribological properties of PTFE and PDA/PTFE coatings in dry contact condition were studied. For the PTFE coating, the roughness of the coating increased gradually with an increasing number of PTFE spin coating deposition cycles. On the other hand, the roughness of the PDA/PTFE coating remained similar after the 2nd (10 μm) PTFE deposition cycle. The PDA/PTFE coating had a much higher roughness than the PTFE coating in both thin and thick coatings. The COF and WCAs of the PDA/PTFE coatings were slightly higher than those of the PTFE coatings, which can be attributed to the higher roughness of the PDA/PTFE coatings. The addition of PDA helped to improve the durability of the PDA/PTFE coatings compared to the PTFE coatings in every thickness studied. The PTFE thickness did not have any significant effect on the durability of the PDA/PTFE coatings until the coating thickness reaches about 30 μm, over which the PDA/PTFE coating showed much enhanced durability. The 42 μm-thick PDA/PTFE coating was 105 times and 4 times more durable than the 3 μm- and 36 μm-thick PTFE coating, respectively. Also, the 42 μm-thick PDA/PTFE coating was 22 times more durable than the 27 μm-thick PDA/PTFE coating. The formation of transfer film on the counterface and better load carrying capacity of the thicker coating due to the larger contact area were responsible for the better tribological properties of thicker coatings. In addition, the addition of PDA helped

the PDA/PTFE coatings to adhere more strongly to the SS substrate than the PTFE coatings, which also contributed to the PDA/PTFE coatings' improved durability over the PTFE coatings.

2.6 Acknowledgement

This material is based upon work supported by the U.S. Department of Energy's Office of Energy Efficiency and Renewable Energy (EERE) under the Next Generation Electric Machines: Enabling Technologies Program Award Number DE-EE0007874. The views and opinions of authors expressed herein do not necessarily state or reflect those of the United States Government or any agency thereof.

References

1. Burris, D. L. and Sawyer, W. G. (2006), "A Low Friction and Ultra Low Wear Rate PEEK/PTFE Composite." Wear 261(3–4), pp 410–18.

2. Unal, H., Kadioglu, U., and Ekiz, H. (2006), "Improved Wear Resistance in Alumina-PTFE Nanocomposites with Irregular Shaped Nanoparticles." Wear 260(7–8), pp 915–18.

3. 3M, (2016), "Scotch-weld structural plastic adhesive," DP8005 technical data, Accessed 24 June 2019.

4. Dupont, (2013), "Dupont Teflon AF: adhesion information," K-26988, Accessed 24 June 2019.

5. Tannenbaum, H. (1999), "Non-stick coating system with PTFE–FEP for concentration gradient," US Patent No. 5230961 A.

6. Eustathios, V. (1977), "Fluoropolymer primer having improved scratch resistance," US Patent No. 4049863 A.

7. Miller, C., Choudhury, D., and Zou, M. (2019), "The Effects of Surface Roughness on the Durability of Polydopamine/PTFE Solid Lubricant Coatings on NiTiNOL 60," Tribology Transactions, 62(5), 919-929.

8. McElwain, S. E., Blanchet, T. A., Schadler, L. S., and Sawyer, W. G. (2008), "Effect of Particle Size on the Wear Resistance of Alumina-Filled PTFE Micro- and Nanocomposites." Tribology Transactions 51(3), pp 247–53.

9. Lee, J. and Lim, D. (2004), "Tribological Behavior of PTFE Film with Nanodiamond." Surface and Coatings Technology 188–189 (1–3 SPEC.ISS.), pp 534–38.

10. Cheng, X., Xue, Y., and Xie, C. (2002), "Friction and Wear of Rare-Earth Modified Glass-Fiber Filled PTFE Composites in Dry Reciprocating Sliding Motion with Impact Loads." Wear 253(7–8), pp 869–77.

11. Yeo, S. M. (2013), "Tribology of Polymeric Coatings for Aggressive Bearing Application," Doctoral Dissertation.

12. Unal, H., Kadioglu, U., and Ekiz, H. (2004), "Sliding Friction and Wear Behaviour of Polytetrafluoroethylene and Its Composites under Dry Conditions." Materials and Design 25(3), pp 239–45.

13. Lee, H. (2008), "Bio-adhesion of mussels and geckos: molecular mechanics, surface chemistry, and nano-adhesives," Doctoral dissertation.

14. Beckford, S. and Zou, M. (2014), “Wear-resistant PTFE thin film enabled by a polydopamine adhesive layer.” Applied surface science 292, pp 350-356.

15. Beckford, S., Cai, J., Fleming, D., and Zou, M. (2016), “The Effects of Graphite Filler on the Tribological Properties of Polydopamine/PTFE Coatings.” Tribology Letters (64-3), pp 41-50.

16. Beckford, S., Mathurin, L., Chen, J., and Zou, M. (2015), “The influence of Cu nanoparticles on the tribological properties of polydopamine/PTFE + Cu films." Tribology Letters (59-1): 1-9.

17. Beckford, S. (2014), “Wear resistant Polydopamine/PTFE nanoparticle composite coating for dry lubrication applications,” Doctoral Dissertation.

18. Doll, G., Evans, R., and Ribaudo, C. (2006), “Coated Rolling Element Bearing Cages”, US Patent No. 6994475 B2.

19. Woelki, P., Petit, D., and Harig, F. (1999), “Self-Lubricating Bearing”, US Patent No. 5971617 A.

20. Tevruz, T. (1998), “Tribological behaviours of Carbon Filled Polytetrafluoroethylene (PTFE) dry Journal Bearings,” Wear (221), pp 61-68.

21. Nunez, E. E., Yeo, S. M., Polychronopoulou, K., and Polycarpou, A. A. (2011), “Tribological study of high bearing blended polymer-based coatings for air-conditioning and refrigeration compressors,” Surface & Coatings Technology (205), pp 2994–3005.

22. Batzar, K. (1993), “Cookware Coating Systems,” US Patent No. 5250356 A.

23. Rossi, S., Chini, F., Straffelini, G., Bonora, P., Moschini, R., and Stampali, A. (2003), “Corrosion protection properties of electroless Nickel/PTFE, Phosphate/MoS2 and Bronze/PTFE coatings applied to improve the wear resistance of carbon steel”, Surface and Coatings Technology (173), pp 235–242.

24. Jiang, Y., Choudhury, D., Brownell, M., Nair, A., Goss, J. A., and Zou, M. (2019), “The effects of annealing conditions on the wear of PDA/PTFE coatings,” Applied surface science (481), pp 723-735.

25. Wenzel R. (1936), “Resistance of solid surfaces to wetting by water,” Industrial and Engineering Chemistry (28), pp 988-994.

Chapter 3

Improving the Tribological Performances of PDA+PTFE Nanocomposite Coatings by Hot Compaction

3.1 Abstract

The tribological performances of compacted and non-compacted polydopamine (PDA)+polytetrafluoroethylene (PTFE) nanocomposite coatings on stainless steel (SS) substrates were investigated. The compaction was accomplished using a combination of heat and pressure. The non-compacted PDA+PTFE coating had an average of 11 times longer durability compared to the pure PTFE coatings. The compaction increased the coating durability by 2.6 times while reducing the coefficient of friction (COF). Furthermore, the compaction helped to reduce the porosity of the PDA+PTFE coating by 63 times compared to non-compacted PDA+PTFE coating. The higher durability and lower COF of the compacted PDA+PTFE coating can be attributed to the reduced coating roughness and porosity, the enhanced adhesion strength to substrates, and the higher load-carrying capacity.

Keywords: PTFE, nanocomposite, hot compaction, durability, COF.

3.2 Introduction

Polytetrafluoroethylene (PTFE) is an engineering polymer that exhibits very low coefficients of friction (COF) and high thermal stability and chemical inertness (1). The self-lubricity of PTFE makes it a desirable material for coating applications where low COF is sought after (1). However, the use of PTFE coatings is hindered due to the low adhesion to metallic substrates, which results in low wear resistance (2-3). Polydopamine (PDA) is a bioinspired adhesive material currently being explored in many coating-related applications due to its ability

to adhere firmly to a variety of surfaces (4-5). A PDA underlayer has been successfully used to increase the adhesion between thin PTFE coatings to different substrates (6-14). Several types of nano/micro-particles have been added to the PTFE layer of thin PDA/PTFE coatings to improve the durability of the coatings (10-14). For example, adding 0.01 wt% of Cu nanoparticles (NPs) improved the durability of thin PDA/PTFE coating by two times (10). Adding 1.0 wt% of graphite particles also improved the durability of thin PDA/PTFE coating by five times (13). Recently, Ag NPs were also incorporated in the PDA underlayer and improved the durability of thin PDA/PTFE coating by 3.6 times (14). Adding a PDA underlayer also improved the durability of thick PTFE coatings on stainless steel (SS) substrate by four times in aggressive wear tests (15). Even though PDA as an underlayer has been studied extensively and shown to improve the durability of both thin and thick PTFE coatings, PDA as a constituent of thick PTFE composite coatings has not been reported.

Thick PTFE coatings are widely used in bearing, compressor, and cookware applications (16-20). For example, the reported thickness for thick coatings for bearing applications varies from five to a few hundred microns (16-20). A 20 - 30 μm thick PTFE coating can outperform the DLC based coating in the compressor of an air conditioner (19). The thickness of the PTFE coatings used in cookware is usually between 32.5 - 45 μm. The durability of the PDA/PTFE coating was found to increase more pronouncedly when the thickness of the coating is 30 μm or higher because of the reduction in contact pressure, better transfer film formation, and better load-carrying capacity (15). However, the PDA/PTFE coatings have needle-like structures after heat treatment (6-15). Although this needle-like structure improved the wear resistance of PDA/PTFE coatings compared to non-heat-treated coatings (8), the structure yielded considerable porosity in the

PDA/PTFE coatings, which is detrimental to coating wear life. We hypothesized that a hot compression could reduce the porosity and result in extended coating wear life.

Different compacting methods can be used to compact a polymer composite system. Cold compression (21), spark plasma compacting (22), roll compacting (23), and hot compression (24-29) have been used to achieve a compacted polymer composite system. Among them, hot compression is the most popular and widespread method to compact different nanocomposites. In hot compression, the composite system is heated to the melting point of the polymer matrix, and pressure is applied simultaneously to compact the composite (24-26). It is crucial to optimize the compacting time and pressure during hot compression to prevent the occurrence of creep and deformation (28). In this research, a hot hydraulic press was used to compact thick PDA+PTFE coatings. The tribological performance of the compacted coatings was compared with the non-compacted coatings.

3.3 Methodology

3.3.1 Sample Preparation

Mirror-finished SS samples with 38.10 mm in diameter and 0.76 mm in thickness were used as substrates. The average roughness, Ra, of a SS substrate, measured over an 80 μm x 80 μm scan area using a 3D laser scanning confocal microscope, was 28 ± 4 nm. The SS substrates were cleaned using deionized (DI) water for 10 min and then soaked in acetone for 10 min in an ultrasonic bath. After cleaning in acetone, the samples were further cleaned in isopropyl alcohol (IPA) for 10 min in an ultrasonic bath. Before beginning the coating deposition process, an actively polymerizing, proprietary mixture of dopamine hydrochloride and PTFE nanoparticle in aqueous dispersion was prepared. The PDA+PTFE nanocomposite coating was then spray coated on the

samples using an in-house designed and assembled spray coater. Once coated, the nanocomposite coatings underwent a heat treatment process that cures the coatings and annealed them. PDA+PTFE coated samples were first heated to 120°C for 5 min to evaporate water from the aqueous dispersion, then heated to 300°C for 5 min to drive off the wetting agents, and finally heated to 372°C for 5 min to anneal the PTFE particles onto the SS substrates. For comparison, a set of PTFE coatings on SS substrates of equivalent thickness was fabricated using the same procedure but using PTFE dispersion only. A pressure of 500 psi was applied for 5 min using a hot press to fabricate the compacted PDA+PTFE nanocomposite samples during the final step of annealing. After the last step of heating, all the PTFE, non-compacted PDA+PTFE, and compacted PDA+PTFE coating samples were cooled in the air.

3.3.2 Coating Characterization

The thicknesses of the coatings were measured using a stylus profilometer with a diamond tip of 12.5 μm-radius over a 12 mm-length at a speed of 400 μm/s. First, part of the coatings was removed from the SS substrates using a Copper bar. The thicknesses of the coatings were then obtained from the height differences between the exposed and coated areas and are reported in Table 1. The surface roughness of the coating, defined to be the arithmetic average of the absolute values of the surface height deviations from the mean of the evaluated surface area, was measured using a 3D laser scanning confocal microscope over 80 μm x 80 μm scan area. Six measurements were performed at randomly selected areas on each coating.

Scanning electron microscopy (SEM) was used to capture the surface morphology. The percentage of porous area was calculated using ImageJ (generic version). The threshold for these measurement was manually adjusted to cover all the porous spot.

Table 3.1 Coating thickness, surface roughness, porosity, and fibril diameter of different coatings.

Coating type	Coating Thickness (µm)	Average Surface Roughness (µm)	Coating Porosity (%)	Fibril Diameter (µm)
PTFE	42.30 ± 4.52	6.18 ± 4.28	22.60 ± 2.12	0.20 ± 0.08
Non-compacted PDA+PTFE	44.60 ± 3.85	4.96 ± 2.12	11.45 ± 1.45	0.26 ± 0.15
Compacted PDA+PTFE	43.10 ± 3.15	0.12 ± 0.04	0.18 ± 0.02	N/A

The water contact angles of the coating surfaces were measured using a water contact angle goniometer. A 3 µl water drop was used to measure the water contact angle between a surface and a water droplet. Six measurements were taken on each coating.

3.3.3 Tribological Study

To evaluate the tribological properties of the PTFE, non-compacted PDA+PTFE, and compacted PDA+PTFE coatings on the SS substrates, samples were tested using a universal mechanical tester (tribometer) with the normal and friction load sensor resolution of 1 mN. Tribological tests were performed using a linear reciprocating motion with an applied normal load of 10 N, a stroke length of 5 mm, and a sliding speed of 10 mm/s with a 0.1-second delay between each testing cycle. This provided an aggressive loading condition with a Hertzian contact pressure of more than 1 GPa (not considering the effect of coating) for expediting the coating failure. All wear tests were performed in a ball-on-disc configuration (Figure 3.1).

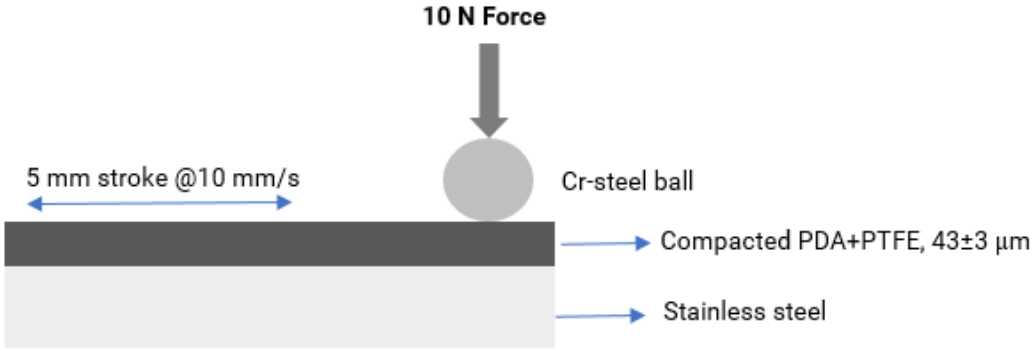

Fig. 3.1 The schematic of the compacted PDA+PTFE coating on SS substrate and the tribological test setup.

A chrome steel ball with a 6.35 mm diameter and 164 ± 8 nm average surface roughness was used as the counterface surface after thorough cleaning using acetone and IPA. The ball was first sonicated in acetone for 10 min, followed by sonicating in IPA for 10 min before being washed in DI water. The ball was then dried using nitrogen gas. The test was programmed to stop once the friction force surpassed 3.0 N, before which a sudden increase in COF was observed, indicating coating failure due to contact between the counterface and the substrate. Six sets of tests were performed on each coating to determine coating durability. The averages, along with the standard deviation, are reported in this article. Wear progression tests were also performed on the non-compacted and compacted PDA+PTFE coatings for 1000, 2000, 4000, and 8000 cycles using the same tribological test routine. Each test was performed independently at a different location on the same samples, varying the number of cycles. After each test, the wear track and counterface were evaluated.

To study the adhesion of PTFE, non-compacted PDA+PTFE, and compacted PDA+PTFE coatings to the SS substrate, scratch tests were performed by linearly varying the normal load from 0.5 to 18 N over a 100-s period at 0.1 mm/s speed over a scratch length of 10 mm. The same type of chrome steel balls as those used in the tribological tests were used as the counterface for the

scratch tests. The wear track and the chrome steel counterface used for tribological and scratch tests were evaluated using a 3D laser scanning confocal microscope.

3.4 Results and Discussion

3.4.1 Coating Thickness and Topography

The topography of spray-coated PTFE, non-compacted PDA+PTFE, and compacted PDA+PTFE coatings were studied, and the SEM and optical microscope images are shown in Figure 2. It can be seen in Figure 3.2(a) and (c) that both PTFE and non-compacted PDA+PTFE coatings have a porous needle-like structure. However, the PTFE coating has thinner and straighter fibrils than the non-compacted PDA+PTFE coating. In contrast, the compacted PDA+PTFE coating has a smooth and compacted topography (Figure 3.2(e)). The optical microscope image shows that PTFE and non-compacted PDA+PTFE coatings have a rough topography with a peak and valley structure (Figure 3.2(b) and (d)), while that of the compacted PDA+PTFE coating shows a smooth topography as a result of the hot compaction process (Figure 3.2(f)).

The average roughness, Ra, of the coatings is plotted in Figure 3.3 and is shown in Table 1, together with the coating thickness (42.30 – 44.60 μm). The PTFE coating has a Ra of 6.18 μm, whereas that of the non-compacted PDA+PTFE coating was 4.96 μm. The addition of PDA has reduced the porosity of the PDA coating. The Ra of the compacted PDA+PTFE coating was 0.12 μm, which is significantly lower than those of both the PTFE and the non-compacted PDA+PTFE coatings.

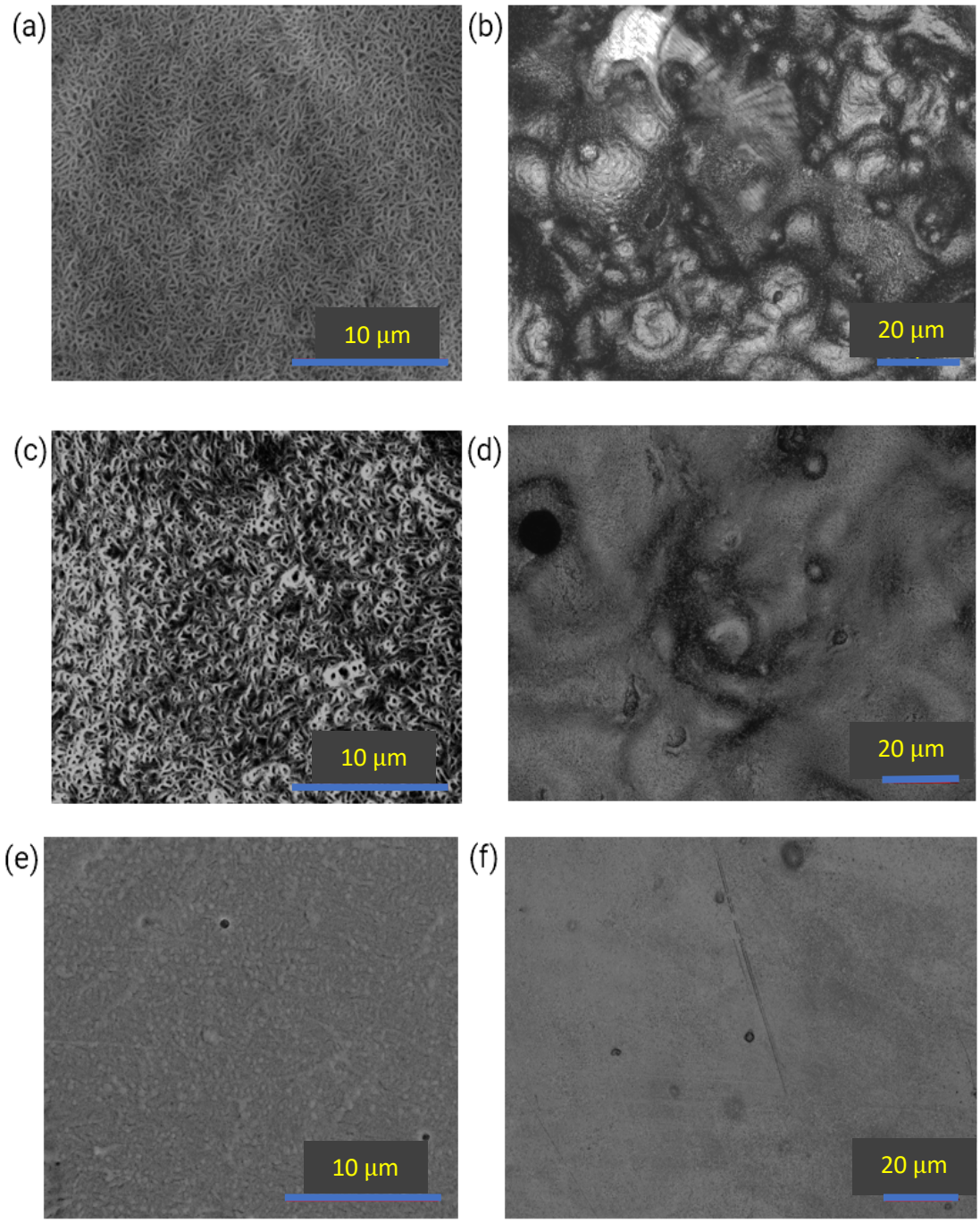

Fig. 3.2 SEM and optical topography images of the PTFE, non-compacted PDA+PTFE, and compacted PDA+PTFE coatings. (a) SEM image of the PTFE coating, (b) optical image of the PTFE coating, (c) SEM image of the non-compacted PDA+PTFE coating, (d) optical image of the non-compacted PDA+PTFE coating, (e) SEM image of the compacted PDA+PTFE coating, and (f) optical image of the compacted PDA+PTFE coating.

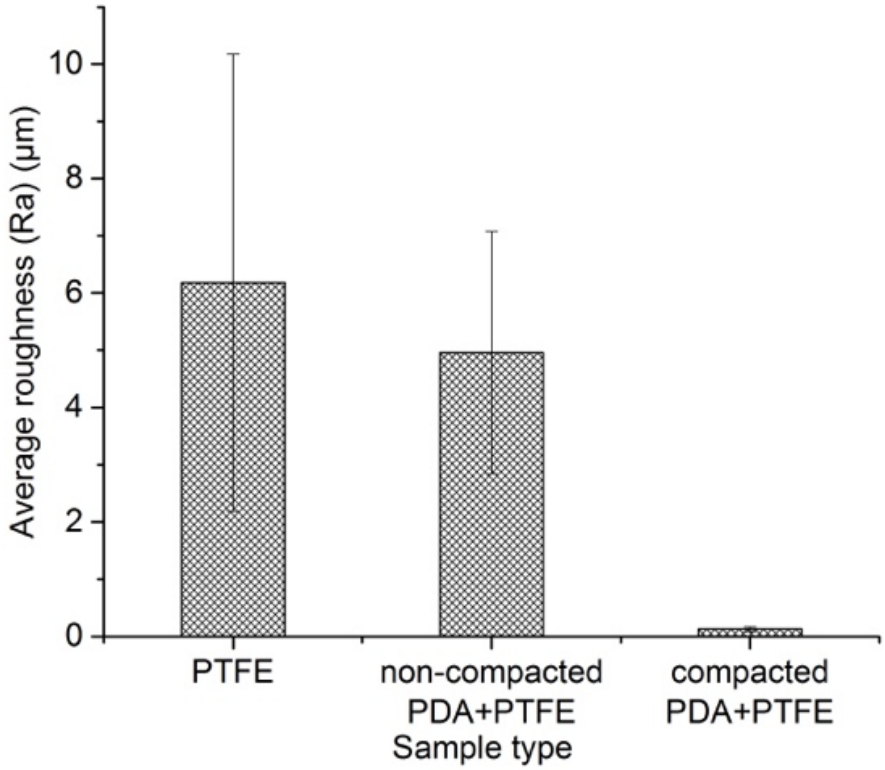

Fig. 3.3 The average roughness of the PTFE, non-compacted PDA+PTFE, and compacted PDA+PTFE coatings.

Figure 3.4 shows the porous area percentage maps of the PTFE, non-compacted PDA+PTFE and compacted PDA+PTFE coatings measured by ImageJ. The porous areas in each image are shown in red. It can be seen from Figure 3.4(a) and (b) that the PTFE coating surface is more porous than the non-compacted PDA+PTFE coating. The average of three measurements of the percentage porous area is 22.60% and 11.45% for the PTFE and non-compacted PDA+PTFE coating, respectively.

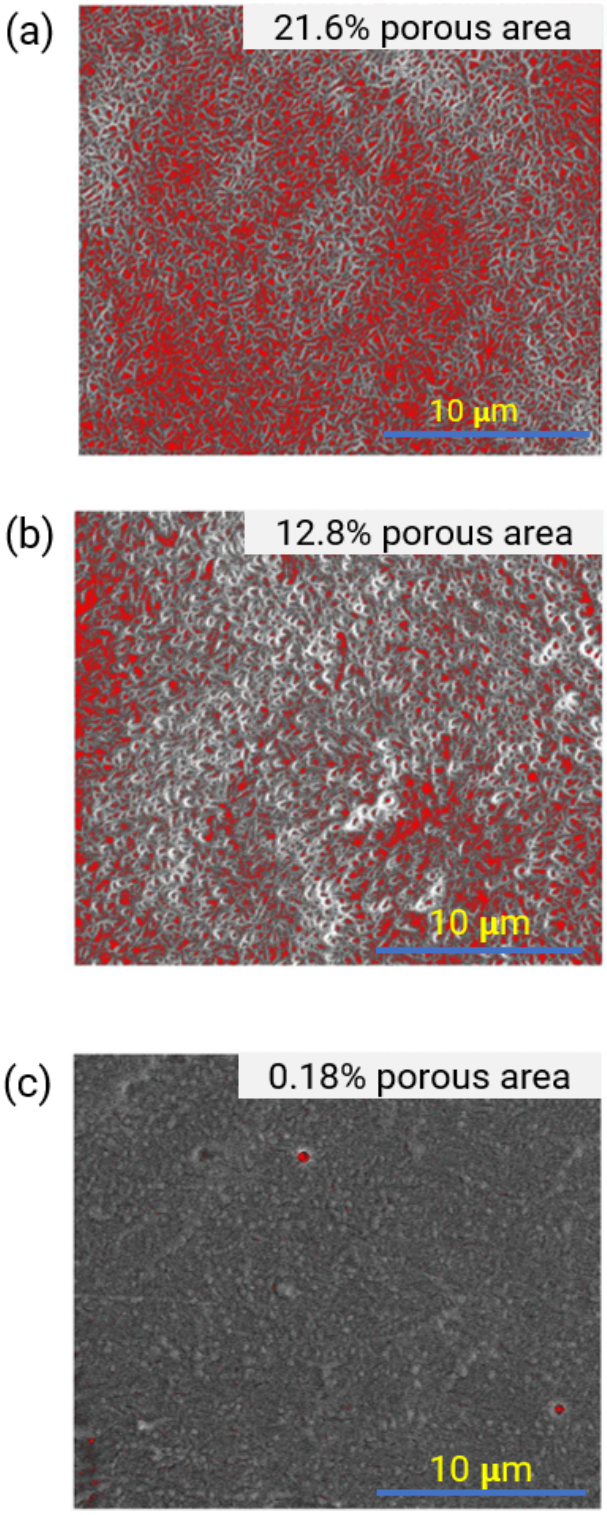

Fig. 3.4 Images of the porous area percentage of the PTFE, non-compacted PDA+PTFE, and compacted PDA+PTFE coatings, where the red areas indicate the porous areas and the remaining areas are PTFE fibrils. (a) PTFE, (b) non-compacted PDA+PTFE, and (c) compacted PDA+PTFE coatings.

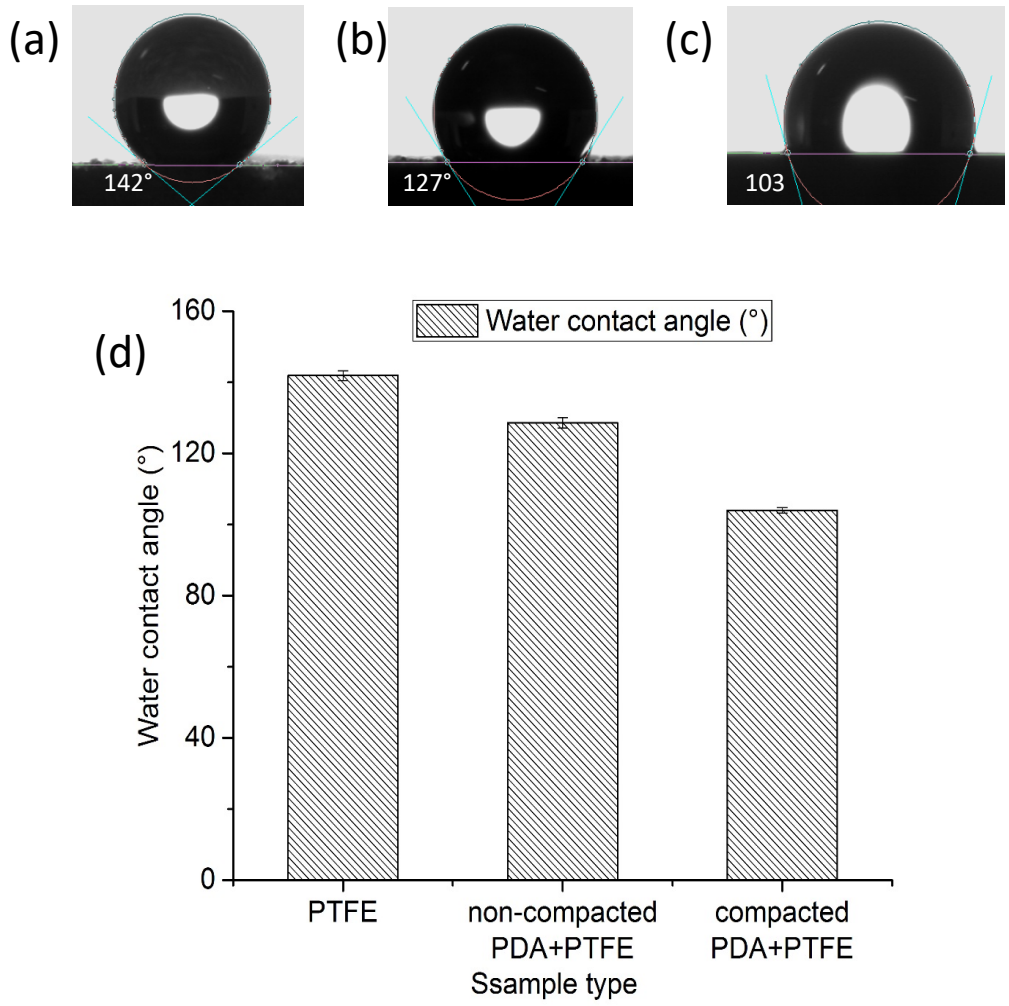

Fig. 3.5 Water droplet images and comparison of WCA among PTFE, non-compacted PDA+PTFE, and compacted PDA+PTFE coatings. (a) PTFE, (b) non-compacted PDA+PTFE, (c) compacted PDA/PTFE, and (d) the comparison of WCAs of the PTFE, non-compacted PDA+PTFE, and compacted PDA+PTFE coatings.

Interestingly, the compacted PDA+PTFE coating shows only a couple of porous spots on the surface with the percentage porous area of only 0.18%, which is significantly lower than the PTFE and non-compacted PDA+PTFE coatings (Figure 3.4(c)). From figures 3.2-4, it can be concluded that the hot compaction can help attain a smoother coating with less surface porosity.

3.4.2 Water Contact Angle

Representative water droplet images on the coatings and the measured WCAs are shown in Figure 3.5. The PTFE coating has hydrophobic behavior with an average WCA of 141º. The addition of PDA reduced the average WCA of the non-compacted PDA+PTFE coating to 128º. The hydrophilic nature of the PDA was responsible for the reduction of the WCA. The compacted PDA+PTFE coating showed an average WCA of 104º, which is significantly lower than the WCA of non-compacted PDA+PTFE and PTFE coatings. The lower WCA of the compacted PDA+PTFE coating can be attributed to the smoother coating topography and lower roughness of the coating.

3.4.3 Tribological Properties

The coating COF changes with testing cycles are shown in Figure 3.6. A transition from a low initial COF to a higher COF was observed on all samples, as shown in Figure 3.6(b). This was due to the easy plowing of loose particles at the beginning of the test. As testing cycles increased, the COF increased due to the coating was compacted from repeated rubbing, resulting in higher interfacial shear strength between the counterface and the coating. The initial COF of non-compacted PDA+PTFE coating was 0.04, which is lower than that of COF of the PTFE coating of 0.06 (Figure 3.6(b)), and this can be attributed to the lower surface roughness of the PDA+PTFE coatings compared to that of the PTFE coating. The sudden increase in the COF of the compacted coating at around 7,000 cycles was due to the coating has worn to the interface between the coating and substrate with higher interfacial shear strength. Six repeating tests were performed on three different samples of each coating. The average COF of the coatings were measured from the entire duration of the testing before a sharp increase in the COF was observed. The average COF and coating durability, along with the corresponding standard deviations, are plotted in Figure 3.7.

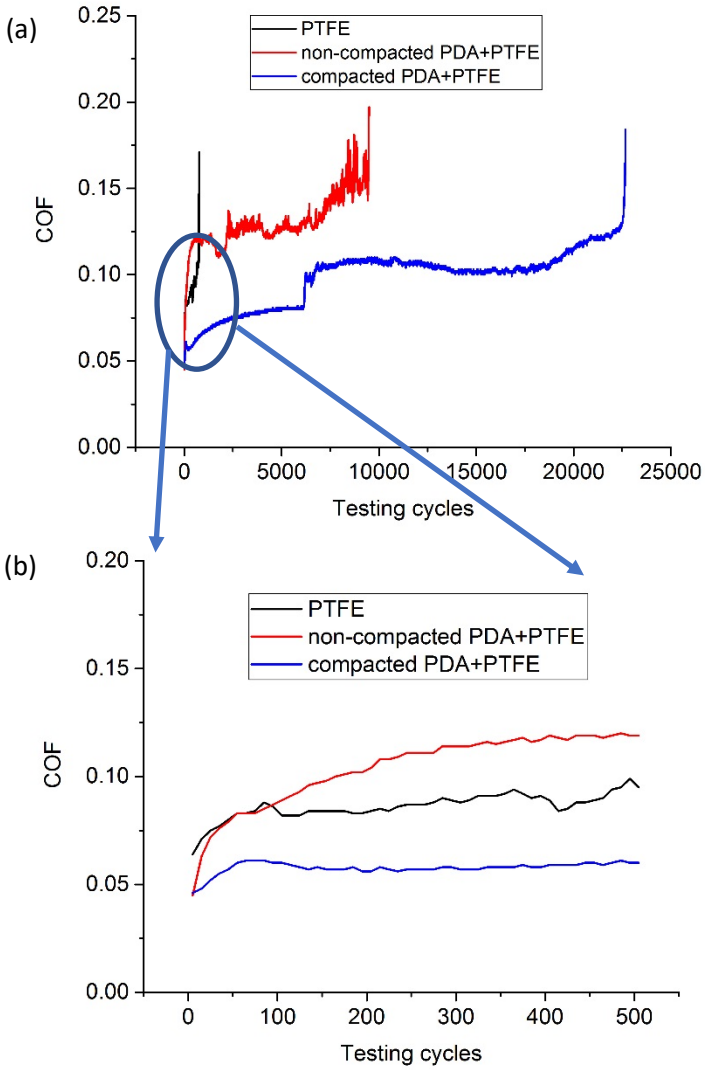

Fig. 3.6 COF profiles of the PTFE, non-compacted PDA+PTFE, and compacted PDA+PTFE coatings tested in dry conditions. (a) The COF profiles for the entire duration of the durability testing and (b) The COF profiles of the initial 500 sec of the testing shown in (a).

It can be seen that the PTFE coating had an average COF of 0.093, while the non-compacted PDA+PTFE coating had a higher COF of 0.128 due to the addition of the adhesive PDA. However, the compacted PDA+PTFE coating had an average COF of only 0.099, which is 22% less than the COF of the non-compacted PDA+PTFE coating. Compaction helped to reduce

the surface porosity and roughness of the PDA+PTFE significantly, which ensured a smoother contact between the counterface and coating. The smoother topography of the coating helped to reduce the COF of the compacted PDA+PTFE coating to a similar level to that of the PTFE coating.

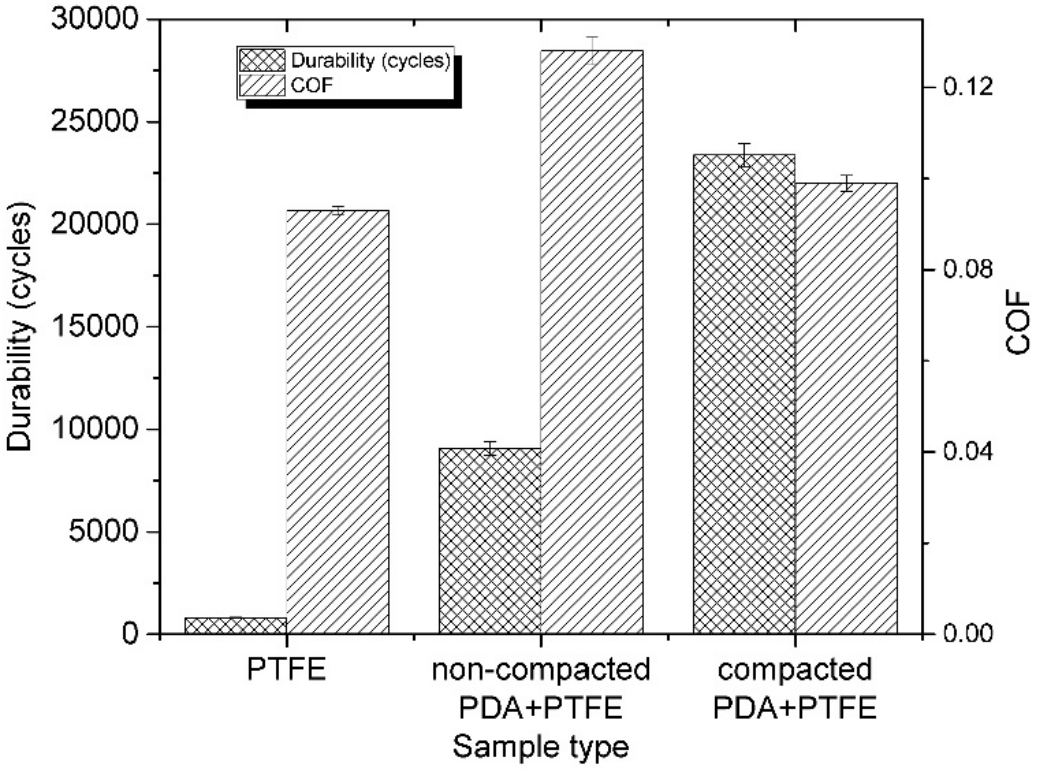

Fig. 3.7 Comparison of the average durability and COF of the PTFE, non-compacted PDA+PTFE, and compacted PDA+PTFE coatings in dry conditions.

The average durability for the PTFE coating was 795 cycles, and for the non-compacted PDA+PTFE coating was 9,050 cycles, which was 11 times higher. The improvement is much more significant than using PDA as an underlayer for the PTFE coating (PDA/PTFE), which was 4.1 times (15). It indicates that the nanocomposite PDA+PTFE not only enhanced the adhesion strength of the coating to the SS substrate but also increased the cohesive strength between PTFE

fibrils. Furthermore, the compacted PDA+PTFE coating showed durability of 23,380 cycles, which is 2.60 and 29.40 times that of the non-compacted coating and PTFE coatings, respectively.

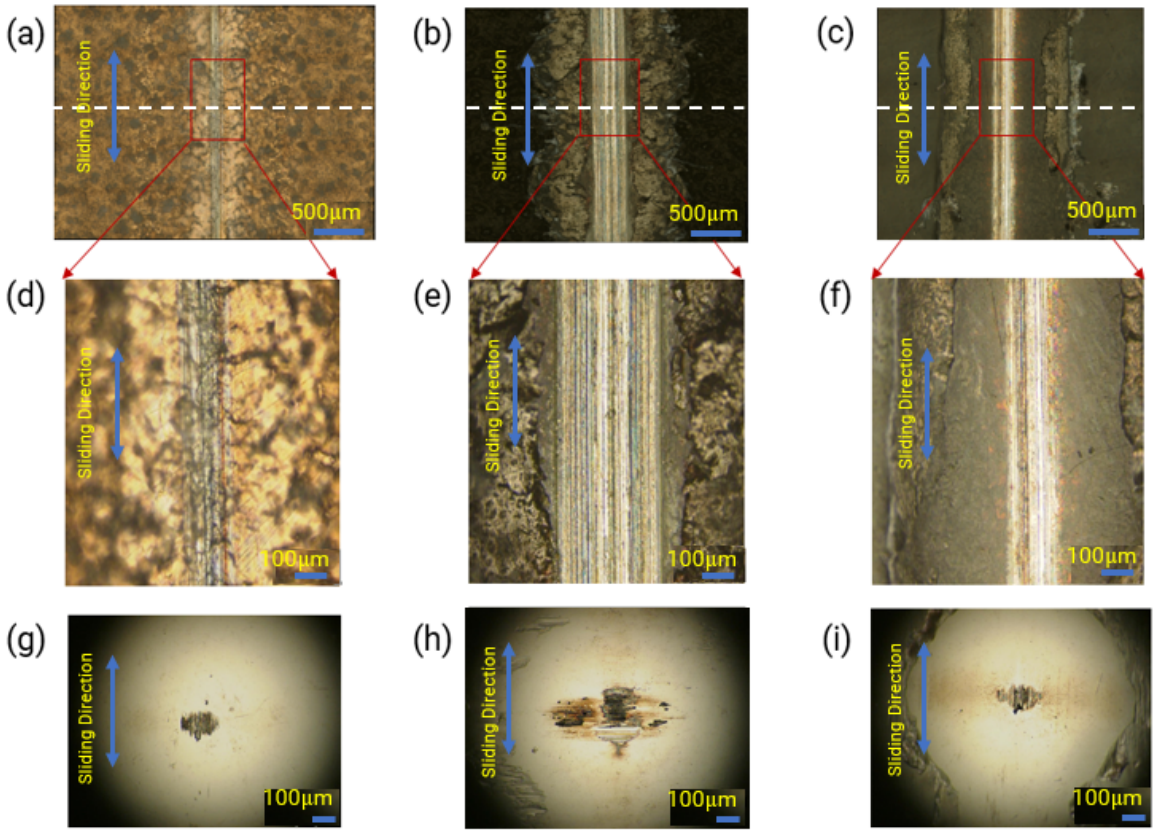

Fig. 3.8 Optical microscope images of the coating wear tracks and the counterfaces after tribological testing. (a) and (d) low and high magnification images of the wear track of PTFE, (b) and (e) low and high magnification images of the wear track of non-compacted PDA+PTFE, (c) and (f) low and high magnification images of the wear track of compacted PDA+PTFE, and (g-i) counterface images of the PTFE, non-compacted PDA+PTFE, and compacted PDA+PTFE coatings, respectively.

Figure 3.8 shows the optical microscope images of the coating wear tracks and the counterfaces after tribological testing. It can be seen in Figure 3.8(a) and 3.8(d) that the PTFE coating showed a line failure where a narrow band of the substrate was exposed. The counterface image showed a small amount of transfer films (Figure 3.8(g)). In contrast, many exposed lines were observed from the wear track of the non-compacted PDA+PTFE coating (Figure 3.8(b) and

(e)). The counter surface image showed more transfer films (Figure 3.8(h)), which could have prevented direct metal-metal contact and prolonged coating life. The compacted PDA+PTFE coating showed multiple exposed SS lines on the wear track, similar to the non-compacted PDA+PTFE coating, but the wear track was much narrower (Figure 3.8(c) and (f)). The amount of the transferred film on the counterface was also smaller (Figure 3.8(i)).

Although the amount of dark transfer films from the PTFE and compacted PDA+PTFE coatings appear to be similar, there is a thin layer of transfer film of PDA+PTFE coating covering a larger area outside the dark area. Furthermore, the coating durability not only depends on the amount of transfer film, but also depends on the bonding strength of the transfer film to the counterface, as well as the coating surface roughness, cohesion, and adhesion to the substrate. PTFE coating was delaminated in the early stage of testing due to its more porous structure, while the compacted PDA+PTFE coating showed a very low wear rate in the early stage of testing. The wear debris of PTFE coating is loosely attached to the counterface due to low adhesion, whereas the PDA in the wear debris of the compacted PDA+PTFE coating adhered the transfer film better to the counterface due to the adhesive nature of PDA.

The wear track cross-sectional profiles of the coatings obtained from the dashed white line shown in Figure 3.8(a) - (c) are plotted in Figure 3.99 to understand the coating failure mechanisms. Interestingly, the wear track of the PTFE coating showed two sets of protrusions above the coating surface. The first set of protrusions are immediately adjacent to the recessed part of the wear track, which is the pile-up wear debris.

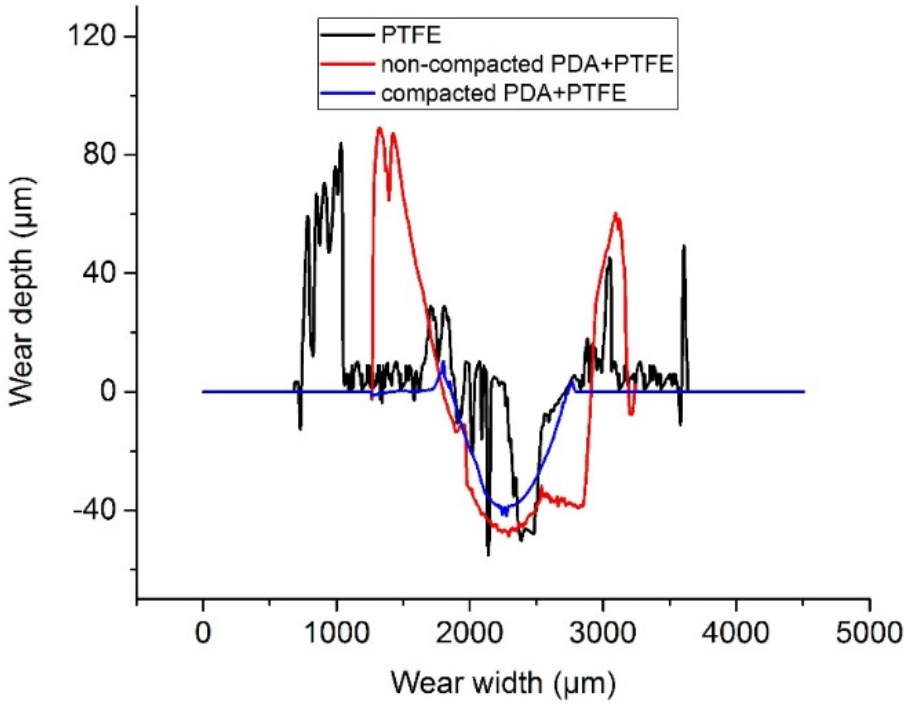

Fig. 3.9 Wear track cross-sectional profiles of the PTFE, non-compacted PDA+PTFE, and compacted DA+PTFE coatings.

The second set of protrusions are much farther from the recessed part of the wear track and one of them is almost double the coating thickness. The volume of the protrusions is larger than the worn material could form. This indicates that the coating had a global delamination. Similarly, the non-compacted PDA+PTFE coating also suffered from global delamination, as indicated by the pile-up height that is twice the coating thickness. However, the wear track profile of the PTFE coating showed the coating was damaged at the center of the wear track but delaminated further way from the center than the non-compacted PDA+PTFE coating, indicating a weaker coating adhesion to the substrate. In comparison, the compacted PDA+PTFE coating failed over a smaller area with only a small amount of piled up of wear debris on either side of the wear track without global delamination. It was hypothesized that the reduction in the surface porosity and the

compacted smooth topography helped to resist global delamination, which in turn improved the durability of the compacted PDA+PTFE coating.

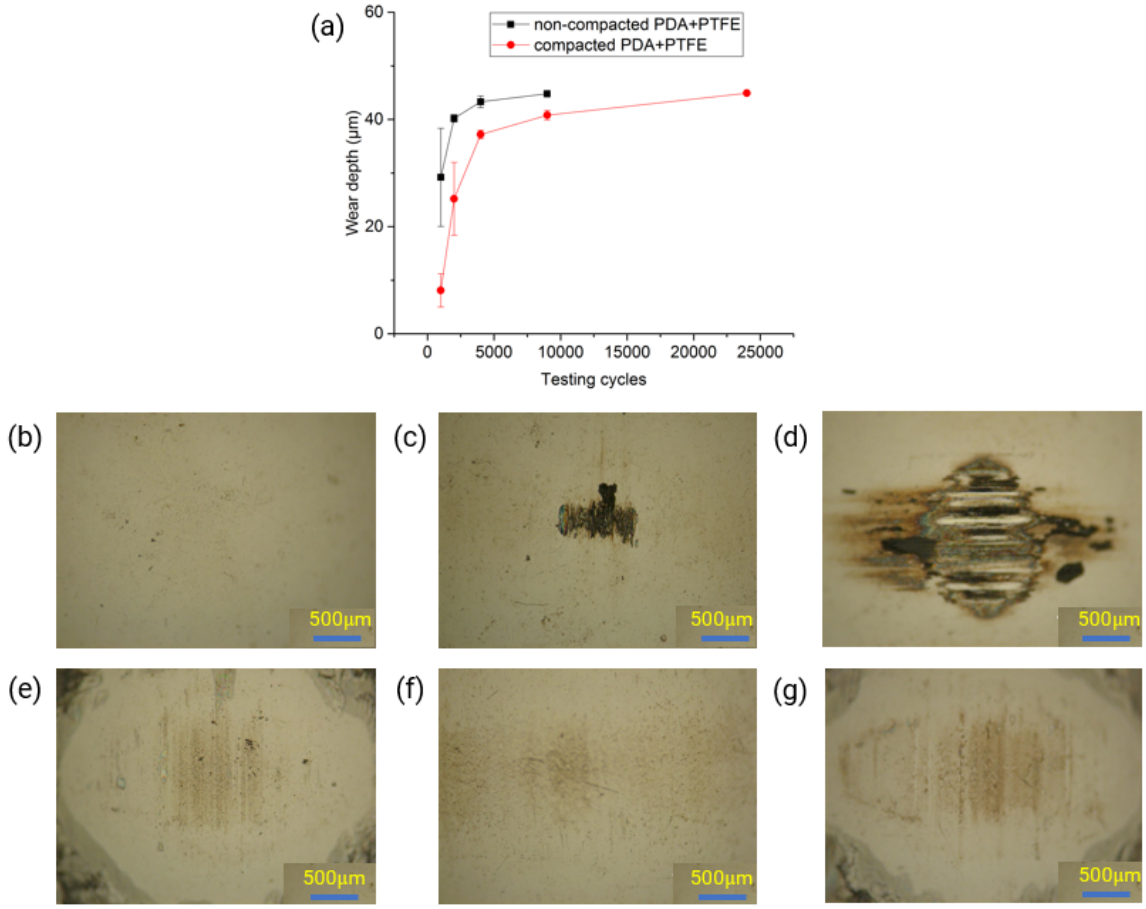

Fig. 3.10 Comparison of the wear depth and counterface images of the non-compacted PTFE and compacted PDA+PTFE coatings after 1,000, 2,000, and 4,000 cycles of testing. (a) comparison of wear depth, (b-d) counterface images after testing for 1,000, 2,000, and 4,000 cycles of testing on non-compacted PDA+PTFE, and (e-g) counterface images after testing for 1,000, 2,000, and 4,000 cycles of testing on compacted PDA+PTFE coatings.

Wear progression tests for 1,000, 2,000, 4,000, and 8,000 cycles on non-compacted, and compacted PDA+PTFE coatings were performed using the same testing routine as the durability study. The wear depth comparison was studied and reported in Figure 3.10(a). It can be seen that the average wear depths of the non-compacted PDA+PTFE coating after 1,000, 2,000, and 4,000

cycles of testing was 29.2, 40.6, and 43.3 μm, respectively; whereas, the wear depths of the compacted PDA+PTFE coating were much smaller in comparison at 8.1, 25.2, and 37.2 μm, respectively. The non-compacted PDA+PTFE coating worn out over 4,000 cycles of the testing because the wear depth was higher than the coating thickness, whereas the compacted PDA+PTFE coating did not fully wear out even after 8,000 cycles. The coatings were much more durable after worn to the coating-substrate interface. The smoother surface topography and the reduction in the surface porosity of the compacted coating were responsible for the lower wear rate.

The counterface images of the wear progression tests are shown in Figure 3.10(b-g). For the non-compacted PDA+PTFE coating (Figure 3.10(b-d)), there is no wear debris deposited on the counterface after 1,000 cycles of testing. After 2,000 cycles, wear debris started to deposit on the counterface. After 4,000 cycles of testing, an enhanced amount of wear debris was deposited on the counterface. It can be concluded that from Figure 3.10 (a-d) that the wear debris on the counterface acts as transfer films which prevent counterface and substrate interaction between 2000 and 4000 cycles and slowed down the coating wear. However, the coating would eventually fail due to global delamination, as shown in Figures 3.6(a) and 3.9. In the case of compacted PDA+PTFE coating, although there was minimum wear debris deposited on the counterface even after 4,000 cycles of testing, a thin layer of transfer film developed on the counterface after 1000 cycles and was also present at 2000 and 4000 cycles, which helped to prolong the coating durability. Furthermore, as shown in Figure 3.9, hot compaction helped to prevent the global delamination of the PDA+PTFE coating, which in turn improved the durability of the compacted PDA+PTFE coating compared to non-compacted PDA+PTFE coating.

3.4.4 Scratch Tests and Wear Resistance

Scratch tests were performed to further investigate the adhesion properties of these coatings. The wear tracks of the coatings generated by scratch tests under linearly increasing normal load and the COF profile are shown in Figure 3.11.

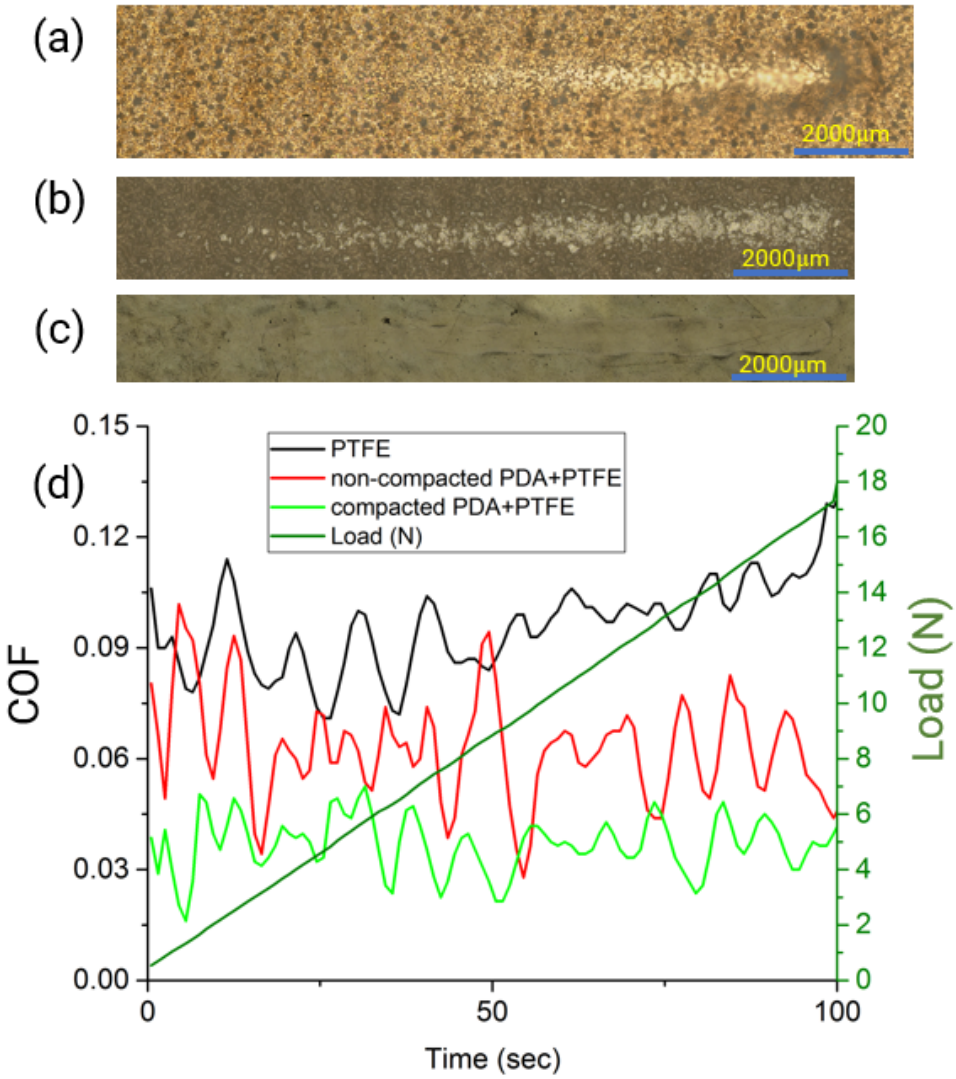

Fig. 3.11 Wear tracks, COF, and normal load profiles of the PTFE, non-compacted PDA+PTFE, and compacted PDA+PTFE coatings after the scratch test. (a) wear track of the PTFE coating, (b) wear track of the non-compacted PDA+PTFE coating, (c) wear track of the compacted PDA+PTFE coating, and (d) COF and normal load profiles of the PTFE, non-compacted PDA+PTFE, and compacted PDA+PTFE coatings after the scratch test.

It was observed in Figure 3.11(a) that the PTFE coating was deformed at 8 N normal load, which is evident from the reduced variation at this load in the COF profile in Figure 3.11(d). It can be seen in Figure 3.11(d) that the PTFE coating showed higher COF than the non-compacted PDA+PTFE and compacted PDA+PTFE coating in scratched tests due to its higher roughness. It was also observed that the PTFE coating showed detachment from the substrate at the end of the scratch tests corresponding to an increase in the COF. It can be seen in Figure 3.11(b) that the non-compacted PDA+PTFE coating was locally deformed early in the scratch tests, and the deformation increased with the normal load but Figure 3.11(d) shows that the variation of COF decreased with normal load due to reduced peak-to-valley distance as a result of coating deformation. Interestingly, no coating delamination from the substrate was observed (Figure 3.11(b)). It can be concluded from the scratch tests that the addition of PDA improved the adhesion of the coating to the substrate. The better adhesion of the coating to the substrate was responsible for the higher durability of the non-compacted PDA+PTFE coating compared to the PTFE coating.

The wear track of the compacted PDA+PTFE coating after the scratch test is shown in Figure 3.11(c). It was observed that the compacted PDA+PTFE coating showed a very smooth wear track without any sign of local and aggressive deformation at the end of the scratch tests. The COF is lower and smoother than that of the non-compacted PDA+PTFE coating. Similar to the non-compacted PDA+PTFE coating, no delamination from the substrate was observed during the scratch test. Therefore, the higher durability and lower COF of the compacted PDA+PTFE coating compared to the non-compacted PDA+PTFE coating can be attributed to the smoother surface, lower porosity, and better load-carrying capacity of the compacted PDA+PTFE coating.

3.5 Conclusions

The effects of adding PDA to PTFE and hot compaction on the tribological properties of PTFE coatings in dry conditions were studied. The thickness of the spray-coated compacted PDA+PTFE coatings was 43±3 μm. Even though all three coatings showed hydrophobic behavior, the addition of PDA lowered the hydrophobicity of the non-compacted PDA+PTFE coating compared to the PTFE coating, and hot compaction further lowered the hydrophobicity of the compacted PDA+PTFE coating. The addition of PDA improved the durability of the non-compacted PDA+PTFE coating 11 times compared to the PTFE coating. The PTFE and the non-compacted PDA+PTFE coating both showed detachment from the substrate during wear tests, whereas the compacted PDA+PTFE coating did not show any form of detachment from the substrate. The non-compacted PDA+PTFE coating was much more durable in the coating-substrate interface due to the better adhesion of the coating to SS substrate, enhanced transfer film formation, and better load-carrying capacity of the coating compared to the PTFE coating. Hot compaction helps to reduce the porosity and the roughness of the PDA+PTFE coating by 63- and 41 times, respectively. Compacted PDA+PTFE coating showed a COF of 0.099, which is 22% lower than the COF of the non-compacted PDA+PTFE coating. The lower COF of the compacted PDA+PTFE coating is due to the lower roughness of the coating. The compacted PDA+PTFE coating showed 2.60- and 29.40-times higher durability than non-compacted PDA+PTFE and PTFE coatings, respectively. In addition to better adhesion to the SS substrate and better load-carrying capacity, reduction of porosity and roughness due to the hot-compaction prevented the local and global deformation of the compacted PDA+PTFE coating during wear tests, which in turn improved the durability of the coating.

3.6 Acknowledgement

This material is based upon work supported by the U.S. Department of Energy's Office of Energy Efficiency and Renewable Energy (EERE) under the Next Generation Electric Machines: Enabling Technologies Program Award Number DE-EE0007874 and by the National Science Foundation (NSF) under Grant Nos. CMMI-1563227 and OIA-1457888. The views and opinions of authors expressed herein do not necessarily state or reflect those of the United States Government or any agency thereof.

References

1. Dhanumalayan, E., and Joshi, G. M. (2018), "Performance Properties and Applications of Polytetrafluoroethylene (PTFE)—a Review." Advanced Composites and Hybrid Materials (1), pp 247–268.

2. Eustathios V. (1977), "Fluoropolymer primer having improved scratch resistance." US Patent No. 4049863 A.

3. Lee, J., and Lim, D. (2004), "Tribological Behavior of PTFE Film with Nanodiamond." Surface & Coatings Technology (188), pp 534-538.

4. Lee, H., Dellatore, S.M., Miller, W.M., and Messersmith, P.B. (2007), "Mussel-Inspired Surface Chemistry for Multifunctional Coatings." Science (318), pp 426-430.

5. Lee, H., Lee, Y., Statz, A.R., Rho, J., Park, T.G., and Messersmith, P.B. (2008), "Substrate-Independent Layer-by-Layer Assembly by using Mussel-Adhesive-Inspired Polymers." Advanced Materials (20), pp 1619-1623.

6. Beckford, S., and Zou, M. (2014), "Wear Resistant PTFE Thin Film Enabled by a Polydopamine Adhesive Layer." Applied Surface Science (292), pp 350-356.

7. Zhao, Y. and Zou, M. (2019), "Experimental Investigation of the Wear Mechanisms of Thin PDA/PTFE Coatings." Progress in Organic Coatings (137), pp 105341.

8. Jiang, Y., Choudhury, D., Brownell, M., Nair, A., Goss, J. A., and Zou, M. (2019), "The effects of annealing conditions on the wear of PDA/PTFE coatings," Applied surface science (481), pp 723-735.

9. Miller, C., Choudhury, D., and Zou, M. (2019), "The Effects of Surface Roughness on the Durability of Polydopamine/PTFE Solid Lubricant Coatings on NiTiNOL 60," Tribology Transactions, 62(5), pp 919-929.

10. Beckford, S., Mathurin, L., Chen, J., and Zou, M. (2015), "The Influence of Cu Nanoparticles on the Tribological Properties of Polydopamine/PTFE + Cu Films." Tribology Letters (59).

11. Beckford, S., Mathurin, L., Chen, J., Fleming, R., and Zou, M. (2016), "The Effects of Polydopamine Coated Cu Nanoparticles on the Tribological Properties of Polydopamine/PTFE Coatings." *Tribology International* (103), pp 87-94.

12. Beckford, S., Cai, J., Chen, J., and Zou, M. (2014), "Use of Au Nanoparticle-Filled PTFE Films to Produce Low-Friction and Low-Wear Surface Coatings." Tribology Letters (56), pp 223-230.

13. Beckford, S., Cai, J., Fleming, R., and Zou, M. (2016), "The Effects of Graphite Filler on the Tribological Properties of Polydopamine/PTFE Coatings." TRIBOLOGY LETTERS (64), pp 1-10.

14. Choudhury, D., Niyonshuti, I., Chen, J., Goss, J., and Zou, M. (2020), "Tribological Performance of Polydopamine + Ag Nanoparticles/PTFE Thin films." *Tribology International* (144), pp 106097.

15. Ghosh, S.K., Miller, C., Choudhury, D., Goss, J.A., and Zou, M. (2020) The Effects of PTFE Thickness on the Tribological Behavior of Thick PDA/PTFE Coatings." Tribology Transactions. DOI: 10.1080/10402004.2020.1728001.

16. Doll, G., Evans, R., and Ribaudo, C. (2006), "Coated Rolling Element Bearing Cages", US Patent No. 6994475 B2.

17. Woelki, P., Petit, D., and Harig, F. (1999), "Self-Lubricating Bearing", US Patent No. 5971617 A.

18. Tevruz, T. (1998), "Tribological behaviours of Carbon Filled Polytetrafluoroethylene (PTFE) dry Journal Bearings," Wear (221), pp 61-68.

19. Demas, N.G., and Polycarpou A.A. (2008), "Tribological performance of PTFE-based coatings for air-conditioning compressors," Surface & Coatings Technology (203), pp 307-316.

20. Batzar, K. (1993), "Cookware Coating Systems," US Patent No. 5250356 A.

21. Reilly J. (1989), "Cold compaction of polyetheretherketone and nickel powders blends." Polymer Engineering and Science 29 (20), pp 1446-1455

22. Li, J., Wang, L., and Jiang, W. (2010), "Super hydrophobic surface of bulk carbon nanotubes compacted by spark plasma sintering followed by modification with polytetrafluoroethylene." Carbon 48(9), pp 2644-2673.

23. Knopp, W.V. (1981), "Roll compacting of polymer powders into fully dense products." US Patent, US 4436682.

24. Hine, P. J., and Ward, I. M. (2006), "Hot compaction of woven nylon 6,6 multifilaments." Journal of Applied Polymer Science 101(2), pp 991-997.

25. Dashevsky, A., Kolter, K., & Bodmeier, R. (2004), "Compression of pellets coated with various aqueous polymer dispersions." International Journal of Pharmaceutics, 279(1-2), pp 19.

26. Zhang, C., Ma, C., and Wang, P. (2005), “Temperature dependence of electrical resistivity for carbon black filled ultra-high molecular weight polyethylene composites prepared by hot compaction.” Carbon (43), pp 2544-2553.

27. Hine, P. J., and Ward, I. M. (1997), “The hot compaction of spectra gel-spun polyethylene fibre.” Journal of Material science (32), pp 4821-4831.

28. Howard, E. G. (1993), “PTFE with improved creep resistance, and preparation thereof.”, US patent, US005420191A.

29. Ghosh S.K. (2016), “On the development of novel multifunctional max reinforced polymers (MRPS) matrix composites.” *Theses and Dissertations, University of North Dakota, Grand Forks, ND.*

Chapter 4

Tribological Properties of PDA+PTFE Coating in Oil-lubricated Condition

4.1 Abstract

In this study, the tribological properties of 45 ± 2 μm-thick polytetrafluoroethylene (PTFE) and polydopamine (PDA)+PTFE coatings in oil-lubricated conditions were investigated under a normal load of 10 N and a linear reciprocating speed of 0.1m/s. Both the PTFE and the PDA+PTFE coatings were deposited using an in-house spray-coating method. The PDA+PTFE coating was five times more durable compared to the PTFE coating in oil-lubricated conditions. Both PTFE and PDA+PTFE coatings showed lower COF in oil-lubricated conditions than in dry conditions. The nanomechanical properties measured by PeakForce Quantitative Nanomechanical (PFQNM) characterization method showed an increase in Young's modulus and adhesion force for the PDA+PTFE coatings compared to the PTFE coatings. Chemical analysis showed that the cross-linking between PDA and PTFE polymer chains occurred during the high-temperature sintering procedure. The higher adhesion of PDA+PTFE coating to the cast iron substrate and the stronger cohesion due to the cross-linking between PDA and PTFE contributed to the higher durability of the PDA+PTFE composite coatings.

Keywords: Durability, Coefficient of friction, Polydopamine, PDA+PTFE, Oil-lubricated condition.

4.2 Introduction

Polytetrafluoroethylene (PTFE) is a popular engineering polymer that shows high thermal and chemical stability [1]. It has a wide range of applications, especially in coatings where non-stick surface properties are desired. PTFE has also been used in different tribological applications

due to its inherently low coefficient of friction (COF), solid lubricity, and chemical inertness [1-3]. However, PTFE coatings have low adhesion to metallic surfaces because of its non-stick properties [4,5], which leads to a high wear rate under shear and frictional loads. Much work has been carried out over the years to increase the wear resistance of PTFE and the adhesion of PTFE coatings to metallic substrate surfaces [4-10]. Using a primer coat composed of an acrylic-based polymer and roughening the surface by sandpaper are the most popular ways to increase adhesion between PTFE and a substrate surface. Inspired by Lee et al. [11-12], S. Beckford et al. [8] used an ultrathin polydopamine (PDA) underlayer to enhance the adhesion between thin PTFE coatings and a stainless steel (SS) substrate, and hence improved the durability of PTFE coatings dramatically in dry sliding contact conditions without the need of modifying the substrate surface. Various micro/nanoparticles (NPs) were also added to further improve the durability of the PTFE coatings [13-17]. Beckford et al. [14] found that the addition of 0.01 wt% of PDA coated Cu NPs can double the durability of the PDA/PTFE thin coating. Similar to Beckford et al.'s study [14], Choudhury et al. [15] found that the addition of 2.0 wt% of Ag NPs in the PDA underlayer improved the durability of the PDA/PTFE coating by 3.6 times. Recently, Miller et al. [18] used PDA to enhance the durability of the PDA/PTFE coating on a Nitinol 60 substrate. However, PDA, as a constituent of the PTFE composite coating has not been studied yet.

Thick PTFE coatings have a wide range of applications, especially in cookware [19], different bearing materials [20-22], and air-conditioner's compressors [23]. The thickness of the coating for bearing applications varies from 5 - 100 μm, whereas the thickness of PTFE coatings for cookware varies from 32.5 - 45 μm [19-22] and the thickness of the PTFE coatings for compressors application varies from 20 - 30 μm [23]. Demas et al. [23] found that a 20 - 30 μm PTFE-based coatings on cast iron substrate can tribologically outperform DLC based coating in

the compressors of air-conditioners. Even though the initial wear in the PTFE coating was higher in compressors application, but the wear debris acted as a third body lubricant, which reduced the COF and further wear [23]. Although the bulk PTFE composite showed better tribological properties in the oil-lubricated condition than in the dry condition [24-32], the tribological behavior of the PTFE coatings in the oil-lubricated condition is still not well understood. The tribological properties of PTFE coatings in oil-lubricated condition are not comparable to bulk PTFE due to the presence of the substrate-coating interface and limited wear volume in the coatings. The low COF of the PTFE coatings in oil-lubricated conditions makes it a suitable material to replace the soft-metal based Babbitt in journal bearings applications where low COF is required for smooth operations. Along with bearing applications, the uses of PTFE coatings in cookware make them very interesting to understand the wear mechanism of PTFE coatings in oil-lubricated conditions.

Nanomechanical properties, such as Young's modulus, hardness, and adhesion, play essential roles in determining the tribological behavior of polymer nanocomposite coatings. These nanomechanical properties of the PDA+PTFE nanocomposite coating can be correlated to their tribological properties, which will be useful to design a polymeric coating in the future for various applications. The reported value of Young's modulus and hardness of the thin PTFE (500-1300 nm) coatings measured by nanoindentation is 1.25 - 2.1 GPa and 45 - 65 MPa, respectively [13,18]. However, Young's modulus and hardness in thick PDA/PTFE (42 μm) coatings, measured by nanoindentation, are 0.72-0.80 GPa and 66.1 – 73.2 MPa, respectively [33]. Moreover, no work was carried out to measure the adhesion between the PTFE top surface and a nanoindentation tip to understand the effect of the filler materials on the adhesion properties of the PTFE composite coating.

In this study, the tribological properties of the thick PTFE and PDA+PTFE coatings in oil-lubricated conditions were studied. The nanomechanical property mappings of these coatings were performed by an atomic force microscope (AFM) using PeakForce Quantitative Nanoscale Mechanical (PFQNM) characterization method. A correlation between the nanomechanical properties and tribological properties of the PTFE and PDA+PTFE coatings was established.

4.3 Experimental Methods

4.3.1 Sample Preparation

The substrates used for this study were 6 mm-thick disks with 40 mm diameter, which were cut from cast iron rods (McMaster-Carr, USA). The substrate was machined to an average surface roughness of 2.54 ± 0.16 μm. For cleaning, the substrates were first sonicated in acetone for 20 min to remove any oil, sand, and organic contaminants. The substrates were then sonicated in isopropyl alcohol for 10 min and dried under nitrogen gas before beginning the spray coating deposition process with a mixture of a proprietary, actively polymerizing aqueous solution of PDA+PTFE composite coating, prepared before the coating deposition. The composite PDA+PTFE coating was deposited via an in-house designed and assembled spray coater apparatus. This method allows for the facile deposition of thick (approximately 45 μm) coatings at fast speeds (under 5 minutes). Once coated, samples underwent a heat treatment process that sinters the coatings. To sinter the coatings to the substrate, the samples were first heated to 120°C for 5 minutes to evaporate water, then 300°C for 5 minutes to remove wetting agents, and finally, heated to 372°C for 5 minutes to sinter the PTFE particles onto the substrate. A set of samples with PTFE coatings were also fabricated using a spray coater apparatus and went through the 3-step heating process. Both the PTFE and the PDA+PTFE coatings were compacted during the final stage of

annealing by using a hot press. Figures 4.1(a) and (b) show the photographs of the PTFE and PDA+PTFE coated samples, respectively.

To study PDA surface chemistry, the PDA coating was fabricated on a mirror-finished stainless-steel (SS) substrate using a rocking shaker method [33]. The SS substrates were submerged in a container contained 700 mL of aqueous solution and placed on a rocking shaker at 60 ºC and 25 Hz rocking frequency. The aqueous solution contained 0.0848 g of Trizma base (Sigma Aldrich, USA) and 1.4 g of dopamine hydrochloride (Sigma Aldrich, USA), and the pH of the solution was kept at ~ 8.5 for 45 minutes for the PDA deposition. After 45 minutes, the SS samples were removed from the rocking shaker and washed in DI water. The SS samples were finally dried in nitrogen gas.

4.3.2 Coating Characterization

The thicknesses of the coatings were measured using a stylus profilometer (Dektak 150, Bruker, USA) with a 12.5 μm-radius diamond tip over a 12,000 μm length at a speed of 400 μm/second. A blade was used to scratch a part of PTFE and PDA+PTFE coatings to expose the cast iron substrate. Figure 4.1(c) shows the thickness profiles of the PTFE and PDA+PTFE coatings. Coating thickness was then measured as the height difference between the cast iron substrate surface and the top of the coating measured by the profilometer. An AFM (Dimension Icon, Bruker, USA) was used to evaluate the sample surface topography and roughness. A silicon tip on nitride cantilever (ScanAssyst air, Bruker, USA) with a spring constant of 0.4 N/m and tip radius of 2-12 nm was used to perform the AFM surface topography measurement. Focused ion beam scanning electron microscopy (FIB-SEM) (XL-30, Phillips/FEI, Hillsboro, OR, USA) was performed to study the cross-section of the PDA+PTFE coating. The water contact angle (WCA)

was measured using a water contact angle goniometer (OCA15, DataPhysics instrument GmbH, Germany). A 2 µl-water droplet was used to measure the coating water contact angle. X-ray Photoelectron Spectroscopy (XPS; PHI 5000 VersaProbe, ULVAC-PHI, Kanagawa, Japan) was used to determine the chemical composition and bonding structure of the PTFE, PDA, and PDA+PTFE coating. Each XPS measurement was performed for a 2-hour duration.

4.3.3 Tribological Testing

The tribological tests were performed in boundary oil-lubricated conditions in a ball-on-disc configuration using a universal mechanical tester (UMT-2, Bruker, USA) under a linear reciprocating motion. The tests were performed under 10 N normal load, 10 mm/s speed, and 5 mm stroke lengths with a chrome-steel counterface ball. For these tests, Mobil DTE-32, the oil commonly used in industry for different roller and journal bearing applications [34], was used as the lubricant. Mobil DTE-32 shows high chemical and thermal stability and high resistance to sludging [34]. A 10 N normal load was used to generate a high contact pressure to accelerate the coating failure in the benchtop test. Figure 4.1(d) shows the schematic of the tribological test setup. The failure criterion for these tests is set to when a frictional force (F_x) reached 3 N, which signifies by a sharp increase in the coefficient of friction when the chrome-steel and cast-iron interact directly. The average and standard deviation of the coating durability and COF from six tests each on PTFE and PDA+PTFE coatings were reported. For studying the coating adhesion, scratch tests were performed by linearly varying the load from 0.5 to 5 N over a 100-s period at 0.1 mm/s speed. A diamond-coated counterface with a tip diameter of 400 µm and a full-cone angle of 120º was used for the scratch tests. The normal load and the corresponding COF for different coatings were reported from the scratch tests. The wear tracks after the tribological tests and the chrome steel

counterface used for the tribological tests were evaluated using a 3D laser scanning confocal microscope (VK X260K, Keyence Corporation, USA).

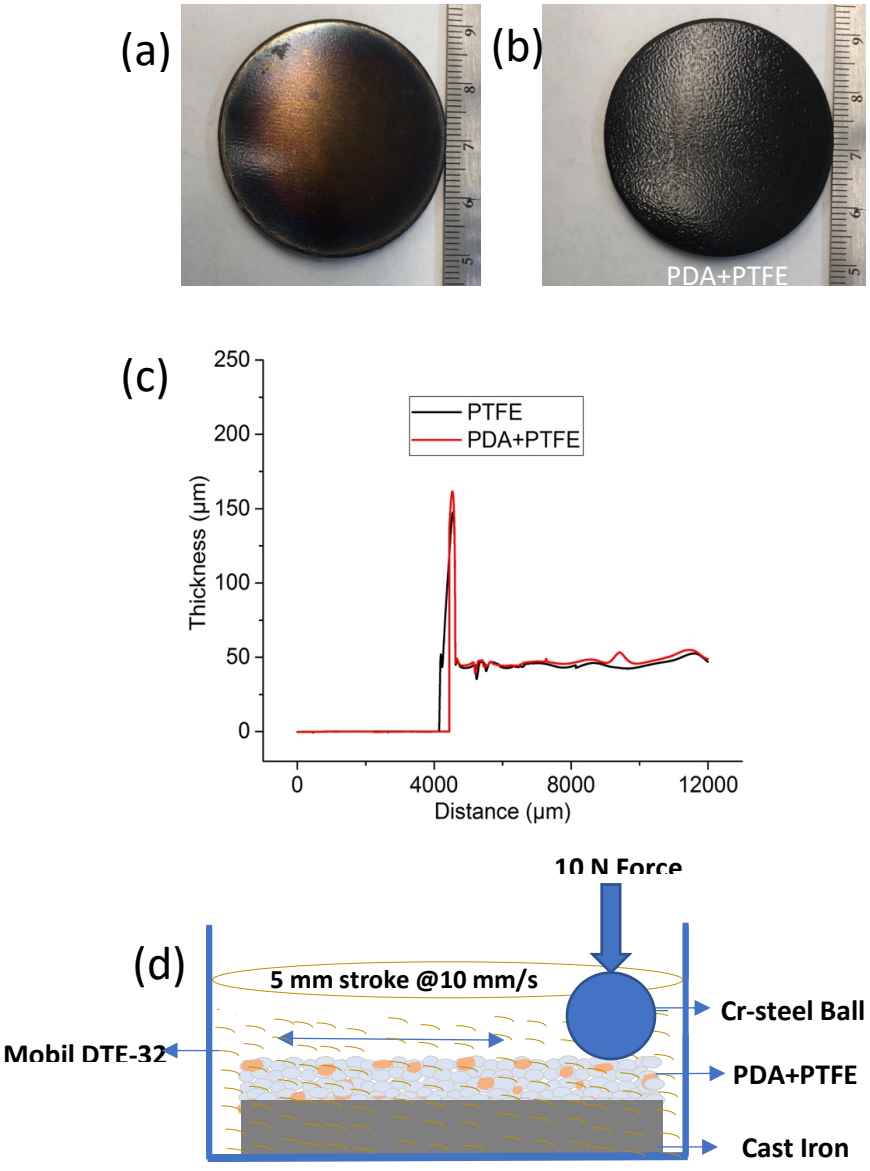

Fig. 4.1 Sample photographs, coating thickness profiles and schematic of the tribological test setup of the PTFE and PDA+PTFE coatings. (a) Photo of PTFE coating sample, (b) Photo of PDA+PTFE coating sample, (c) thickness profiles of the PTFE and PDA+PTFE coatings, and (d) schematic of the tribological tests setup.

4.3.4 Nanomechanical Property Characterization

The PFQNM was performed by using an AFM (Dimension Icon, Bruker, USA) to measure the nanomechanical properties (Young's modulus and adhesion) of PTFE and PDA+PTFE coatings. PFQNM is a technique where a single imaging technique that can measure the surface topography and nanomechanical properties, such as Young's modulus, deformation, and adhesion. A special AFM probe, RTESPA-300-30 with a 32 nm probe radius, a half-angle of 20º, and a spring constant of 45.67 N/m was used to perform the nanomechanical mapping on the coating surfaces. The AFM probe can measure the elastic modulus in the range of 0.5 to 20 GPa. The PFQNM methods generate maps for the nanomechanical properties in scanned areas. Both the nanomechanical property maps and the average values of 5 different measurements were reported in this study.

The hardness of the PTFE and PDA+PTFE coatings were measured using a nanoindenter (TI-900, Hysitron, USA). The indents were made using a spheroconical diamond probe with a 1-μm tip radius and a 60° cone angle. The indentation load was 50 μN and the loading and unloading rates were 10 μN/s with a 5-second holding time. Each coating was indented five times, and the average and standard deviation values of hardness were determined.

4.4 Results and Discussion

4.4.1 Coating Topography

Figure 4.2 shows the AFM images of the PTFE and PDA+PTFE coatings at two different scan sizes. It can be seen from the AFM images that both the PTFE and the PDA+PTFE coatings have a compacted topography. Press marks on the surfaces of both the PTFE and the PDA+PTFE

coatings, resulting from the countersurface during compaction, can be observed. There was no porous area on the surface of both the PTFE and the PDA+PTFE coatings.

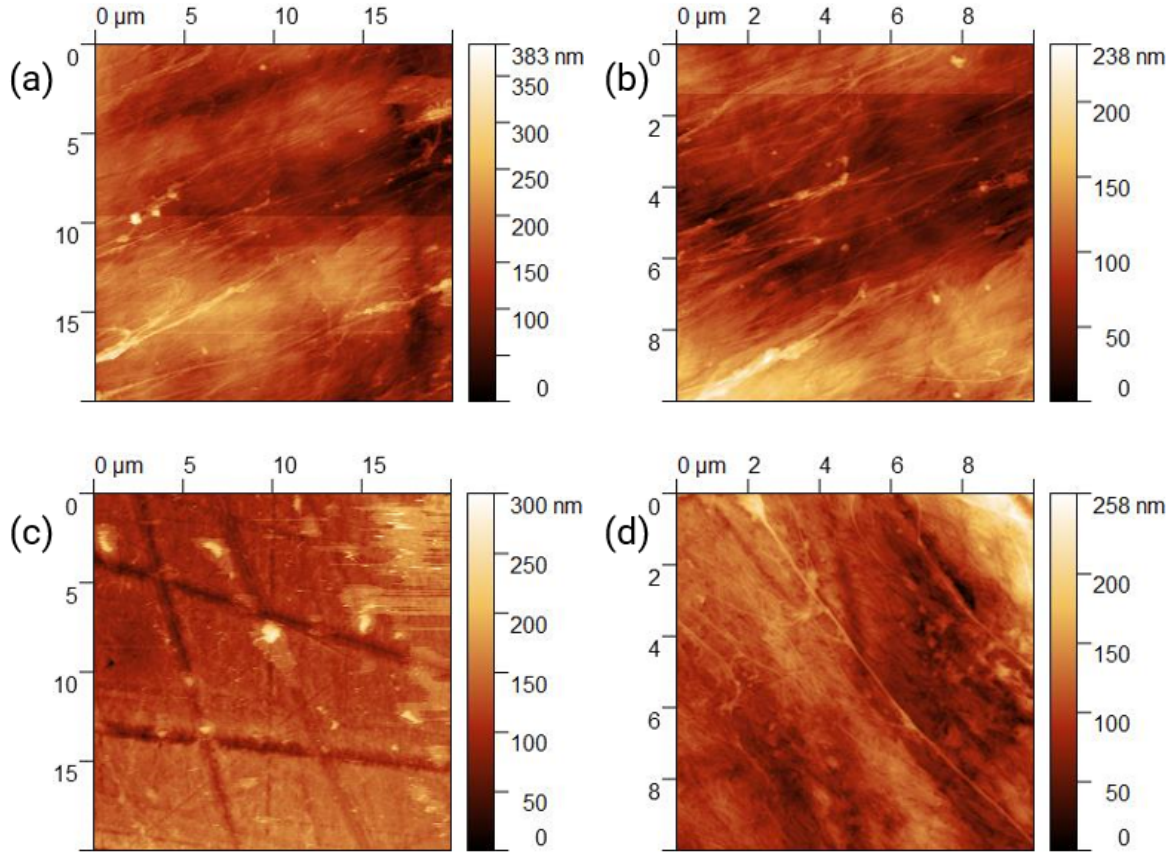

Fig. 4.2 AFM images of PTFE and PDA+PTFE coatings at two different scan sizes. (a) PTFE (20 µm x 20 µm scan), (b) PTFE (10 µm x 10 µm scan), (c) PDA+PTFE (20 µm x 20 µm scan), and (d) PDA+PTFE (10 µm x 10 µm scan).

Figure 4.3(a) shows the roughness parameters of the PTFE and the PDA+PTFE coatings. The PTFE coating has an average roughness, Ra, of 40 nm, whereas PDA+PTFE coating has a Ra of 48 nm due to the addition of PDA. Even though the PTFE coating showed a slightly lower Ra and root mean square roughness, Rq, than the PDA+PTFE coating, the T-test results show that the differences are not statistically significant ($P = 0.076$). Both PTFE and PDA+PTFE coating has a similar negative skewness number, which indicates both coatings are valley dominated (Figure

4.3(a)). The roughness profile agrees with the skewness and proves the valley dominated structure of the PTFE and PDA+PTFE coating (Figure 4.3(b)).

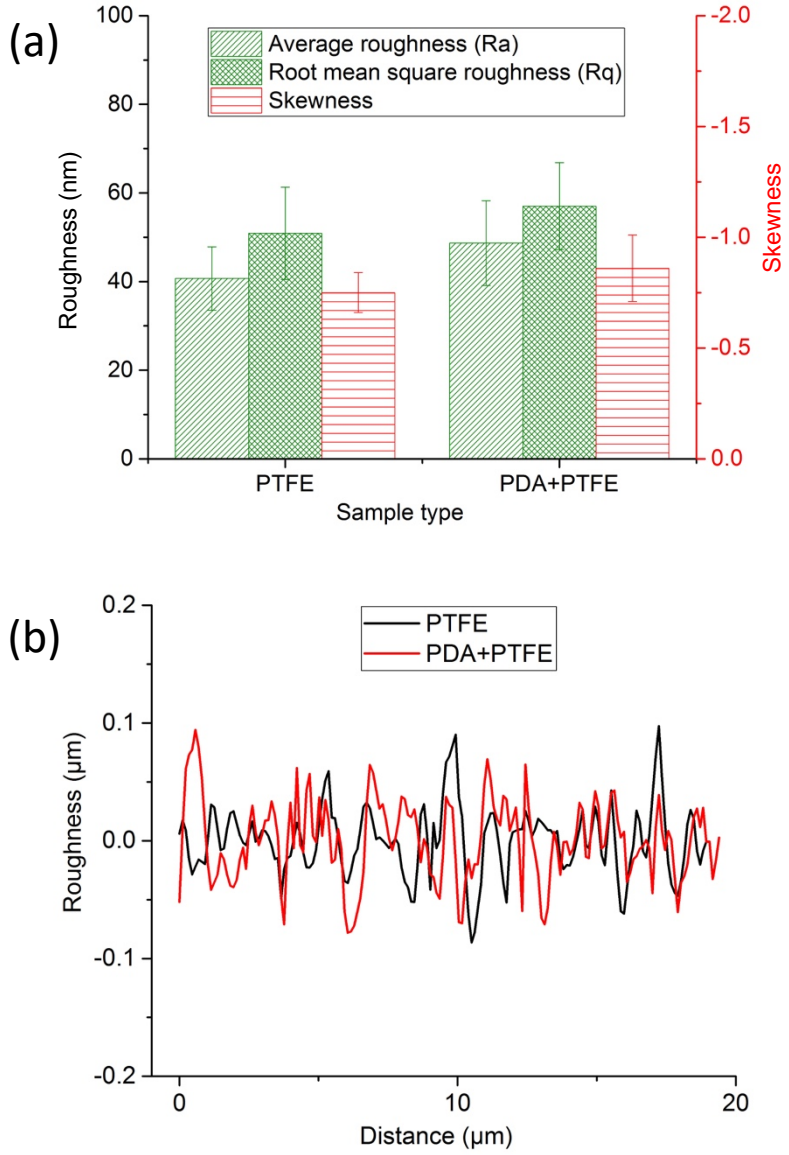

Fig. 4.3 The roughness parameters and roughness profiles of the PTFE and PDA+PTFE coatings. (a) the average roughness, Ra, root mean square roughness, Rq, and skewness and (b) roughness profiles of the PTFE and PDA+PTFE coatings.

4.4.2 Water Contact Angle

Figure 4.4 shows the WCA measurement of the PTFE and PDA+PTFE coatings. The PTFE coating showed hydrophobic behavior with an average WCA of 119.3º. The addition of PDA to the PTFE matrix reduced the average WCA of the PDA+PTFE coating to 105.9º. The hydrophilic nature of the PDA (WCA = 58 ± 2.4º) is responsible for the reduction in the WCA of the PDA+PTFE coating. Even though the addition of PDA decreased the hydrophobic behavior of the PTFE coating, the PDA+PTFE coating remained hydrophobic.

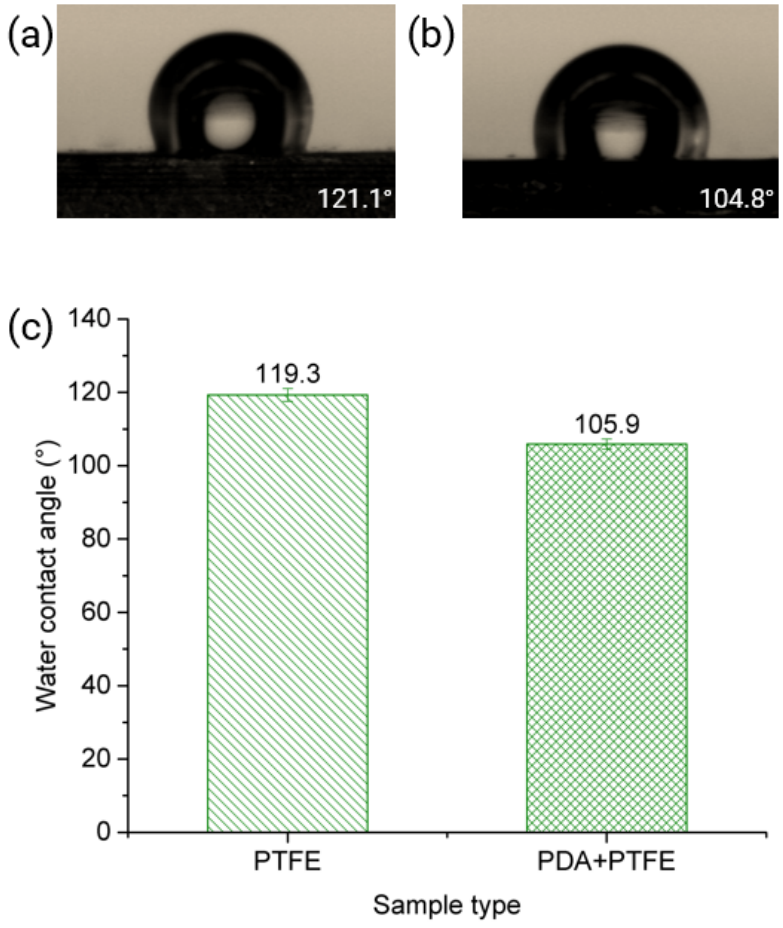

Fig. 4.4 Water droplet images and comparison of the water contact angle of the PTFE and PDA+PTFE coatings. (a) water droplet image on PTFE coating, (b) water droplet image on PDA+PTFE coating, and (c) the comparison of the water contact angle of PTFE and the PDA+PTFE coatings.

4.4.3 Nanomechanical Properties

The surface topography, Young's modulus, and adhesion maps of PTFE and PDA+PTFE coatings obtained by PFQNM are shown in Figure 4.5. It can be seen that Young's modulus and adhesion values are consistent throughout the imaged areas of both the PTFE and the PDA+PTFE coatings. These values measured using PFQNM were summarized and shown in Figure 4.6. Young's modulus of the PTFE coating was 0.61 + 0.07 GPa that is similar to the reported Young's modulus of thick PTFE coating [33].

Figure 4.6(a) shows that the addition of PDA increased the Young's modulus of the PTFE coating from 0.61 GPa to 0.97 GPa. The higher Young's modulus of the PDA (2.3 GPa) is responsible for the increase in Young's modulus of the PDA+PTFE coating [35]. However, the hardness of the PTFE and PDA+PTFE coating was measured using nanoindentation, and no significant change in the hardness was observed, as shown in Figure 4.6(b). Additionally, it was hypothesized that the cross-linking between the PDA and PTFE might be responsible for the higher Young's modulus of the PDA+PTFE coating compared to the PTFE coating. To check this hypothesis, XPS was performed on both the PTFE and the PDA+PTFE coatings. The bonding structure will be discussed later. The PDA + PTFE coating showed a higher adhesion force of 172 nN than the 154 nN adhesion force of the PTFE coating. The more adhesive PDA is responsible for the increase in the adhesion force of the PDA+PTFE coating compared to the PTFE coating.

4.4.4 Friction and Durability

The COF profiles of the PTFE and PDA+PTFE coatings tested in Mobil DTE-32 oil for 3,000 cycles and 15,000 cycles, respectively, were plotted in Figure 4.7. It is observed that the starting COF of the PTFE coating is 0.03, which is comparable to the bulk PTFE in oil-lubricated

conditions [32]. The COF of the PTFE coating increased to 0.045 gradually over the 3,000 cycles of the testing until the coating failed.

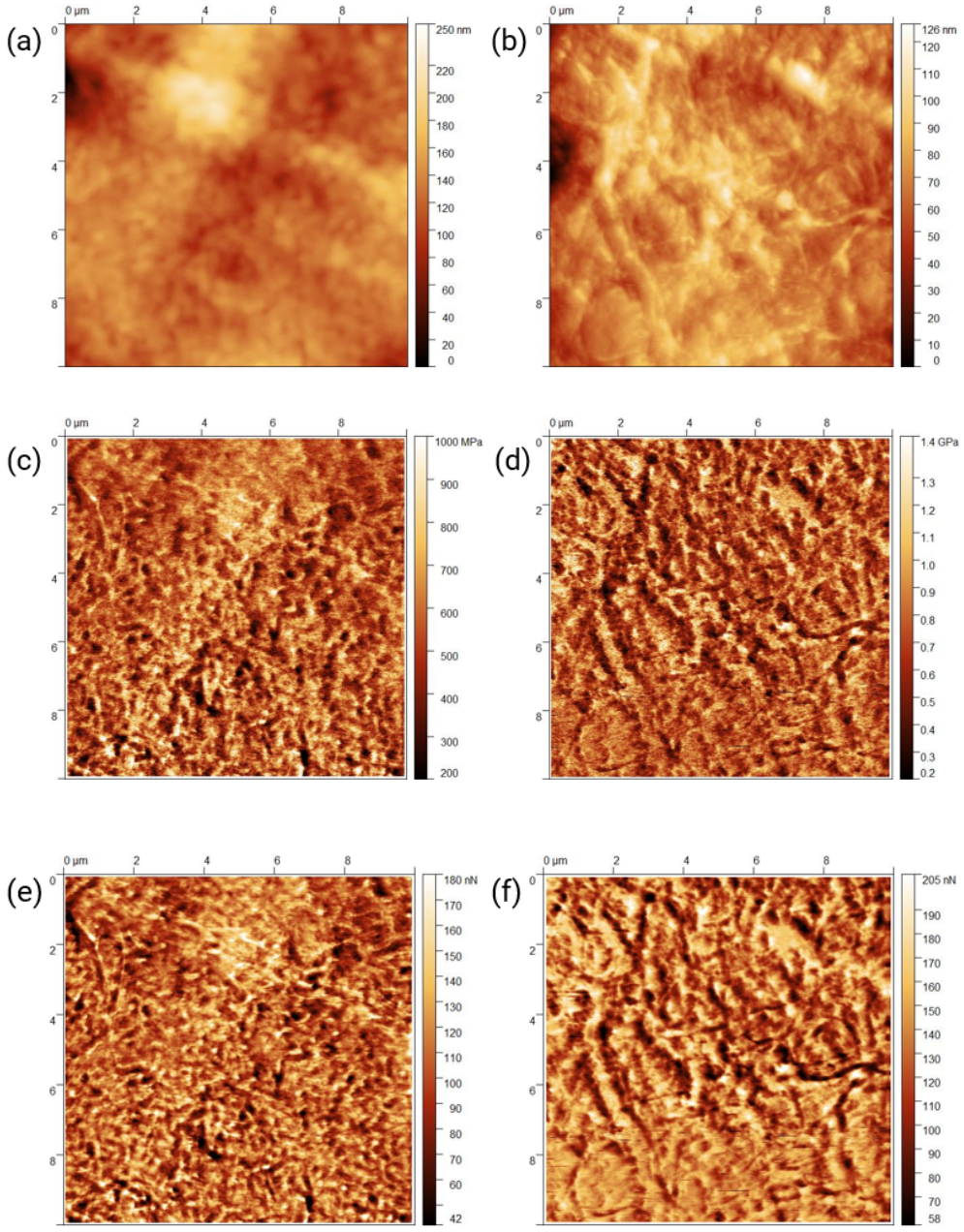

Fig. 4.5 Nanomechanical property maps of the PTFE and PDA+PTFE coatings. (a) and (b) shows the topography of the PTFE and PDA+PTFE coatings, respectively, (c) and (d) shows the modulus of elasticity maps of the PTFE and PDA+PTFE coatings, respectively, and (e) and (f) shows the adhesion maps of the PTFE and PDA+PTFE coatings, respectively.

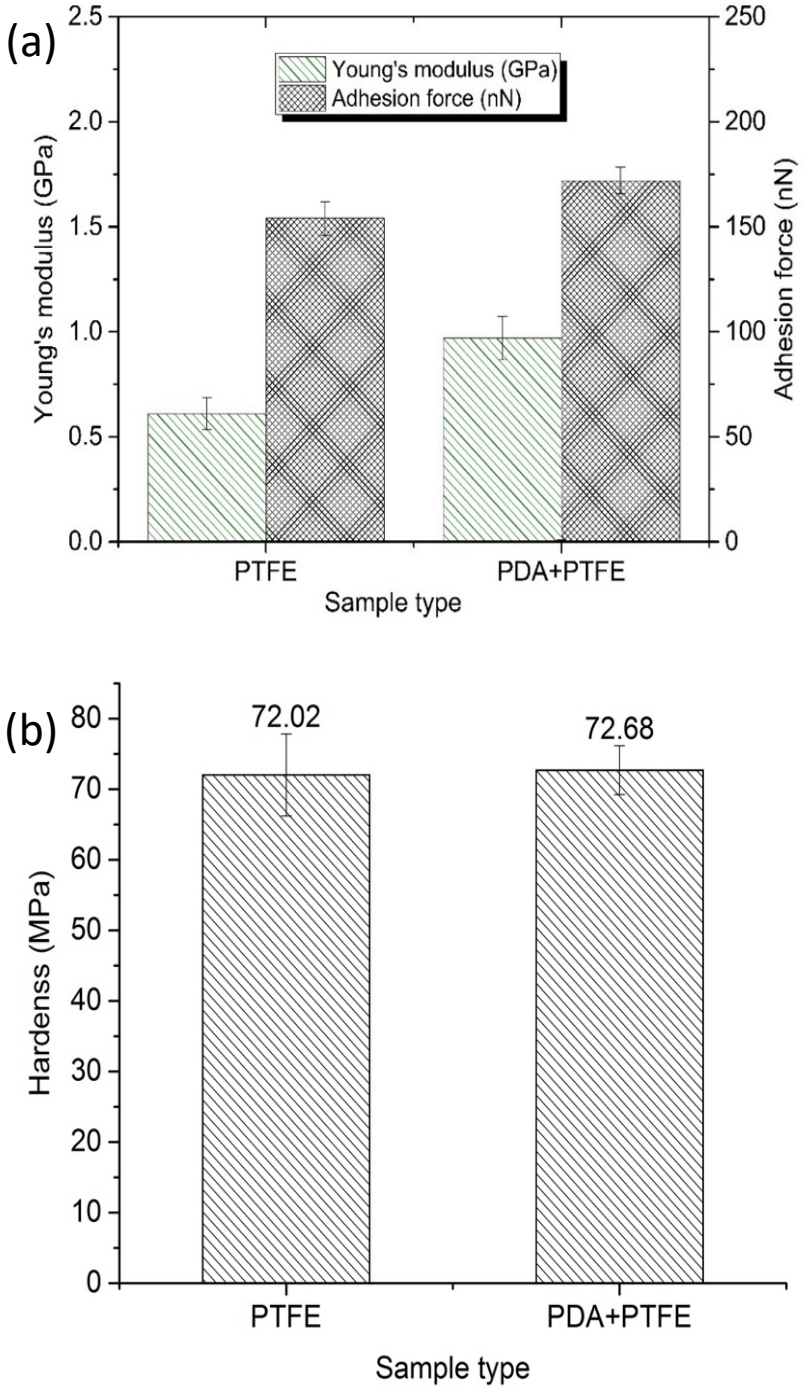

Fig. 4.6 Comparison of the nanomechanical properties (Young's modulus, adhesion force, and hardness) of PTFE and PDA+PTFE coatings. (a) Young's modulus and adhesion force and (b) hardness.

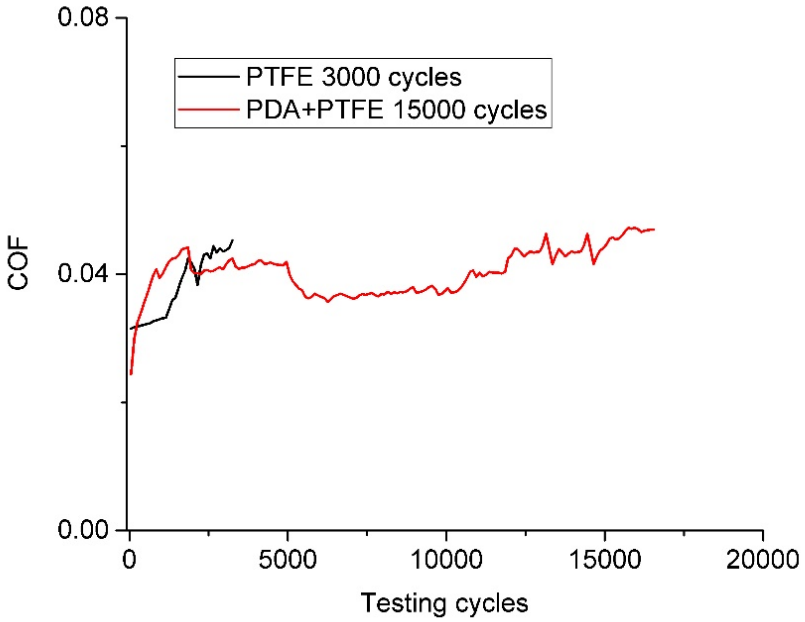

Fig. 4.7 COF profile of the PTFE and PDA+PTFE coatings tested in oil-lubricated conditions.

However, no pronounced increase in the COF profile was observed due to the chrome steel, and the cast-iron interface was in oil-lubricated conditions. The wear progression tests were performed to study the coating failure and will be discussed later. The starting COF of the PDA+PTFE coating is much lower (0.02) than the PTFE coating (0.03). The COF of the PDA+PTFE coating transitioned into 0.04 at the first 2,000 cycles and held below this value until 12,500 cycles of testing. The COF of the PDA+PTFE coating then transitioned into 0.051 for the rest of the test. Interestingly, the COF of the PDA+PTFE coating did not show any significant difference from the PTFE coating, even though adhesive PDA were added.

The coefficient of friction of the PTFE coating reported in the literature is 0.12 in dry conditions [8,9,14,15]. As shown in Figure 4.8, the COF of the PTFE coating in the oil-lubricated condition was found to be 0.045, which is 62.5% less than that tested in dry conditions. The average COF of the PDA+PTFE coating was found to be 0.049, which is not significantly higher

than the PTFE coating, indicating that the addition of PDA does not negatively impact the COF of the PTFE coating.

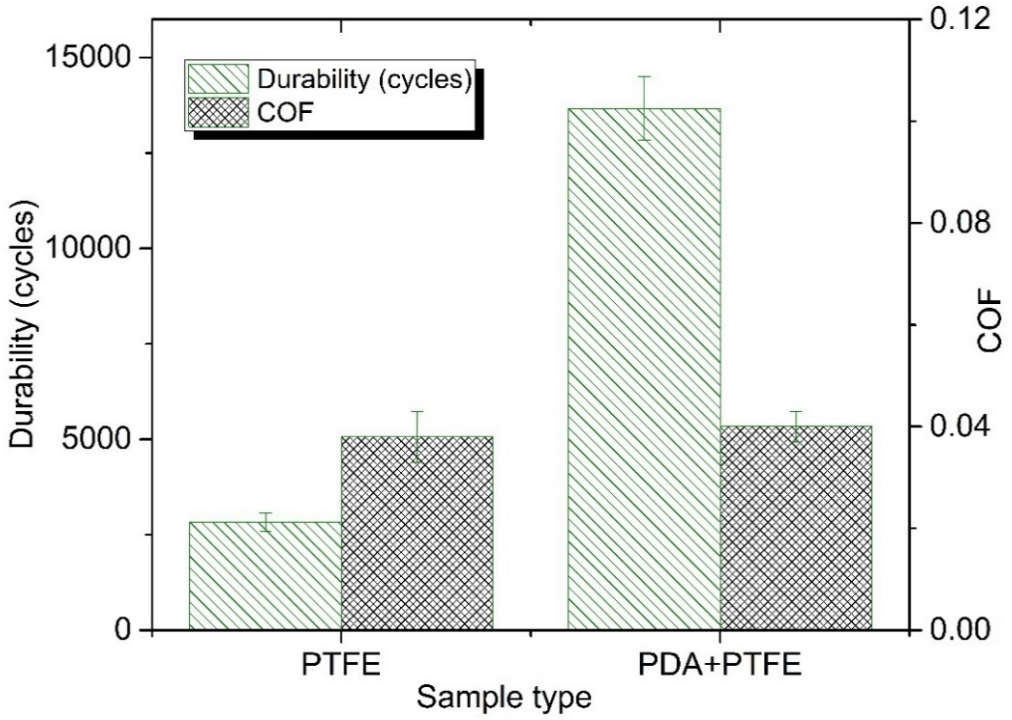

Fig. 4.8 Comparison of the average durability and COF of the PTFE and PDA+PTFE coatings in oil-lubricated conditions.

The durability of the PTFE and PDA+PTFE coatings in oil-lubricated conditions was also plotted in Figure 4.8. The PTFE coating lasted for 2,765 cycles, whereas the PDA+PTFE coating lasted for 13,667 cycles. The better durability of the PDA+PTFE coating can be attributed to the higher Young's modulus of the coating, which gives the coating a better load carrying capacity under normal load. To check this hypothesis, scratch tests were performed on the PTFE and PDA+PTFE coatings and will be discussed later.

4.4.5 Wear Progression

A set of wear progression tests were performed to determine the durability of the PTFE and PDA+PTFE coatings. Figure 4.9(a) shows the comparison of the wear depths of the coatings tested for 1,000, 2,000, and 3,000 cycles in oil-lubricated conditions. It can be seen that the PTFE coating has rapidly worn out during the 3,000 cycles of testing, whereas the PDA+PTFE coating wore at a much slower rate during the 3,000 cycles of testing. The PDA+PTFE coating was further tested tribologically for 4,000, 6,000, 8,000, 10,000, and 15,000 cycles in oil-lubricated conditions, and the wear depths were plotted in Figure 4.9(b). It was observed that the wear depth increased linearly for the first 8,000 cycles of testing and reached 11.12 μm, and the wear depth started to increase rapidly when the coating was tested for 10,000 and 15,000 cycles with the wear depth reaching 31.2 μm and 44.57 μm, respectively. It was hypothesized that the higher wear rate after 8,000 cycles might be due to the presence of porosity in the coating underneath the compacted top surface. To prove this hypothesis, FIB-SEM was used to cut and image the cross-section of the PDA+PTFE coating. AFM images were also taken on the bottom surface of the PDA+PTFE coating after peeling it off from the substrate.

Figure 4.10 shows the cross-section FIB-SEM image of the PDA+PTFE coating. It can be seen from the SEM image that the top surface of the PDA+PTFE coating (inside the red circle) does not have any porosity. Porosities can be seen underneath the top compacted coating (inside the yellow circle). The porous structure on the left side of the SEM image was from the deformation of the PDA+PTFE coating surface under the FIB irradiation. Even though a porous structure underneath the compacted PDA+PTFE coating was observed, the morphology of the PDA+PTFE coating was not fully understood due to the deformation caused by the FIB.

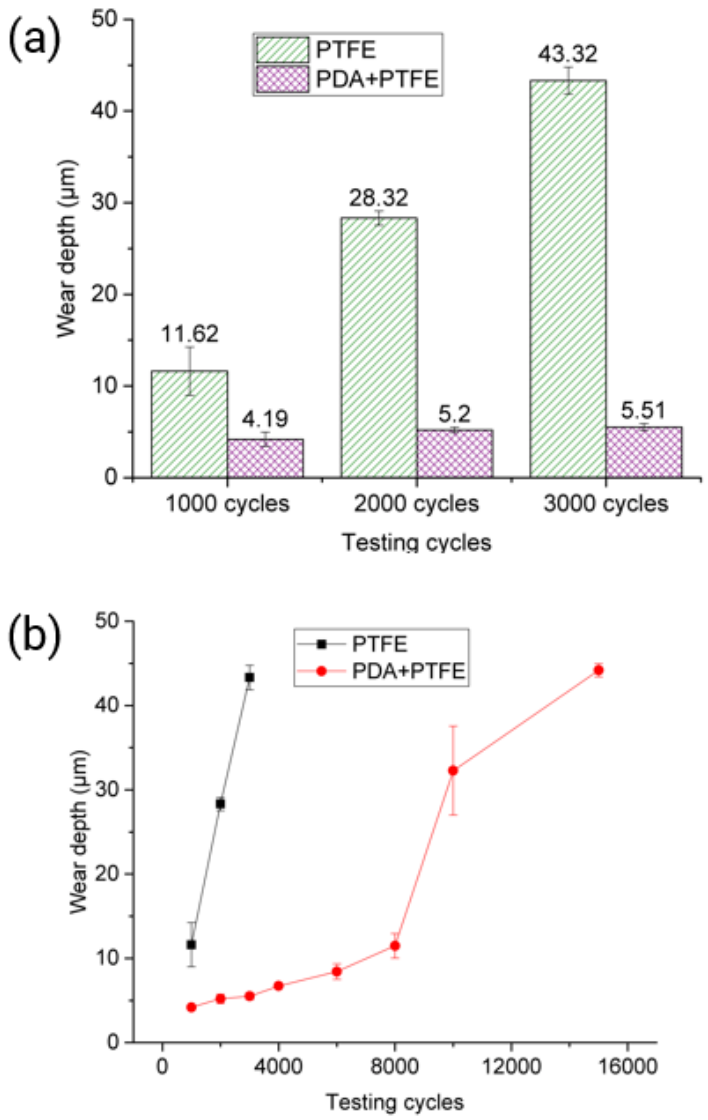

Fig. 4.9 Study of the wear depth of the PTFE and PDA+PTFE coatings in progressive wear tests in oil-lubricated conditions. (a) comparison of the wear depth of the PTFE and PDA+PTFE coatings at 1,000, 2,000, and 3,000 cycles of testing and (b) progressive wear depth of the PTFE and PDA+PTFE coating at different cycles of testing.

Figure 4.10 shows the cross-section FIB-SEM image of the PDA+PTFE coating. It can be seen from the SEM image that the top surface of the PDA+PTFE coating (inside the red circle) does not have any porosity. Porosities can be seen underneath the top compacted coating (inside the yellow circle). The porous structure on the left side of the SEM image was from the

deformation of the PDA+PTFE coating surface under the FIB irradiation. Even though a porous structure underneath the compacted PDA+PTFE coating was observed, the morphology of the PDA+PTFE coating was not fully understood due to the deformation caused by the FIB.

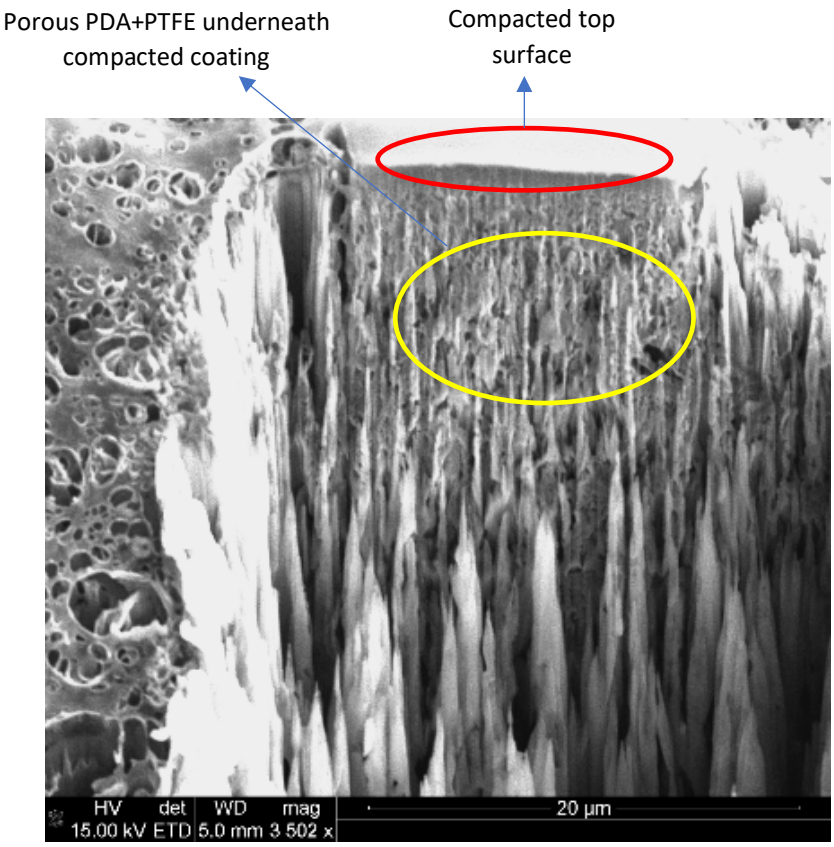

Fig. 4.10 Cross-sectional FIB-SEM image of the PDA+PTFE coating.

To further investigate the morphology of the coating, AFM imaging was performed on the bottom surface of the PDA+PTFE coating after peeling it off from the substrate. The AFM images of the bottom surface are shown in Figures 4.11. From Figure 4.11(a), it was observed that the PDA+PTFE coating has porous spots throughout the area of the image. It was also observed that the PTFE particle at the bottom of the surface did not show the usual needle-like structure observed

previously [13,27]. Higher-resolution AFM image in Figure 4.11 (b) shows the PDA+PTFE coating had a pellet-like structure on the bottom surface. The highly porous structure of the PDA+PTFE coating bottom surface was also visible from Figure 4.11(b). Jiang et al. [9] found that the PTFE coating showed a pellet-like structure before annealing at 372º C. The pellet-like structure on the bottom of the PDA+PTFE coating indicates that the 45 μm-thick PDA+PTFE coating was not fully annealed at the bottom of the coating. During the annealing process, the top surface of the PDA+PTFE coating was annealed and compacted, whereas the bottom of the coating was not annealed and compacted. Combining the SEM and AFM study of the cross-section and bottom surface of the PDA+PTFE coating, it can be concluded that the porous and non-annealed PDA+PTFE coating underneath the compacted PDA+PTFE coating were responsible for the higher wear rate of the PDA+PTFE coating after 8,000 cycles of testing in oil-lubricated condition. Figure 4.12 shows the optical wear track images of the PTFE and PDA+PTFE coatings tested for 3,000 and 15,000 cycles, respectively. The PTFE wear track shows the machining line of the substrate underneath the coating due to the transparent nature of the PTFE coating. The PDA+PTFE coating has a black color and does not show the machining marks on the substrate. The wear track image of the PTFE coating (Figure 4.12(a)) shows that after 3,000 test cycles, there was no PTFE coating left on the wear track. The white areas on the wear track (Figure 4.12(a) and (b)) indicate there was a counter surface-to-substrate interaction during the tribological testing. The counter surface image in Figure 4.12(c) shows some wear scuff, which proved the earlier assertion that there was some metal-metal interaction during the tribological testing of the PTFE coating for 3,000 cycles in oil-lubricated condition. It can be concluded that there was no observable transfer film formation during wear tests, and the wear debris was swept away by the oil during wear test (Figure 4.12(c)). Figure 4.12(d) shows the wear track image of the PDA+PTFE

coating after 15,000 cycles of testing in oil-lubricated conditions. It can be seen that the PDA+PTFE coating was mostly worn out from the substrate after 15,000 cycles, but the substrate is not exposed. There was no metal-metal interaction during the tribological tests, and there was no wear scuff and no transfer film on the counterface ball after testing.

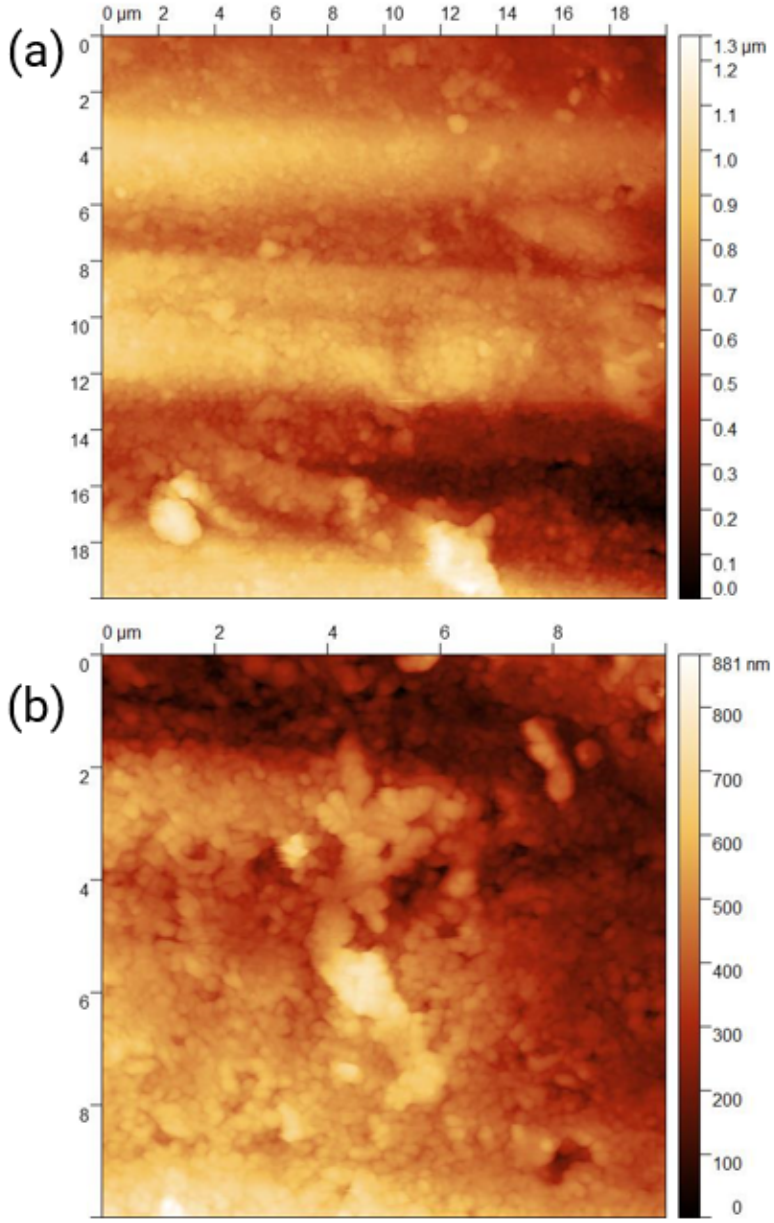

Fig. 4.11 AFM images of the bottom of the PDA+PTFE coating at two different scan sizes. (a) 20 µm x 20 µm, and (b) 10 µm x 10 µm.

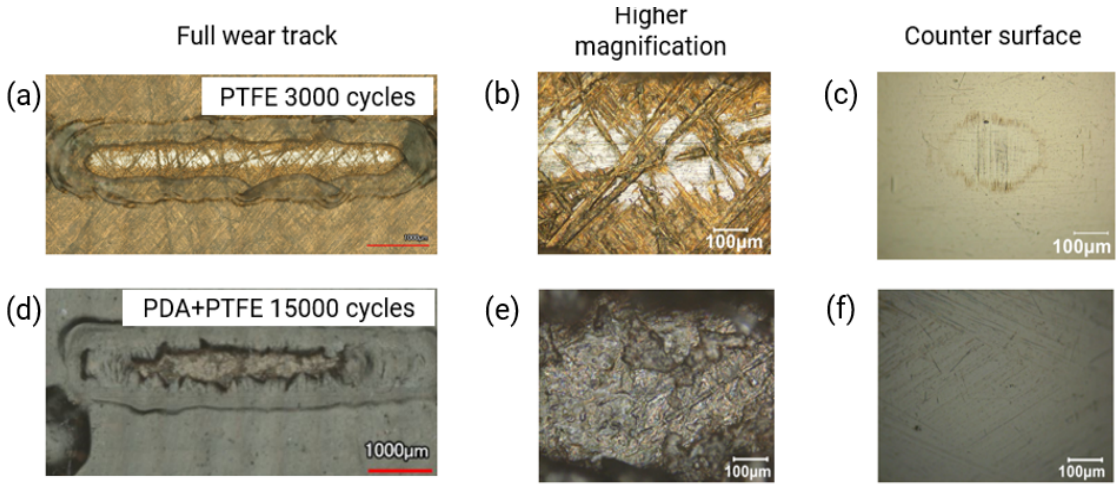

Fig. 4.12 Optical microscope images of the PTFE and PDA+PTFE coatings tested for 3,000 and 15,000 cycles in oil-lubricated conditions. (a) and (d) show wear tracks of the PTFE and PDA+PTFE coating, (b) and (e) show higher magnification images of the wear tracks, and (c) and (f) show the counter surfaces after the tribological testing.

4.4.6 Scratch Test

To investigate the coating adhesion to the substrate, scratch tests were performed on the PTFE and PDA+PTFE coatings using a diamond-coated tip with 400 µm diameter and 120º cone angle. The optical images of the wear tracks and the normal load and COF profiles of the scratch tests are plotted in Figure 4.13. It can be seen from Figure 4.13(a) and (b) that both PTFE and PDA+PTFE coatings were deformed at the start of the scratch tests. For PTFE coating, more aggressive wear starts around 2.2 N normal load, where wrinkles started to form in the coating due to coating delamination. The PDA+PTFE coating showed a smoother wear track until 4 N normal load. After this point, the wear track width increased, but no wrinkle formation and coating delamination on the wear track was observed. The change in the wear width of the PDA+PTFE coating was also evident by the abrupt change in the COF in Figure 4.13(c). The addition of PDA gives the PDA+PTFE coating a better load carrying capacity, which translated into better

durability of the PDA+PTFE coating. The higher force required to delaminate the PDA+PTFE coating can be attributed to the higher Young's modulus of the PDA+PTFE coating. Stiffer PDA+PTFE coating needed a higher loading condition to cause elastic deformation in the coating compared to PTFE coating. In addition to the better nanomechanical properties, it was hypothesized that there was cross-linking between the PDA+PTFE, which in turn gave the better durability of the PDA+PTFE coating. To check this hypothesis, XPS was performed on the PTFE and PDA+PTFE coatings, and their chemical bonding was analyzed.

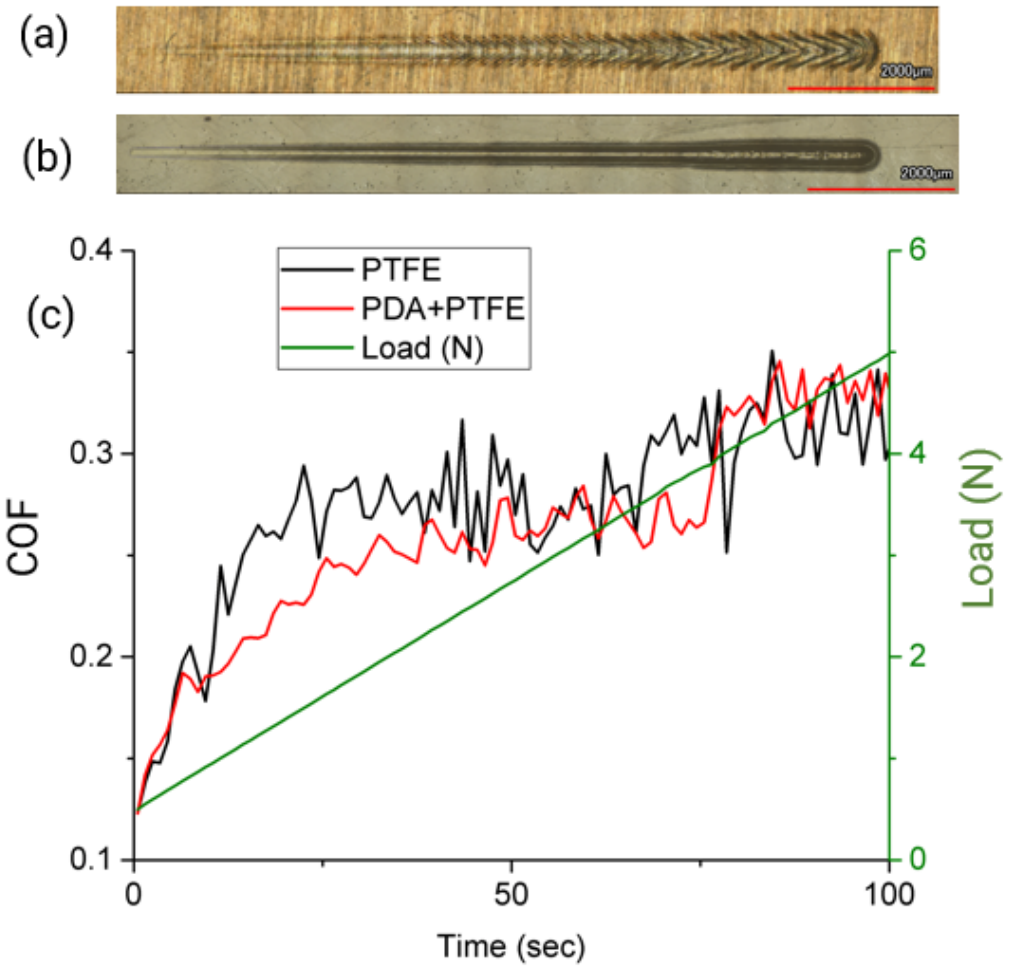

Fig. 4.13 Optical microscope images of wear tracks, the COF profiles, and the load profile of PTFE and PDA+PTFE coatings from the scratch test. (a) The PTFE wear track, (b) the PDA+PTFE wear track, and (c) the COF profiles and the load profile over time.

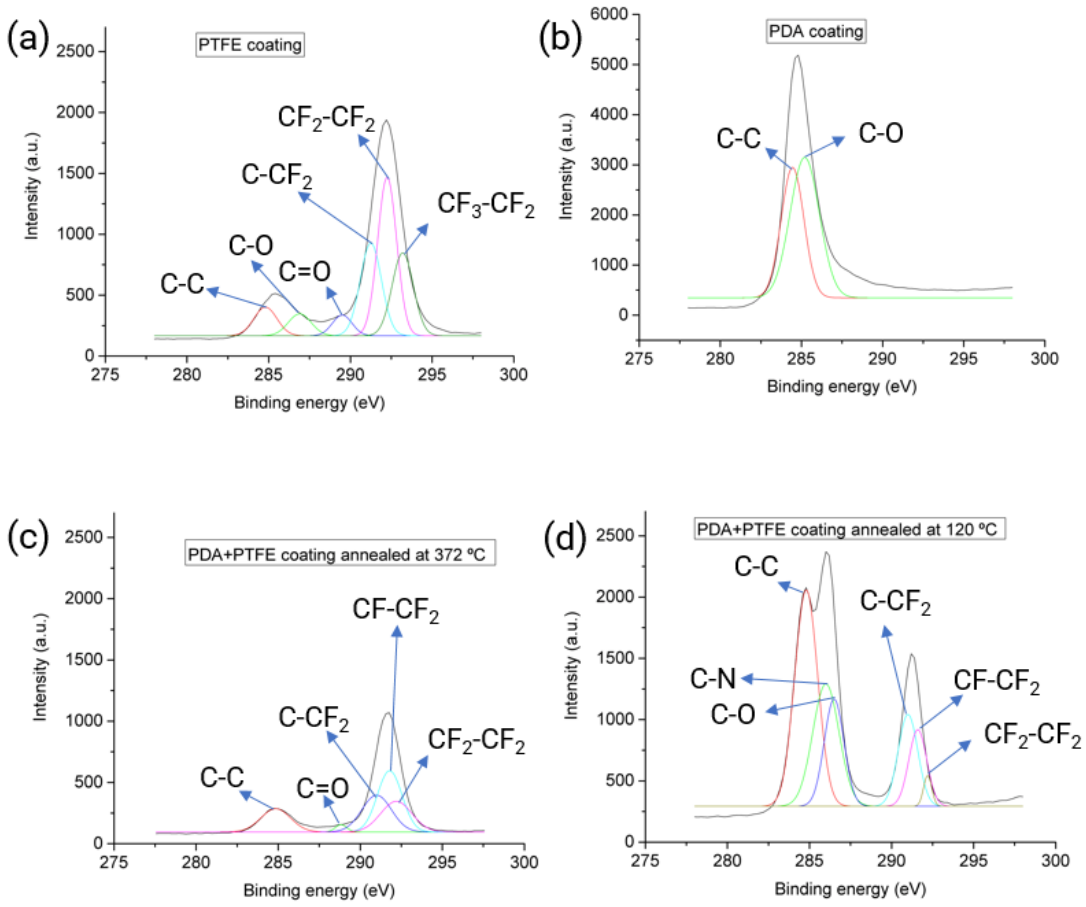

Fig. 4.14 Chemical bonding analysis of the PTFE, PDA, and PDA+PTFE coatings by XPS. XPS spectrum and bonding analysis of (a) PTFE coating, (b) PDA coating, (c) PDA+PTFE coating annealed at 372 ºC, and (d) PDA+PTFE coating annealed at 120 ºC.

4.4.7 Chemical Analysis

Figure 4.14 shows the XPS spectra of C1s of the PTFE, PDA, and PDA+PTFE coatings annealed at 372 ºC and 120 ºC. Table 4.1 summarizes the different bonding types and their proportion (%) present in the different coatings. It can be seen from Table 4.1 that the PTFE coating has a large percent of CF_2-CF_2 bonds (39.1%) and have a small percent of C-C bonds

(7.1%), while the PDA was dominated by C-C and C-O bonds. Interestingly, there were differences between the bonding structures of the PDA+PTFE and PTFE coatings annealed at 372 ºC. The PDA+PTFE coating has a higher percentage of C-C bonds (14.6%) due to the addition of PDA. Remarkably, a lower percent of the CF_2-CF_2 bonds (19.3%) were found, and 38.5% of CF-CF_2 bonds were also formed in the PDA+PTFE coating. This indicates some of the CF_2-CF_2 bonds were broken and converted to CF-CF_2 bonds, which facilitated the cross-linking between the PDA and PTFE molecules, thus resulting in improved nanomechanical properties and hence better durability of the PDA+PTFE coating annealed at 372 ºC.

Table 4.1: The proportion of different bonds (%) obtained by XPS on different coatings.

Bonding Type	**PDA (%)**	**PTFE (%)**	**PDA+PTFE annealed at 372º C (%)**	**PDA+PTFE annealed at 120º C (%)**
C-C	48.1	7.1	14.6	33.5
C-O	51.9	5.4	0.0	19.0
C=O	0.0	5.1	4.5	0.0
C-N	0.0	0.0	0.0	16.6
C-CF_2	0.0	22.9	23.1	14.3
CF_2-CF_2	0.0	39.1	19.3	4.8
CF_3-CF_2	0.0	20.4	0.0	0.0
CF-CF_2	0.0	0.0	38.5	11.8
CF-C	0.0	0.0	0.0	0.0

It is not clear exactly when the cross-linking between PDA and PTFE polymer chains occurred, but it is hypothesized that the cross-linking may have happened during the final curing of the PDA+PTFE coating at 372 ºC. To check this hypothesis, XPS was performed on the PDA+PTFE coating heated to 120 ºC without the final curing step, and the XPS spectrum is shown in Figure 4.14(d). It was observed in figure 4.14(c) and 4.14(d) that the PDA+PTFE coating heated to 120 ºC and 372 ºC have a different XPS spectrum. The former had distinct peaks for both PTFE

and PDA. The higher percentage of the C-C (33.5%), C-O (19.0%), and C-N (16.6%) bonds in the XPS spectra of the PDA+PTFE coating heated to 120 ºC are from the PDA, whereas the CF_2-CF_2, CF-CF_2, and C-CF_2 came from the PTFE. It is interesting to see that the percentage of the stable CF_2-CF_2 bonds (19.3%) in the PDA+PTFE coating heated to 372 ºC is higher than that heated to 120 ºC (4.8%). Decreases in the distinct peaks for the PDA coating (C-C and C-O, and C-N) were observed in the PDA+PTFE coating heated at 372 ºC compared to the coating heated at 120 ºC due to the cross-linking between the PDA and PTFE particles. Therefore, it can be concluded from Figure 4.14(c) and (d) that the high-temperature curing process was responsible for the cross-linking between PDA and PTFE.

4.5 Conclusion

The tribological properties of PTFE and PDA+PTFE coatings in oil-lubricated conditions were studied. Both coatings showed hydrophobic behavior. The coatings also showed similar COF in oil-lubricated conditions, which is 62.5% lower than that in dry conditions. The PDA+PTFE coating lasted five times longer than the PTFE coating in an oil-lubricated condition when tested under a normal load of 10 N and a linear reciprocating speed of 0.1m/s. The coating life could be further improved by better compaction of the coatings. The addition of PDA helped to increase the Young's modulus of the PTFE coating from 0.61 GPa to 0.97 GPa. The adhesion of the PDA+PTFE coating was slightly higher than that of the PTFE coating. XPS chemical analysis showed that cross-linking occurred between the PDA and PTFE molecules during the high-temperature annealing process as the results of broken CF_2-CF_2 bonds and the formation of the more active CF-CF_2 bond. The better nanomechanical properties of the PDA+PTFE coating and

the cross-linking between the PDA and PTFE contributed to the better durability of the PDA+PTFE coating than the PTFE coating in oil-lubricated condition.

4.6 Acknowledgment

This material is based upon work supported by the U.S. Department of Energy's Office of Energy Efficiency and Renewable Energy (EERE) under the Next Generation Electric Machines: Enabling Technologies Program Award Number DEEE0007874 and by the National Science Foundation (NSF) under Grant Nos. CMMI-1563227 and OIA-1457888. The views and opinions of authors expressed herein do not necessarily state or reflect those of the United States Government or any agency thereof.

References

1. E. Dhanumalayan, G.M. Joshi, Performance Properties and Applications of Polytetrafluoroethylene (PTFE)—a Review, Advanced Composites and Hybrid Materials, 1 (2018), 247–268. https://doi.org/10.1007/s42114-018-0023-8.

2. H. Unal, A. Mimaroglu, U. Kadıoglu, H. Ekiz, Sliding friction and wear behaviour of polytetrafluoroethylene and its composites under dry conditions, Materials and Design, 25 (2004), 239-245. https://doi.org/10.1016/j.matdes.2003.10.009.

3. D. Pan, B. Fan, X. Qi, Y. Yang, X. Hao, Investigation of PTFE Tribological Properties Using Molecular Dynamics Simulation, TRIBOLOGY LETTERS, 67 (2019), 28. https://doi.org/10.1007/s11249-019-1141-3.

4. V. Eustathios, Fluoropolymer primer having improved scratch resistance, US Patent No. 4049863 A (1977).

5. J. Lee, D. Lim, Tribological Behavior of PTFE Film with Nanodiamond, Surface & Coatings Technology, 188 (2004), 534-538. https://doi.org/10.1016/j.surfcoat.2004.07.102.

6. D.L. Burris, W.G. Sawyer, Improved Wear Resistance in Alumina-PTFE Nanocomposites with Irregular Shaped Nanoparticles, Wear, 260 (2006), 915-918. https://doi.org/10.1016/j.wear.2005.06.009.

7. S.E. McElwain, T.A. Blanchet, L.S. Schadler, W.G. Sawyer, Effect of Particle Size on the Wear Resistance of Alumina-Filled PTFE Micro- and Nanocomposites, Tribology Transactions, 51 (2008), 247-253. https://doi.org/10.1080/10402000701730494.

8. S. Beckford, M. Zou, Wear Resistant PTFE Thin Film Enabled by a Polydopamine Adhesive Layer, Applied Surface Science, 292 (2014), 350-356. https://doi.org/10.1016/j.apsusc.2013.11.143.

9. Y. Jiang, D. Choudhury, M. Brownell, A. Nair, J.A. Goss, M. Zou, The Effects of Annealing Conditions on the Wear of PDA/PTFE Coatings, Applied Surface Science, 481 (2019), 723-735. https://doi.org/10.1016/j.apsusc.2019.03.076.

10. Y. Zhao, M. Zou, Experimental Investigation of the Wear Mechanisms of Thin PDA/PTFE Coatings, Progress in Organic Coatings, 137 (2019), 105341. https://doi.org/10.1016/j.porgcoat.2019.105341.

11. H. Lee, S.M. Dellatore, W.M. Miller, P.B. Messersmith, Mussel-Inspired Surface Chemistry for Multifunctional Coatings, Science, 318 (2007), 426-430. https://doi.org/10.1126/science.1147241.

12. H. Lee, Y. Lee, A.R. Statz, J. Rho, T.G. Park, P.B. Messersmith, Substrate-Independent Layer-by-Layer Assembly by using Mussel-Adhesive-Inspired Polymers, Advanced Materials, 20 (2008), 1619-1623. https://doi.org/10.1002/adma.200702378

13. S. Beckford, J. Cai, R. Fleming, M. Zou, The Effects of Graphite Filler on the Tribological Properties of Polydopamine/PTFE Coatings, TRIBOLOGY LETTERS, 64 (2016), 1-10. https://doi.org/10.1007/s11249-016-0777-5.

14. S. Beckford, L. Mathurin, J. Chen, R. Fleming, M. Zou, The Effects of Polydopamine Coated Cu Nanoparticles on the Tribological Properties of Polydopamine/PTFE Coatings, Tribology International, 103 (2016), 87-94. https://doi.org/10.1016/j.triboint.2016.06.031.

15. D. Choudhury, I. Niyonshuti, J. Chen, J.A. Goss, M. Zou, Tribological Performance of Polydopamine + Ag Nanoparticles/PTFE Thin films, Tribology International, 144 (2020), 106097. https://doi.org/10.1016/j.triboint.2019.106097.

16. S. Beckford, L. Mathurin, J. Chen, M. Zou, The Influence of Cu Nanoparticles on the Tribological Properties of Polydopamine/PTFE + Cu Films, Tribology Letters,59 (2015), 11. https://doi.org/10.1007/s11249-015-0543-0.

17. S. Beckford, J. Cai, J. Chen, M. Zou, Use of Au Nanoparticle-Filled PTFE Films to Produce Low-Friction and Low-Wear Surface Coatings, Tribology Letters, 56 (2014), 223-230. https://doi.org/10.1007/s11249-014-0402-4.

18. C. Miller, D. Choudhury, M. Zou, The Effects of Surface Roughness on the Durability of Polydopamine/PTFE Solid Lubricant Coatings on NiTiNOL 60, Tribology Transactions, 62 (2019), 919-929. https://doi.org/10.1080/10402004.2019.1641645.

19. K. Batzar, Cookware Coating Systems," US Patent No. 5250356 A (1993).

20. T. Tevruz, Tribological Behaviours of Carbon Filled Polytetrafluoroethylene (PTFE) Dry Journal Bearings, Wear, 221 (1998), 61-68. https://doi.org/10.1016/S0043-1648(98)00258-0.

21. G.L. Doll, R.D. Evans, C.R. Ribaudo, C. R., Coated Rolling Element Bearing Cages, US Patent No. 6994475 B2 (2006).

22. P. Woelki, D. Petit, F. Harig, Self-Lubricating Bearing, US Patent No. 5971617 A (1999).

23. N.G. Demas, A.A. Polycarpou, Tribological performance of PTFE-based coatings for air-conditioning compressors, Surface & Coatings Technology, 203 (2008), 307-316. https://doi.org/10.1016/j.surfcoat.2008.09.001.

24. Z. Zhang, Q. Xue, W. Liu, W. Shen, Friction and Wear Characteristics of Metal Sulfides and graphite-filled PTFE Composites Under Dry and oil-lubricated Conditions, Journal of Applied Polymer Science, 72 (1999), 751-761. https://doi.org/10.1002/(SICI)1097-4628(19990509)72:6%3C751::AID-APP3%3E3.0.CO;2-W.

25. B. Jia, T. Li, S. Liu, P. Cong, Tribological Behaviors of several Polymer-Polymer Sliding Combinations Under Dry Friction and Oil-Lubricated Conditions, Wear, 262 (2007), 1353-1359. https://doi.org/10.1016/j.wear.2007.01.011.

26. Z. Zhang, Q. Xue, W. Liu, W. Shen, Friction and Wear Characteristics of Lead and its Compounds Filled Polytetrafluoroethylene Composites Under Oil Lubricated Conditions, Tribology International, 31 (1998), 361-368. https://doi.org/10.1016/S0301-679X(98)00045-0.

27. Q. Xue, Z. Zhang, W. Liu, W. Shen, Friction and Wear Characteristics of Fiber- and whisker-reinforced PTFE Composites Under Oil Lubricated Conditions, Journal of Applied Polymer Science, 69 (1998), 1393-1402. https://doi.org/10.1002/(SICI)1097-4628(19980815)69:7%3C1393::AID-APP14%3E3.0.CO;2-V.

28. K.W. Liew, S.Y. Chia, C.K. Kok, K.O. Low, Evaluation on Tribological Design Coatings of Al2O3, Ni–P–PTFE and MoS2 on Aluminium Alloy 7075 Under Oil Lubrication, Materials and Design, 48 (2013), 77-84. https://doi.org/10.1016/j.matdes.2012.08.010.

29. Q. Shangguan, X. Cheng, On the Friction and Wear Behavior of PTFE Composite Filled with Rare Earths Treated Carbon Fibers Under Oil-Lubricated Condition, Wear, 260 (2006), 1243-1247. https://doi.org/10.1016/j.wear.2005.08.009.

30. Z. Zhang, Q. Xue, W. Liu, W. Shen, Friction and Wear Behaviors of several Polymers Under oil-lubricated Conditions, Journal of Applied Polymer Science, 68 (1998), 2175-2182. https://doi.org/10.1002/(SICI)1097-4628(19980627)68:13%3C2175::AID-APP14%3E3.0.CO;2-Z.

31. A. Golchin, G.F. Simmons, S.B. Glavatskih, Break-Away Friction of PTFE Materials in Lubricated Conditions, Tribology International, 48 (2012), 54-62. https://doi.org/10.1016/j.triboint.2011.03.025.

32. Z. Zhang, W. Liu, Q. Xue, Effects of various Kinds of Fillers on the Tribological Behavior of Polytetrafluoroethylene Composites Under Dry and oil-lubricated Conditions, Journal of Applied Polymer Science, 80 (2001), 1891-1897. https://doi.org/10.1002/app.1286.

33. S.K. Ghosh, C. Miller, D. Choudhury, J.A. Goss, M. Zou, The Effects of PTFE Thickness on the Tribological Behavior of Thick PDA/PTFE Coatings, Tribology Transactions (2020). https://doi.org/10.1080/10402004.2020.1728001.

34. Exxon Mobil, Mobil DTE Oil Named Series. https://www.mobil.com/en-US/Industrial/pds/GL-XX-Mobil-DTE-Named-Series, 2020, (accessed 20 May 2020).

35. H. Li, J. Xi, Y. Zhao F. Ren, Mechanical Properties of polydopamine (PDA) thin films, Materials Advances, 4 (2019), 405-412. https://doi.org/10.1557/adv.2019.52.

Chapter 5

Effect of Cu Nanoparticles on the Tribological Performance of PDA+PTFE Coatings in Oil-lubricated Condition

5.1 Abstract

The effect of Cu nanoparticles (NPs) on the tribological performance of the thick polydopamine (PDA)+polytetrafluoroethylene (PTFE) coatings in DTE-32 Mobil lubricated condition was investigated. PDA+PTFE+Cu NP coatings with 45 μm thickness were spray-coated with 0.12, 0.25, and 0.50 wt% of Cu NPs in an aqueous PDA+PTFE solution, respectively. The mechanical properties were studied by PeakForce quantitative nanomechanical (PFQNM) characterization and nanoindentation. The Young's modulus increased, and the coefficient of friction (COF) reduced with the addition of Cu NPs compared to PDA+PTFE coating. The PDA+PTFE+0.25 wt% Cu and PDA+PTFE+0.50 wt% Cu coatings increased the durability by 52% and 33% compared to the coating without Cu NPs, respectively. The better tribological performance of the nanocomposite coatings is contributed by the better mechanical properties, better adherence, and enhanced cross-linking between the constituents of the nanocomposite coatings due to the presence of Cu NPs. The addition of 0.25 wt% Cu NPs in PDA+PTFE increased the thermal conductivity by 12%.

Keywords: Nanocomposite coating, Copper nanoparticles, Durability, Thermal conductivity, PFQNM

5.2 Introduction

Polytetrafluorethylene (PTFE) exhibits low friction, but very high wear rate under shear force [1]. Even though, a 5-100 μm PTFE film has a widespread application in cookware, bearings, and compressors [2-6], the high wear rate and delamination is limiting the use of PTFE coating in oil-lubricated condition. Different nanoparticles (NPs) have been added to the PTFE matrix to improve the durability of thin PTFE films [7-16]. NPs, even at smaller quantities, can affect the tribological performance of polymer composites due to higher specific surface area, low interparticle separation, and interfacial reaction between the polymer and NPs [17-19]. However, at higher concentration, the NPs aggregate themselves due to strong Van Der Waals attraction and it inversely affect the physical and mechanical properties of the polymeric nanocomposites [17-19].

Copper (Cu) has been used to improve the tribological behavior of PTFE films [10-11]. The high mechanical strength of the Cu NPs makes it a very prominent filler material for coating applications. Beckford et al. used 0.01wt% Cu in the PTFE layer to enhance the longevity of the polydopamine (PDA)/PTFE thin films by two-fold [10]. Cu NPs melt at a much lower melting temperature than that of bulk Cu [20]. The melting of Cu NPs helps to spread and compact the film, which resulted in increased cohesion between the constituents of the films. The cohesive films adhere better to the cast iron substrate [10]. In addition to cohesion, NPs show an anchoring property to the substrate, which also helps to improve the adhesion between the film and the substrate [12]. Furthermore, a PDA coated Cu NP can increase the longevity of the PDA/PTFE films by 2-times [11]. Inspired by Lee et al. [21-22], polydopamine (PDA) has been used as an adhesive layer to adhere to the PTFE coating better to different substrates and enhance the wear resistance of the coating [23-27]. PDA, a bioinspired adhesive, shows high adhesion to metallic

surfaces and PTFE coating [23-27]. The better adhesion and load carrying capacity helps increasing the durability of the PDA/PTFE coating of different thickness compared to the PTFE coating itself [25].

Even though the PDA/PTFE coating has been studied extensively in dry conditions, not much progress has been made to study the tribology of the PTFE in different lubricated states [28-33]. In oil lubricated conditions the wear of the PTFE coating is dominated by the delamination of the coating [34]. Recently, Ghosh et al. reported that PDA's addition in the PTFE matrix helps to increase the durability of the PTFE thick films in Mobil DTE-32 lubricated tribological setup [34]. It was reported that better nanomechanical properties, change in bonding structure, and improved adherence to the cast iron was accounted for the enhanced longevity of the PDA+PTFE thick films [34].

PTFE is a thermal and electrical insulator [1]. However, in oil lubrication conditions, it is essential to have a higher thermal conductivity to dissipate the heat generated during tribo-contact. Recently, polymer matrix composites have been widely used in heat exchangers and electronic packaging due to the light weight of the polymers [35]. Metallic NPs have been added to the polymers to improve the thermal conductivity of those polymer matrix composites [35]. Due to their high thermal conductivity, Cu NPs are widely used to improve the thermal conductivity of different polymersNP. It is hypothesized that the addition of Cu NPs, even at a minimal amount, can significantly improve the thermal conductivity of the PDA+PTFE coatings.

The effect of Cu NPs on the thermal conductivity and tribological behavior of PDA+PTFE thick films in Mobil DTE-32 lubricated condition in a single load setup is reported in this article. The change in Young's modulus, adhesion, and hardness of the PDA+PTFE nanocomposite

coatings due to the introduction of Cu particles and how these changes affect the tribology of the PDA+PTFE thick films were also reported in this study.

5.3 Experimental Methods

5.3.1 Sample Preparation

A cast iron substrate (McMaster-Carr, USA) with a thickness, diameter, and roughness of 6 mm, 40 mm, and 2.39 μm, respectively, was used for this study. The roughness of the cast iron substrate was measured by optical microscopy over an 80 μm × 80 μm scan size. Three different measurements were taken, and the average roughness is reported here. The cast iron substrates were cleaned in acetone for 20 min using a sonicator to remove dirt and oil. After the acetone cleaning, the samples were cleaned in isopropyl alcohol in a sonicator for 10 min, followed by drying using nitrogen gas. Three sets of coatings were prepared by first mixing dopamine hydrochloride (Sigma Aldrich, USA), PTFE NP (with an average particle diameter of 230 nm) aqueous dispersion (Teflon™ PTFE DISP 40, The Chemours Company, USA), and 0.12, 0.25, or 0.50 wt% of Cu NPs (US Research Nanomaterials, Inc.), respectively, in a beaker on a magnetic stir plate, and the coating was polymerized using the combination of temperature, time, light, and oxidizers. Once polymerized, the coating mixture was then spray coated over the cast iron substrates. The coated substrates were placed over a hot plate for 5 min at 120°C to remove water, and then in an oven at 300°C for 5 min to remove the wetting agent in the PTFE dispersion, and finally, cured at 372°C for 5 min while applying a pressure of 500 psi using a hot press. A set of control samples without Cu NPs in the PDA+PTFE matrix were prepared using the same procedure as PDA+PTFE+Cu nanocomposite coatings.

5.3.2 Coating Characterization

The size of the Cu NPs was investigated using a transmission electron microscope (TEM) (FEI Titan 80-300, Thermo Fisher Scientific, USA). A drop of Cu NPs diluted to 0.005 vl% in water was placed on a EMS300-Cu TEM grid for imaging. The distribution of Cu NPs in the coating spray mixture was studied by using TEM. A drop of diluted PDA+PTFE+0.25 wt% Cu coating mixture was deposited on the TEM grid for imaging. The thickness of the coating was measured using a stylus profilometer (Dektak, Bruker, USA). The bonding structures of the coatings were studied using an X-ray photoelectron spectroscopy (XPS; PHI 5000 VersaProbe, ULVAC-PHI, Kanagawa, Japan).

5.3.3 Tribological Testing

A set of linear reciprocating wear tests were carried out using a universal mechanical tester (UMT-2, Bruker, USA). The tribological behavior of the coatings in boundary oil-lubricated conditions was studied with a ball-on-disc arrangement under 10 N normal load at a speed of 0.1 m/s and with a stroke length of 5 mm. Mobil DTE-32, a common oil used in various journal and roller bearing operations, was used as the oil for this study to evaluate the PDA+PTFE coating as a replacement for tin Babbitt in journal bearings. The Mobil DTE-32 shows high chemical and thermal stability and high resistance to sludging [36]. A chrome steel ball with 6.35 mm diameter and 162 ± 7 nm average roughness was used as the counterface. The durability of the coatings was determined by performing progressive tribological tests because it is hard to determine when the coating failed due to the similar coefficient of friction (COF) of the coated and the bare cast iron in oil-lubricated condition. A series of tribological tests were performed on each coating at different number of cycles and the wear depth of the coating was monitored. The coating was

characterized as failed when the wear depth reached to a critical value (> 44 μm), just 1 μm less than the coating thickness to avoid the interaction of the counterface and cast iron substrate in durability measurement. Scratch tests were performed using a diamond tip with a 400 μm diameter and a 120º full cone angle. The scratch tests were performed under a linearly varying load from 0.5 to 8 N at a speed of 0.01 cm/seconds over 1 cm length using the UMT-2. A 3D laser scanning confocal microscope (VK X260K, Keyence Corporation, USA) was used to study the wear tracks and understand the wear mechanisms of the nanocomposite and control coatings.

5.3.4 Nanomechanical Property Characterization

The surface morphology, Young's modulus, and adhesion force of the PDA+PTFE and the PDA+PTFE+Cu nanocomposite coatings were measured using the PeakForce quantitative nanomechanical (PFQNM) module of an AFM (Dimension Icon, Bruker USA). A RTESPA-300-30 AFM probe (Bruker, USA) with a radius of 30 nm was used for the PFQNM mapping. Each scan line contains 512 measurement data points. An average of 3 different measurements, along with the property maps, are presented in this article. The hardness and Young's modulus of the coatings was determined by nanoindentation using a TriboIndenter (TI-900, Hystrion, USA) using a spheroconical diamond tip with a 1-μm tip radius and a 60º cone angle. A maximum of 50 μN nanoindentation load was used with a loading and unloading rate of 10 μN/s. The average depth of indents was maintained at 200-300 nm [33]. The average of 10 measurements for each coating is reported in this study.

5.3.5 Thermal Conductivity Measurement

The thermal conductivity measurements of the coatings were performed using a custom-built tester according to the ASTM 5470-06 standard. Data was collected by placing a circular sample of stand-alone PDA+PTFE coating with a diameter of 38.1 mm and thickness of 800 µm between two cylindrical copper bars; one provided a constant thermal flux via an internal cartridge heater, and the other removed the heat through a circulating water line.

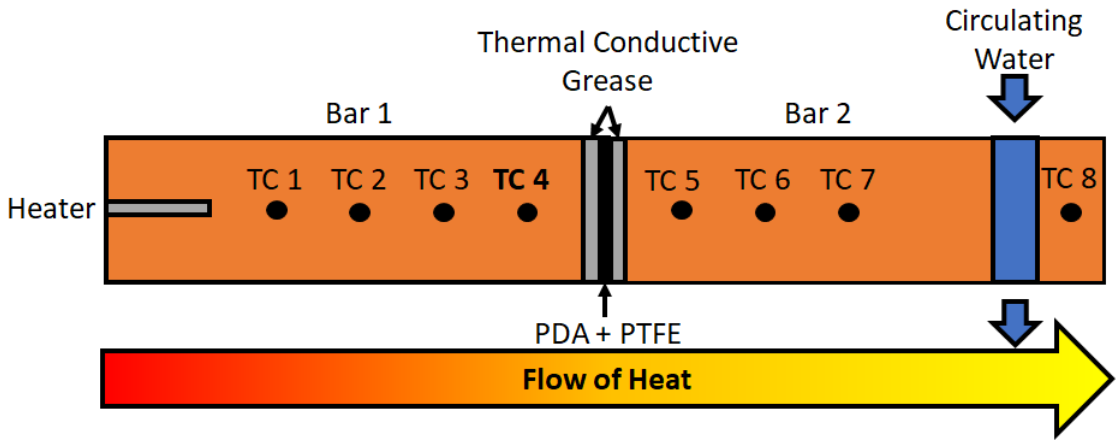

Fig. 5.1 The schematic of the thermal conductivity measurement of the coatings using an in-house setup.

Embedded thermocouples allowed the linear thermal gradient across each bar to be measured in real-time. From this data, both the temperature difference across the sample area, as well as the average heat flux through the two copper bars, can be determined at a steady-state condition. Figure 5.1 illustrates the heat flow setup from the heater (left) to the heat sink (circulating water on the right). Assuming that the thickness of the sample is known and possesses the same cross-sectional area of copper bars, the experimental thermal conductivity can be extracted from Equation 1:

$$R = \frac{\Delta T}{Q} = \frac{L}{kA} \tag{5.1}$$

where k is the thermal conductivity (W/mK), R is thermal resistance (°C/W), A is the cross-sectional area (m^2), L is the thickness of the sample (m), ΔT is the temperature drop across the sample (°C), and Q is the heat flux (W).

For each coating sample, the steady-state thermal conductivity was measured in a way to minimize the surface contact resistance. First, a known mass of Wakefield 120 series thermal grease was compressed between the end of the two copper bars, the system was allowed to come to a steady state; and a baseline thermal resistance measurement was taken. After recording the baseline, the stand-alone PTFE sample was then compressed between the two copper bars with the thermal grease, allowed to come to a steady-state, and a total thermal resistance value was recorded. The baseline resistance measurement was then subtracted from this total measured thermal resistance value; and with a known sample thickness, the thermal conductivity was extracted using Equation 5.1. It was assumed that the interfacial resistance between the PTFE and thermal grease was negligible.

5.4 Results and Discussion

5.4.1 Coating Topography

The size and shape of the Cu NPs were studied using a TEM and is reported in Figure 5.2. The TEM image was acquired from a 0.005 vl% Cu NP in water. It can be observed from the TEM image that even at a low concentration, the Cu NPs coagulate with each other and stack themselves. The size of the Cu NPs was 40-50 nm.

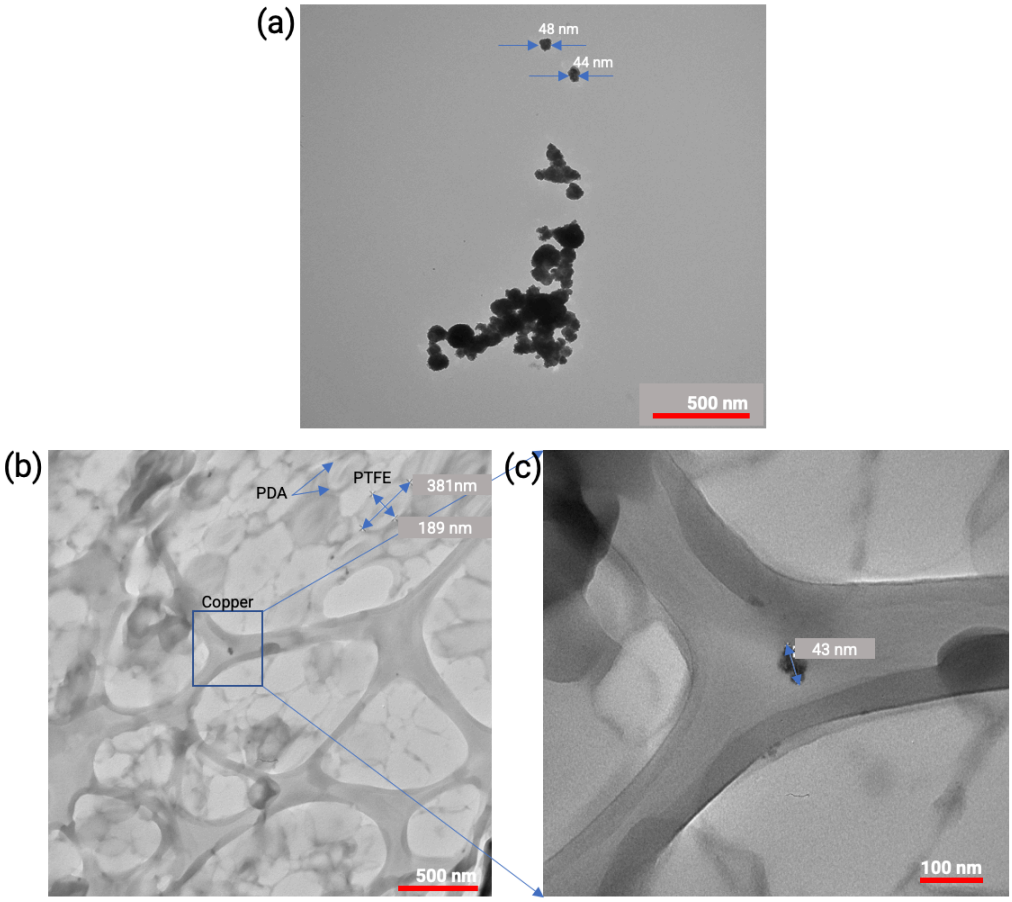

Fig. 5.2 A TEM image of the Cu nanoparticles and PDA+PTFE+0.25 wt% Cu coating. (a) Cu nanoparticles, (b) diluted PDA+PTFE+0.25 wt% Cu coating, and (c) high resolution image of the Cu NPs.

The TEM image of the PDA+PTFE+0.25 wt% Cu NPs coating mixture shows that the Cu NPs are uniformly distributed throughout the coating (Figure (5.2b)). The TEM image clearly shows the Cu and PTFE particles as well as the PDA connecting the PTFE particle aggregates (Figure 5.2(b)). A higher magnification TEM image shows the size of Cu NP is 43 nm (Figure 5.2(c)).

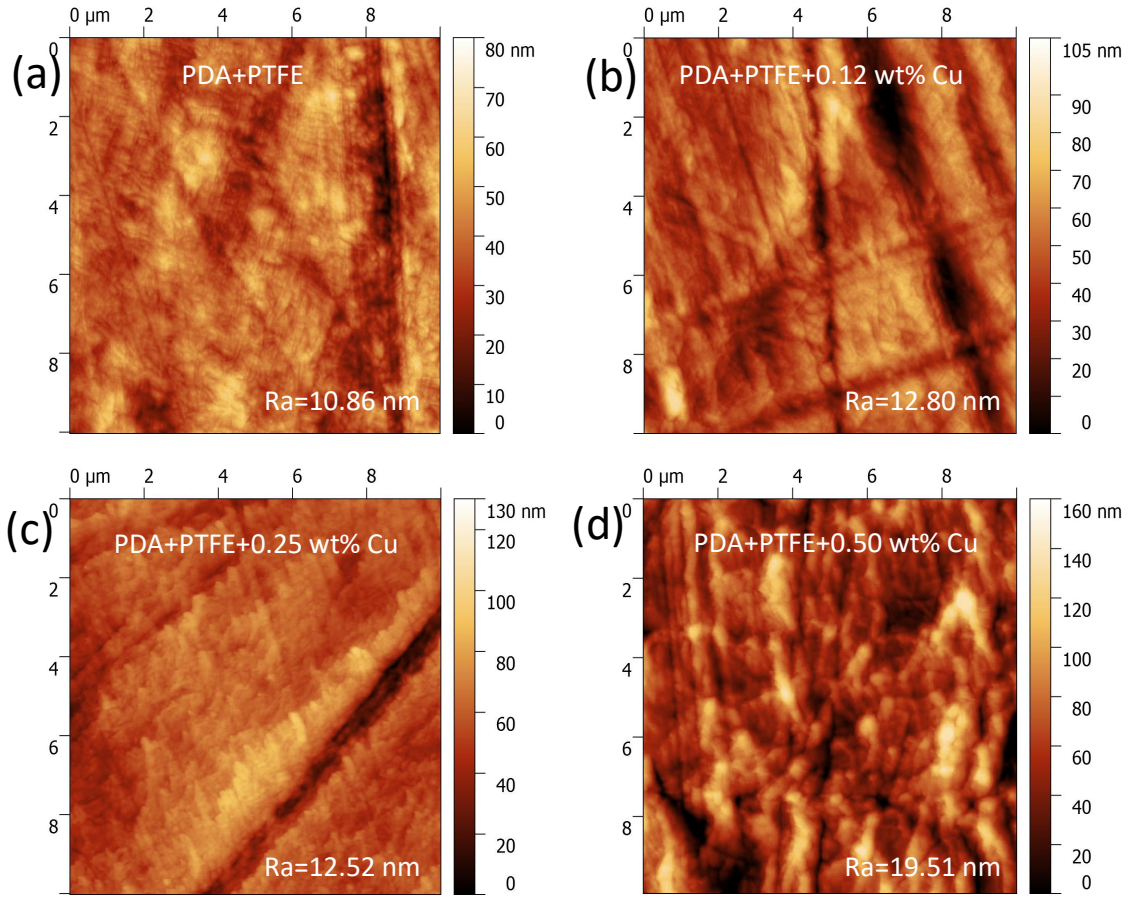

Fig. 5.3 AFM images of the coatings showing compacted surface topography (a) PDA+PTFE (control), (b) PDA+PTFE+0.12 wt% Cu, (c) PDA+PTFE+0.25 wt% Cu, and (d) PDA+PTFE+0.50 wt% Cu.

The AFM topography images of the PDA+PTFE and PDA+PTFE+Cu nanocomposite coatings are presented in Figure 5.3. It was observed from Figure 5.3 that all coatings are compact without porous spots. Compression marks was observed over all the samples. However, the PDA+PTFE+0.50 wt% Cu coatings show a rougher topography. The average roughness of the coatings measured from the AFM images is shown in Figure 5.4. Since the average roughness of these coatings is 11-19 nm, which is 2 orders of magnitude lower than that of the substrate of 2.39 µm, the roughness should not come from the substrate. While adding a small amount of Cu NPs

in the coating did not change the average roughness much, adding more Cu NPs (0.50 wt%) resulted in a significantly increased roughness. The increasing aggregation of Cu NPs was responsible for the observed roughness increase.

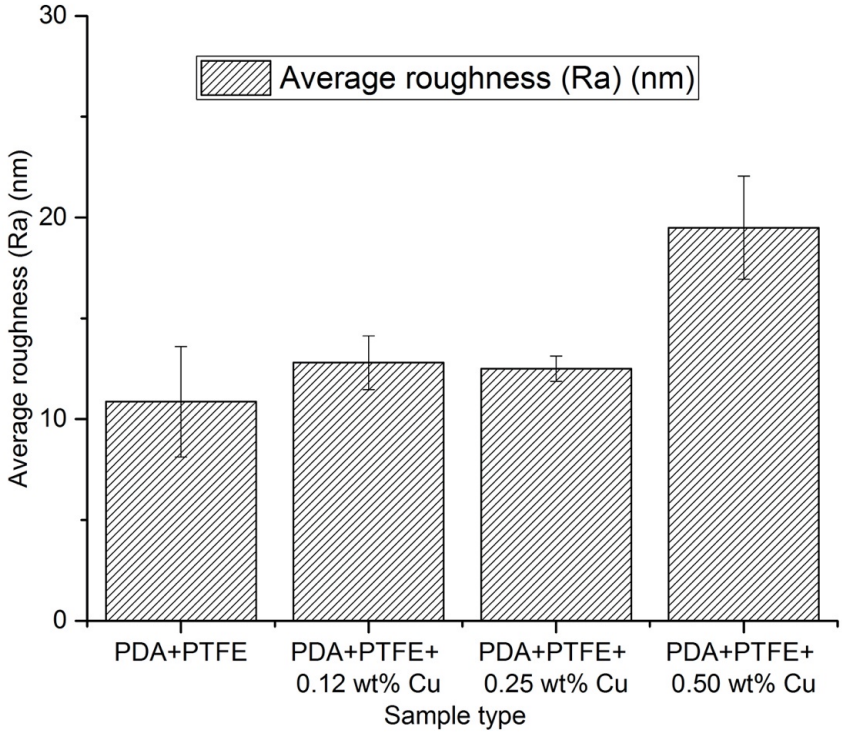

Fig. 5.4 Comparison of average roughness (Ra) among PDA+PTFE and PDA+PTFE+Cu nanocomposite coatings.

5.4.2 Nanomechanical Properties

The Young's modulus and adhesion maps of the control and the nanocomposite coatings are reported in Figure 5.5 and 5.6, respectively. It was observed from Figure 5.5 that the Young's modulus of the PDA+PTFE coating is uniform throughout the mapped area.

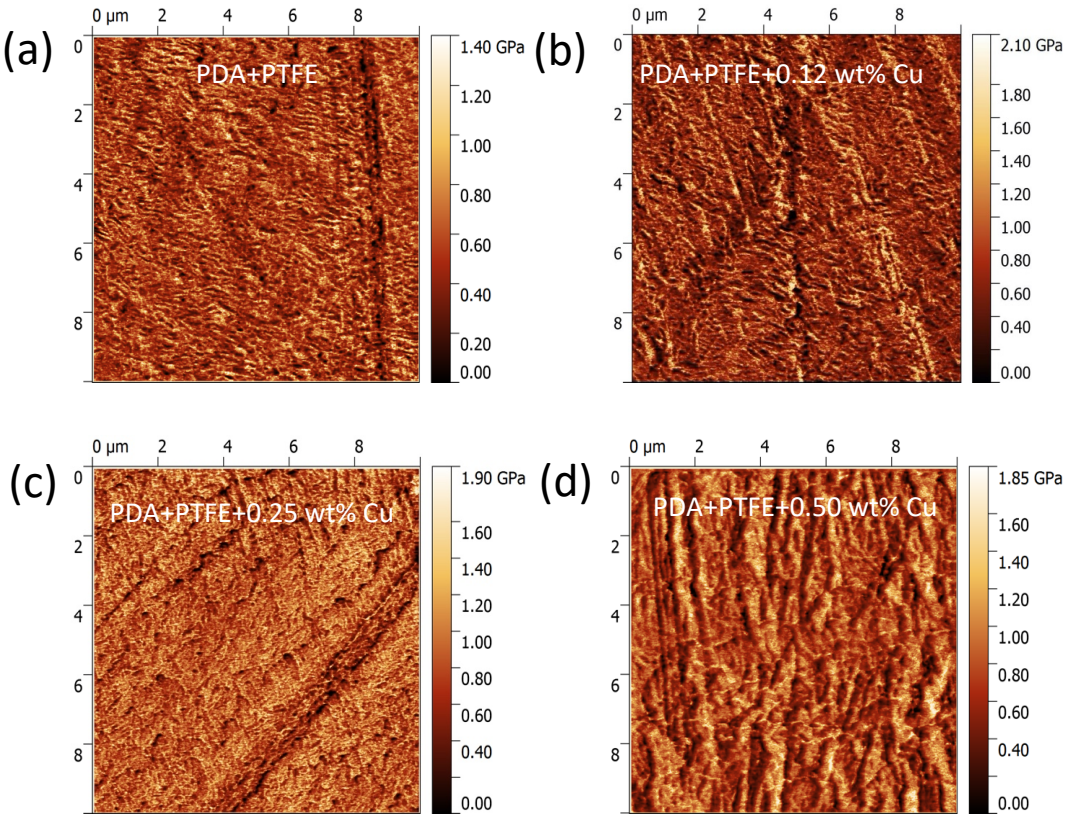

Fig. 5.5 Young's modulus map from PFQNM measurement of the PDA+PTFE and PDA+PTFE+Cu coatings. (a) PDA+PTFE, (b) PDA+PTFE+0.12 wt% Cu, (c) PDA+PTFE+0.25 wt% Cu, and (d) PDA+PTFE+0.50 wt% Cu.

The PDA+PTFE+0.12 wt% Cu and PDA+PTFE+0.25 wt% Cu coatings also showed very uniform Young's modulus in the mapped area due to the homogenous distribution of the Cu NPs in the PDA+PTFE matrix. However, the mapped area of the PDA+PTFE+0.50 wt% Cu coating showed variation in the Young's modulus due to the non-uniform dispersion of the Cu NPs. Similarly, the adhesion maps of the PDA+PTFE, PDA+PTFE+0.12 wt% Cu, and PDA+PTFE+0.25 wt% Cu NP coatings are also uniform compared to that of the PDA+PTFE+0.50

wt% Cu coating, as shown in Figure 5.6. The non-uniformity of the adhesion in the mapped area is related to the roughness of the PDA+PTFE+0.50 wt% Cu NP coating.

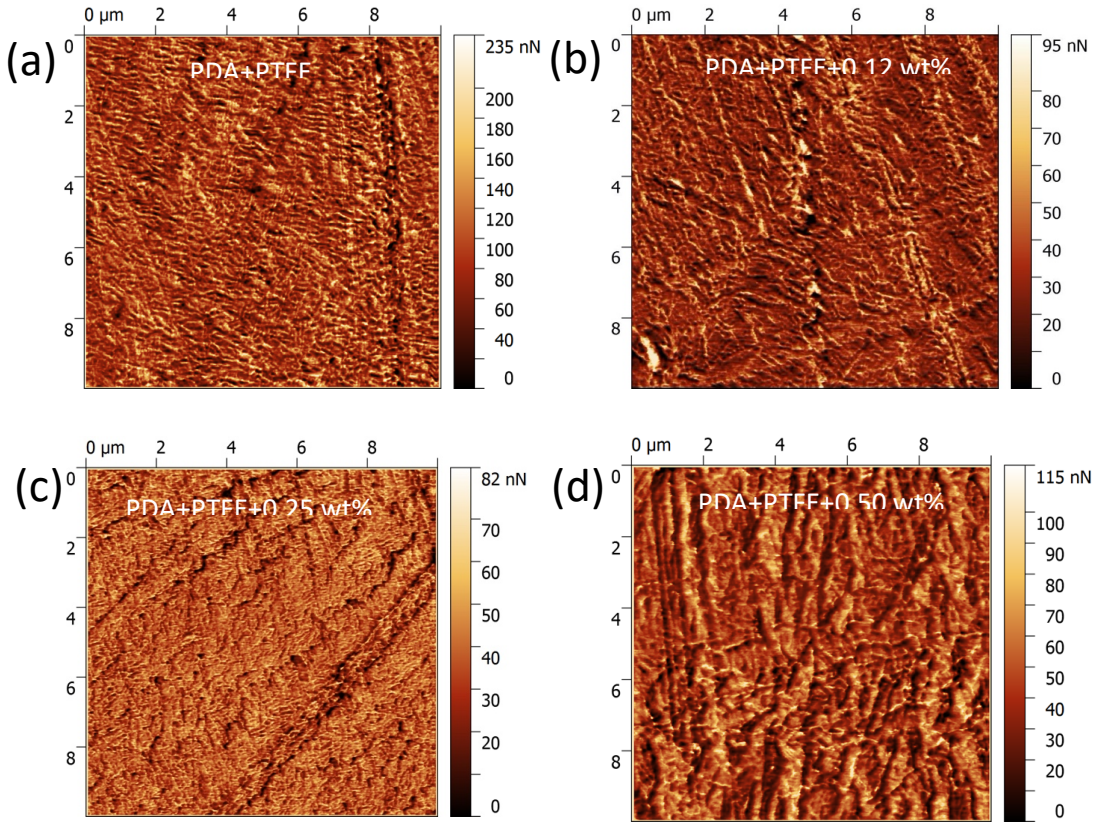

Fig. 6 Adhesion force map from PFQNM measurement of the PDA+PTFE and PDA+PTFE+Cu coatings. (a) PDA+PTFE, (b) PDA+PTFE+0.12 wt% Cu, (c) PDA+PTFE+0.25 wt% Cu, and (d) PDA+PTFE+0.50 wt% Cu.

The average Young's modulus from three AFM PFQNM measurements and ten nanoindentation measurements, along with their standard deviations, are presented in Figure 5.7(a). The Figure shows that the PDA+PTFE coatings with Cu NPs have a higher Young's modulus than the control coating. The increase was ascribed to the superior Young's modulus of the copper. Higher stiffness of the PDA+PTFE+Cu NPs coating means higher load required to cause elastic deformation in the coating [33].

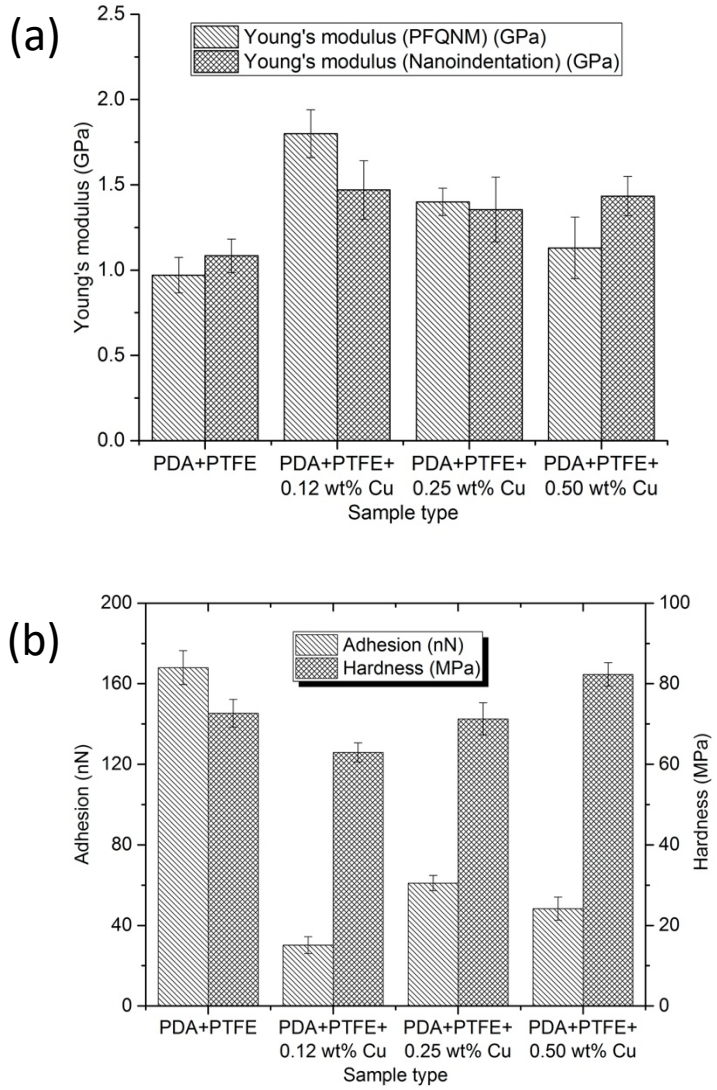

Fig. 5.7 Comparison of the mechanical properties (Young's modulus, adhesion force, and hardness) of the control and PDA+PTFE+Cu nanocomposite coatings. (a) Young's modulus and adhesion force and (b) hardness.

It is noted that, in Figure 5.7(a), the average Young's modulus of the coatings contains Cu NPs measured from the AFM PFQNM decreased slightly with the Cu NP concentration, while that measured by nanoindentation did not. This could be attributed to the tendency of Cu NPs to stack themselves to form bigger particles and thus lower the dispersity of the Cu NPs at higher

concentrations. The non-uniform distribution of NPs leaves most part of the coating without Cu NPs, which resulted in lower Young's modulus with increased Cu NP concentration. Unlike AFM mapping, nanoindentation is only performed at isolated locations, and therefore, it is less sensitive to local material variations from the Cu NP concentration changes.

In contrast, the adhesion force between the AFM probe and the control coating surface was much higher than the adhesion force of the nanocomposite coatings, as shown in Figure 5.7(b). The lower adhesion of the control coating is likely caused by larger contact area between the AFM tip and the coating due to lower Young's modulus.

Hardness plays a critical role in the plastic deformation of the polymeric coating. The nanohardness of the coating was measured by nanoindentation and presented in Figure 5.7(b). It can be observed that the addition of 0.12 wt% Cu NPs slightly reduced the hardness. A small amount of creep was observed during the indentation of the PDA+PTFE+0.12 wt% Cu coating, indicating a slight less compaction of this sample, which contributed to the measured lower hardness of the coating. Further increase of Cu NPs concentration showed a slight increasing in the hardness. The aggregated harder Cu NPs were responsible for the increased hardness of these coatings.

5.4.3 Tribological Performance

The COF profiles of the control sample, the PDA+PTFE+0.12 wt% Cu, PDA+PTFE+0.25 wt% Cu, and PDA+PTFE+0.50 wt% Cu coatings evaluated in boundary oil-lubricated condition for 15,000, 15,000, 20,000, and 18,000 cycles, respectively, are reported in Figure 5.8.

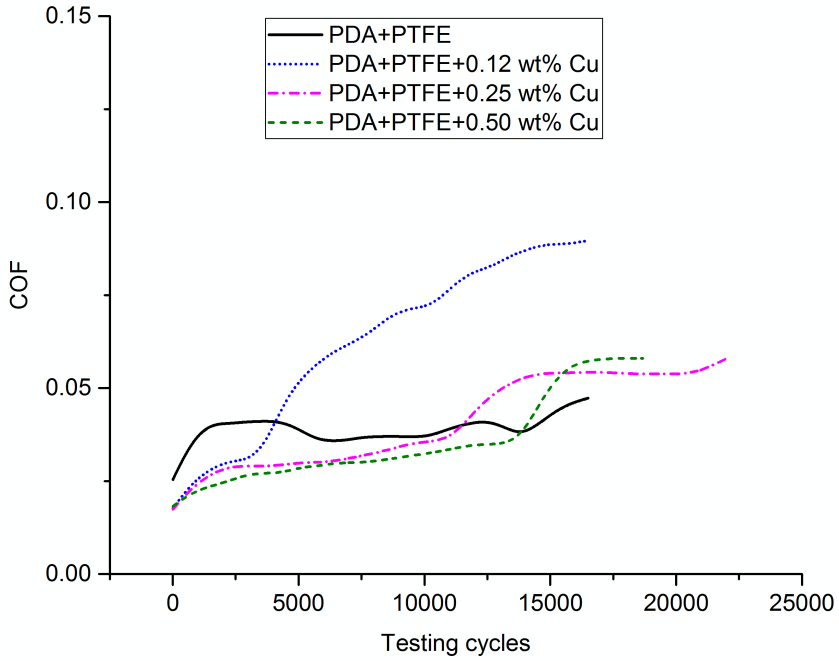

Fig. 5.8 COF profiles of the PDA+PTFE, PDA+PTFE+0.12 wt% Cu, PDA+PTFE+0.25 wt% Cu, and PDA+PTFE+0.50 wt% Cu coatings tested in boundary oil-lubricated condition for 15,000, 15,000, 20,000, and 18,000 cycles, respectively.

The starting COF of the control coating was 0.025, which transitioned into 0.045 after 1000 cycles of testing and remained there until 4000 cycles of testing (Figure 5.8), after which the COF dropped to 0.035 and then increased rapidly after 13,000 cycles of testing. All the nanocomposite coatings containing Cu NPs showed a lower starting COF, which can be attributed to the significantly lower adhesion force of the coatings than the control coating. The nanocomposite coating contains 0.12 wt% Cu NPs showed a rapid increase in the COF at about 3000 cycles of testing. It was hypothesized that the early deformation in the coating was responsible for the transition. The nanocomposite coatings containing 0.25 and 0.50 wt% Cu NPs show a rapid increase in the COF after 11,000 and 13,000 cycles, respectively.

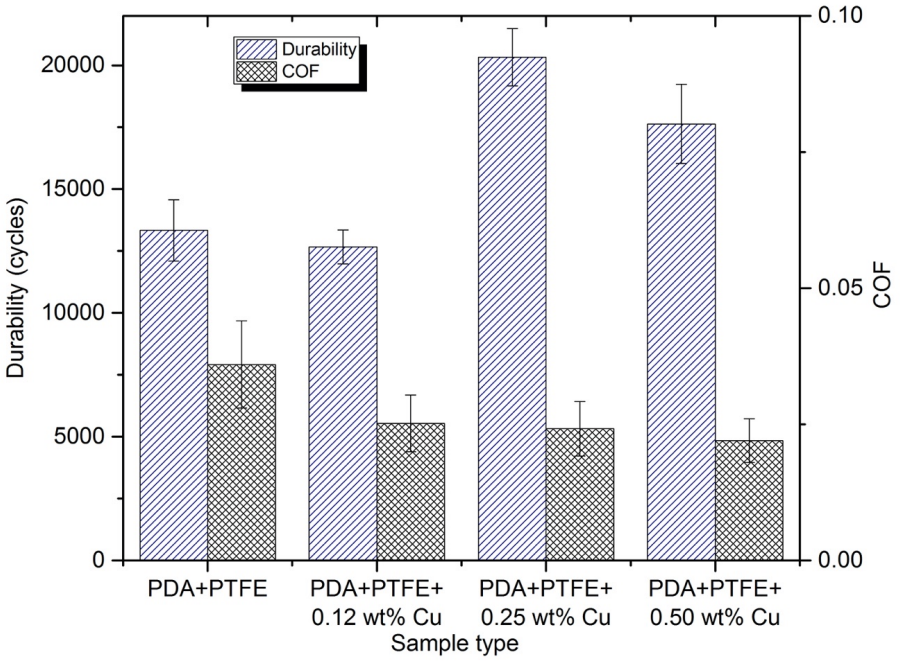

Fig. 5.9 Comparison of average COF and durability of the PDA+PTFE, PDA+PTFE+0.12 wt% Cu, PDA+PTFE+0.25 wt% Cu, and PDA+PTFE+0.50 wt% Cu coatings tested in boundary oil-lubrication.

Figure 5.9 shows the average COF and durability of the control and the nanocomposite coatings measured over the wear lifespan of these coatings. The average COF of the coatings were determined from the COF of first 2500 cycles of testing to eliminate the effect of delamination in the COF. It can be seen in Figure 5.9 that the PDA+PTFE coating has an average COF of 0.036. All the PDA+PTFE+Cu NPs coatings showed lower average COF than the control coatings. The higher adhesion of the PDA+PTFE coating was responsible for the higher COF of the control coating. The durability testing indicated that the control coating was durable for 13,333 cycles in Mobil DTE-32 lubricated conditions. The addition of 0.12 wt% Cu NPs had a detrimental effect on the durability of the coatings, resulting in a slight decrease in durability to 12,667 cycles. The slight decrease was attributed to the decrease in the hardness of the coating. It was hypothesized

that the PDA+PTFE+0.12 wt% Cu coating deformed earlier to the critical wear depth of 11-12 μm due to the lower hardness compared to PDA+PTFE coating, thus start the delamination process sooner than the control coating. Interestingly, adding 0.25 and 0.50 wt% of Cu NPs increased the durability of the coating to 20,333 cycles and 17,633 cycles, respectively. The enhanced durability is attributed to the formation of micro cracks that helps decrease the debris size [10] and the better coating adherence to the substrate compared to the PDA+PTFE due to the pinning effect of the NPs. The decrease in the durability of the coating containing 0.50 wt% Cu NPs compared to the coating containing 0.25 wt% Cu can be ascribed to the Cu NP aggregation at a higher concentration. The aggregation of the Cu NPs is responsible for abrasive third-body wear, which accelerates the delamination process. To further study the adhesion and wear mechanism of these nanocomposite coatings, scratch tests using a diamond tip were conducted and will be explained later.

Figure 5.10 shows the wear track images of the different types of coatings tested. It was observed that after 15,000 cycles, the control coating was worn out, but the cast iron was not exposed, and there were minimum wear scars on the counterface (Figures 5.10(a) and (b)). The wear track of the PDA+PTFE+0.12 wt% Cu coating, on the other hand, showed severe wear after 15,000 cycles with exposed cast iron and severe wear on the counterface (Figures 5.10(c) and (d)). However, PDA+PTFE+0.25 wt% Cu coating showed minimum exposed cast iron after 20,000 cycles, but there was no wear scuff on the counterface (Figures 5.10(e) and (f)). Similarly, PDA+PTFE+0.50 wt% Cu coating after 18,000 cycles, showed some exposed cast iron but no white severe wear line was observed and there was no wear scuff on the counterface (Figures 5.10(g) and (h)). Figure 7-10 shows that the addition of 0.25 and 0.50 wt% Cu NPs helped to delay the coating delamination, which improved the coating durability in oil-lubricated condition.

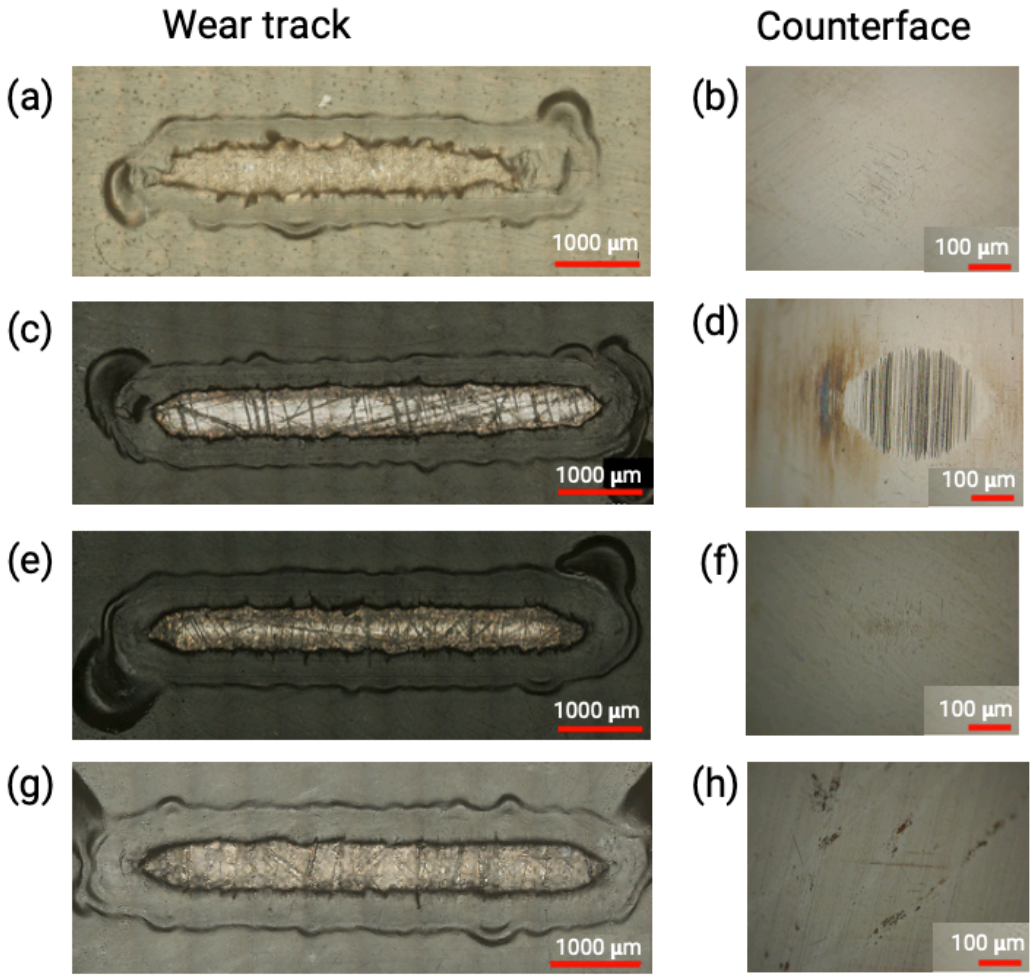

Fig. 10 Optical microscope images of the wear tracks and counterfaces of the PDA+PTFE, PDA+PTFE+0.12 wt% Cu, PDA+PTFE+0.25 wt% Cu, and PDA+PTFE+0.50 wt% Cu coatings tested in boundary oil-lubricated condition for 15,000, 15,000, 20,000, and 18,000 cycles, respectively. (a), (c), (e), and (g) are the wear tracks of the PDA+PTFE, PDA+PTFE+0.12 wt% Cu, PDA+PTFE+0.25 wt% Cu, and PDA+PTFE+0.50 wt% Cu coatings and (b), (d), (f), and (h) are the counter surfaces for (a), (c), (e), and (g), respectively.

5.4.4 Scratch Test

Scratch tests were conducted to understand the adhesion and wear mechanism of the various types of coatings.

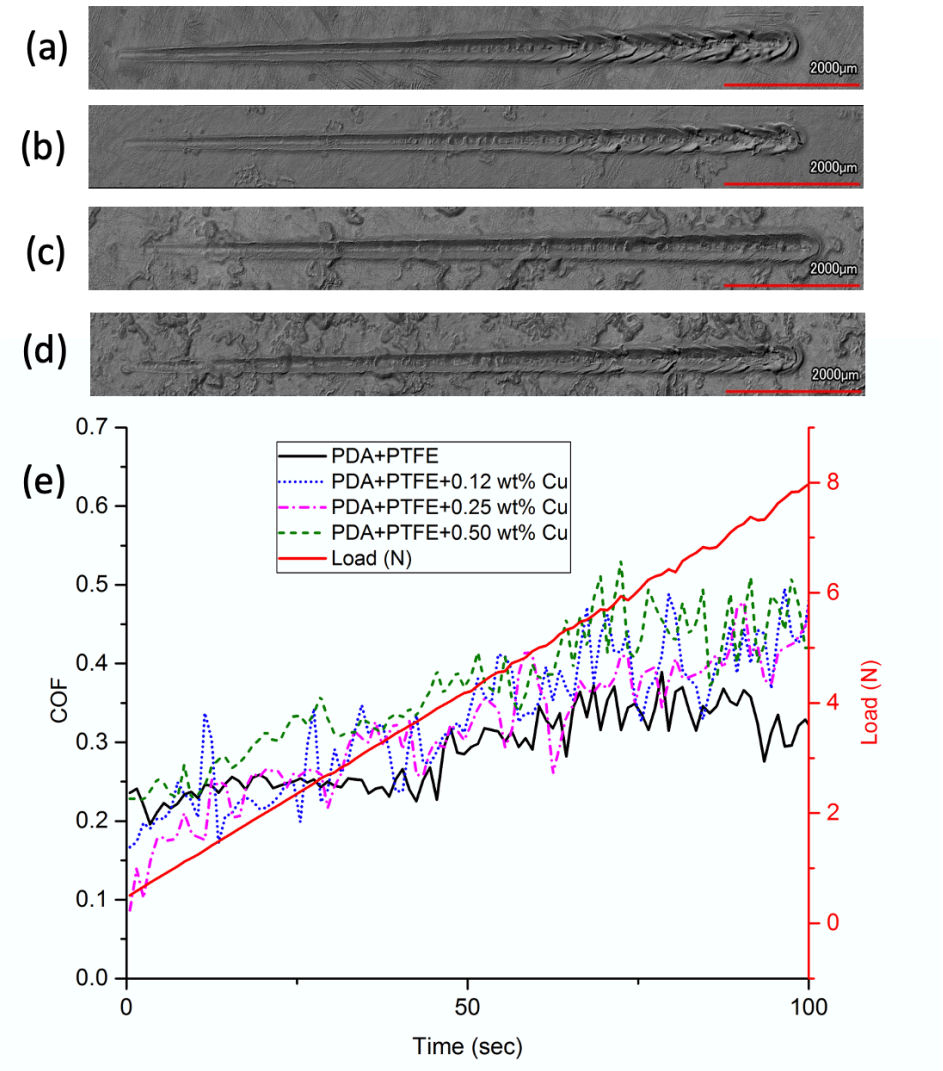

Fig. 5.11 Optical microscope images of the wear tracks of (a) PDA+PTFE, (b) PDA+PTFE+0.12 wt% Cu, (c) PDA+PTFE+0.25 wt% Cu, and (d) PDA+PTFE+0.50 wt% Cu coatings after the scratch test and (e) the COF profiles of the PDA+PTFE, PDA+PTFE+0.12 wt% Cu, PDA+PTFE+0.25 wt% Cu, and PDA+PTFE+0.50 wt% Cu coatings and the load profile from the scratch test.

The images of the wear tracks, the normal load, and the COF profiles of the scratch tests are shown in Figure 5.11. The PDA+PTFE coating was deformed and started to form wrinkle at 4 N (Figure 5.11(a)), which was also evident from the sudden increase in the COF (Figure 5.11(e)). The PDA+PTFE+0.12 wt% Cu coating had slightly less deformation under the same loading conditions (Figure 5.11(b)). Interestingly, the PDA+PTFE+0.25 wt% Cu coating showed a much smoother wear track, and there was no trace of wrinkle formation even at 8 N force (Figure 5.11(c)). The better load carrying capacity contributed to the higher resistance to the deformation of the PDA+PTFE+0.25 wt% Cu coating. However, the PDA+PTFE+0.50 wt% Cu coating started to form wrinkles at around 6 N, caused by the third-body wear of the bigger copper particle aggregates (Figure 5.11(d)).

5.4.5 Wear Progression

To further compare the wear mechanism, wear progression tests were performed on the control and the best-performing PDA+PTFE+0.25 wt% Cu coatings using the same linear reciprocating tribological test routine.

The coatings were tested for 1000, 2000, 4000, 8000, 10,000, 15,000, 18,000, 20,000 cycles, and the wear depth of the coatings was reported in Figure 5.12. The control coating exhibited a sharp increase in the wear rate after 8,000 cycles, which indicates that the coating has delaminated. This can be attributed to the more porous and the not fully annealed coating at the substrate-coating interface, as previously reported [31].

The PDA+PTFE+0.25 wt% Cu coating showed this transition occurred after 15,000 cycles of testing. The delayed transition to the higher wear rate and delamination of the PDA+PTFE+0.25 wt% Cu coating can be attributed to the better load carrying capacity of the coating, the spreading

of the films due to low melting point of copper, smaller debris size, and the better adhesion of the PDA+PTFE+0.25 wt% Cu coating to the cast iron substrate.

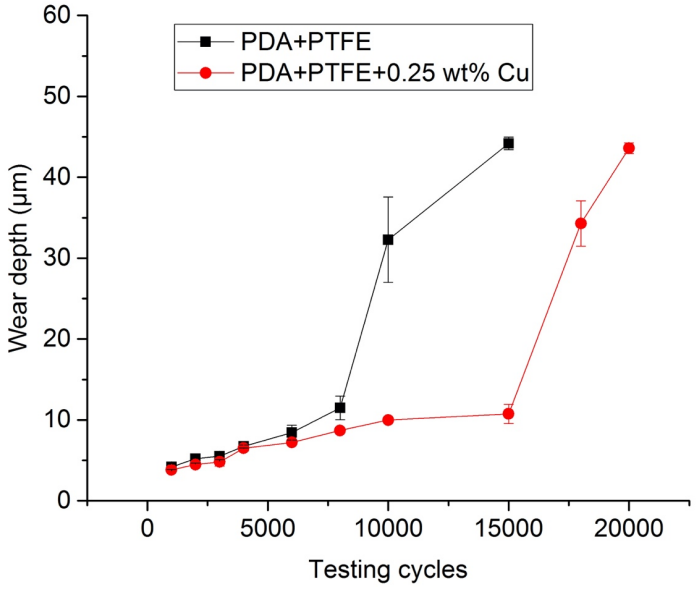

Fig. 5.12 Comparison of wear depth of the control and PDA+PTFE+0.25 wt% Cu coatings after 1000, 2000, 4000, 8000, 10,000, 15,000, 18,000, and 20,000 cycles of testing to investigate the wear progression.

5.4.6 Chemical Analysis

The XPS spectra of the control and PDA+PTFE+0.25 wt% Cu coatings are reported in Table 5.1 and Figure 5.13. Similar to previously reported [34], PDA and PTFE particles cross-linked during the high temperature annealing process and changed the XPS spectra of PTFE coating, as evidenced by the additional bonding other than CF_2-CF_2 as shown in Table 5.1 and Figure 5.13.

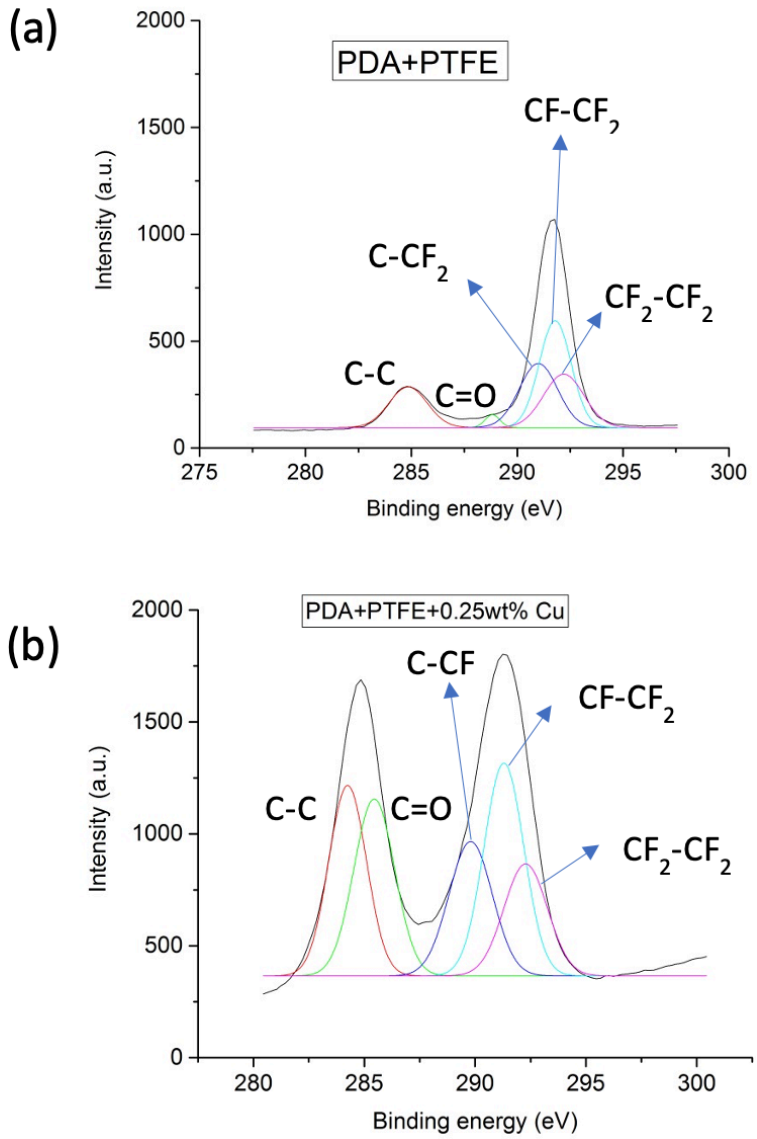

Fig. 5.13 XPS pattern and changes in the bonding structure of (a) PDA+PTFE coating and (b) PDA+PTFE+0.25 wt% Cu coating.

Table 5.1 also show that the percentage of C-C, C=O, and C-CF increased in the coating contain 0.25 wt% Cu compared to the control coating. A decrease in the C-CF_2, CF_2-CF_2, and CF-CF_2 was noticed in the PDA+PTFE+0.25 wt% Cu coating. It was concluded that the presence of Cu NP helped facilitate further shifts in the bonding structure of the control coating. Breaking down of the C-CF_2, CF_2-CF_2, and CF-CF_2 bonds facilitated the shifts to a more carbon dominated

C-C and C-CF bonds. The increased durability of the control coating due to the addition of 0.25 wt% Cu NPs can be attributed to the enhancement in the cross-linking between the constituent PTFE and PDA polymers.

Table 5.1: XPS bonding comparison of different coatings.

Bonding	PDA+PTFE	PDA+PTFE+0.25 wt% Cu
C-C	14.63	23.04
C=O	4.54	16.26
C-CF_2	23.25	0.00
CF_2-CF_2	19.37	13.55
CF-CF_2	38.21	25.75
C-CF	0.00	21.41

5.4.7 Thermal Conductivity

The thermal conductivity of PTFE and Cu is 0.25 and 385 W/mK, respectively [35]. The thermal conductivity of the control coating was 0.25 W/mK, which is the same as that of bulk PTFE [35]. It was noticed that the introduction of PDA particles did not influence the thermal performance of the PTFE. The thermal conductivity of the PDA+PTFE+0.25 wt% Cu nanocomposite coating was 0.28, which is 12% higher than the thermal conductivity of the control coating. The higher thermal conductivity of Cu NPs contributed to the increase in the thermal conductivity of PDA+PTFE coating.

5.5 Conclusion

The effects of the addition of Cu NPs on the friction, wear, and thermal performance of the PDA+PTFE coating was studied. The addition of Cu NPs did not change the hydrophobic behavior

of the PDA+PTFE coatings. The Cu NPs increased the Young's modulus of the coating in every concentration of Cu NP, whereas the nanocomposite coating's adhesion values decreased with the addition of Cu NPs. All PDA+PTFE+Cu NPs coatings showed lower COF compared to PDA+PTFE coating due to the lower adhesion force between the coatings and the counterface. The addition of 0.25 and 0.50wt% Cu NPs enhanced the durability of the PDA+PTFE coating by 52% and 33%, respectively. The enhanced tribological performance of the PDA+PTFE+0.25 wt% Cu and PDA+PTFE+0.50 wt% Cu coatings can be attributed to the lower adhesion force to the counterface, enhanced cross-linking between the PTFE and PDA in the presence of Cu NPs, better adherence to the substrate, and the better load carrying capacity of these coatings. In addition to the better durability, the PDA+PTFE+0.25 wt% Cu coating showed a 12% improvement in the coating thermal conductivity due to the presence of Cu NPs with higher thermal conductivity.

5.6 Acknowledgment

This material is based upon work supported by the U.S. Department of Energy's Office of Energy Efficiency and Renewable Energy (EERE) under the Next Generation Electric Machines: Enabling Technologies Program Award Number DE-EE0007874 and by the National Science Foundation (NSF) under Grant Nos. CMMI-1563227 and OIA-1457888. The views and opinions of authors expressed herein do not necessarily state or reflect those of the United States Government or any agency thereof.

References

1. Dhanumalayan, E., Joshi, G. M.: Performance Properties and Applications of Polytetrafluoroethylene (PTFE)—a Review. Advanced Composites and Hybrid Materials. 1, 247–268 (2018). DOI:10.1007/s42114-018-0023-8

2. Batzar, K.: Cookware Coating Systems, US Patent No. 5250356 A (1993).

3. Tevruz, T.: Tribological Behaviours of Carbon Filled Polytetrafluoroethylene (PTFE) Dry Journal Bearings. Wear. 221, 61-68 (1998). DOI: 10.1016/s0043-1648(98)00258-0

4. Doll, G. L., Evans, R. D., Ribaudo, C. R.: Coated Rolling Element Bearing Cages. US Patent No. 6994475 B2 (2006)

5. Woelki, P., Petit, D., Harig, F.: Self-Lubricating Bearing. US Patent No. 5971617 A (1999)

6. Demas, N.G., Polycarpou A.A.: Tribological performance of PTFE-based coatings for air-conditioning compressors. Surface & Coatings Technology. 203, 307-316 (2008). DOI: 10.1016/j.surfcoat.2008.09.001

7. Beckford, S., Cai, J., Chen, J., Zou, M.: Use of Au Nanoparticle-Filled PTFE Films to Produce Low-Friction and Low-Wear Surface Coatings. Tribology Letters. 56, 223-230 (2014). DOI: 10.1007/s11249-014-0402-4

8. Beckford, S., Cai, J., Fleming, R., Zou, M.: The Effects of Graphite Filler on the Tribological Properties of Polydopamine/PTFE Coatings. TRIBOLOGY LETTERS. 64, 1-10 (2014). DOI: 10.1007/s11249-016-0777-5

9. Choudhury, D., Niyonshuti, I., Chen, J., Goss, J., Zou, M.: Tribological Performance of Polydopamine + Ag Nanoparticles/PTFE Thin films. *Tribology International*. 144,106097 (2020). DOI: 10.1016/j.triboint.2019.106097

10. Beckford, S., Mathurin, L., Chen, J., Zou, M.: The Influence of Cu Nanoparticles on the Tribological Properties of Polydopamine/PTFE + Cu Films. Tribology Letters. 59 (2015). DOI: 10.1007/s11249-015-0543-0

11. Beckford, S., Mathurin, L., Chen, J., Fleming, R., Zou, M.: The Effects of Polydopamine Coated Cu Nanoparticles on the Tribological Properties of Polydopamine/PTFE Coatings. *Tribology International*. 103, 87-94 (2016). DOI: 10.1016/j.triboint.2016.06.031

12. Unal, H., Mimaroglu, A., Kadıoglu, U., Ekiz, H.: Sliding friction and wear behaviour of polytetrafluoroethylene and its composites under dry conditions. Materials and Design. 25, 239-245 (2004). DOI: 10.1016/j.matdes.2003.10.009

13. Pan, D., Fan, B., Qi, X., Yang, Y., Hao, X.: Investigation of PTFE Tribological Properties Using Molecular Dynamics Simulation. TRIBOLOGY LETTERS. 67, (2019). DOI: 10.1007/s11249-019-1141-3

14. Eustathios V.: Fluoropolymer primer having improved scratch resistance. US Patent No. 4049863 A (1977)

15. Zare, Y.: Evaluation of nanoparticle dispersion and its influence on the tensile modulus of polymer nanocomposites by a modeling method. Colloid & Polymer Science. 295(2), 363-369 (2017). DOI: 10.1007/s00396-017-4016-x

16. Zaïri F., Gloaguen J. M., Naït-Abdelaziz M., Mesbah A., Lefebvre J.M.: Study of the effect of size and clay structural parameters on the yield and post-yield response of polymer/clay nanocomposites via a multiscale micromechanical modelling. Acta Mater. 59(10), 3851–3863(2011). DOI: 10.1016/j.actamat.2011.03.009

17. Fu S.Y., Feng X.Q., Lauke B., Mai Y.W.: Effects of particle size, particle/matrix interface adhesion and particle loading on mechanical properties of particulate–polymer composites. Compos Part B. 39(6):933–961 (2008). DOI: 10.1016/j.compositesb.2008.01.002

18. Lee, H., Dellatore, S.M., Miller, W.M., Messersmith, P.B.: Mussel-Inspired Surface Chemistry for Multifunctional Coatings. Science. 318, 426-430 (2007). DOI: 10.1126/science.1147241

19. Lee, H., Lee, Y., Statz, A.R., Rho, J., Park, T.G., Messersmith, P.B.: Substrate-Independent Layer-by-Layer Assembly by using Mussel-Adhesive-Inspired Polymers. Advanced Materials. 20, 1619-1623 (2008). DOI: 10.1002/adma.200702378

20. Beckford, S., Zou, M.: Wear Resistant PTFE Thin Film Enabled by a Polydopamine Adhesive Layer. Applied Surface Science. 292, 350-356 (2014). DOI: 10.1016/j.apsusc.2013.11.143

21. Jiang, Y., Choudhury, D., Brownell, M., Nair, A., Goss, J.A., Zou, M.: The Effects of Annealing Conditions on the Wear of PDA/PTFE Coatings. Applied Surface Science. 481, 723-735 (2019). DOI: 10.1016/j.apsusc.2019.03.076

22. Ghosh, S.K., Miller, C., Choudhury, D., Goss, J.A., Zou M.: The Effects of PTFE Thickness on the Tribological Behavior of Thick PDA/PTFE Coatings. Tribology Transactions, DOI: 10.1080/10402004.2020.1728001(2020). DOI: 10.1080/10402004.2020.1728001

23. Zhao, Y., Zou, M.: Experimental Investigation of the Wear Mechanisms of Thin PDA/PTFE Coatings. Progress in Organic Coatings. 137, 105341(2019). DOI: 10.1016/j.porgcoat.2019.105341

24. Miller, C., Choudhury, D., Zou, M.: The Effects of Surface Roughness on the Durability of Polydopamine/PTFE Solid Lubricant Coatings on NiTiNOL 60. Tribology Transactions, 62, 919-929 (2019). DOI: 10.1080/10402004.2019.1641645

25. Zhang, Z., Xue, Q., Liu, W., Shen, W.: Friction and Wear Characteristics of Metal Sulfides and graphite-filled PTFE Composites Under Dry and oil-lubricated Conditions. Journal of Applied Polymer Science. 72, 751-761 (1999). DOI: 10.1002/(SICI)1097-4628(19990509)72:6<751::AID-APP3>3.0.CO;2-W

26. Jia, B., Li, T., Liu, X., Cong, P.: Tribological Behaviors of several Polymer-Polymer Sliding Combinations Under Dry Friction and Oil-Lubricated Conditions. Wear. 262, 1353-1359 (2007). DOI: 10.1016/j.wear.2007.01.011Get

27. Zhang, Z., Xue, Q., Liu, W., Shen, W.: Friction and Wear Characteristics of Lead and its Compounds Filled Polytetrafluoroethylene Composites Under Oil Lubricated Conditions. Tribology International. 31, 361-368 (1998). DOI: 10.1016/S0301-679X(98)00045-0

28. Xue, Q., Zhang, Z., Liu, W., Shen, W.: Friction and Wear Characteristics of Fiber- and whisker-reinforced PTFE Composites Under Oil Lubricated Conditions. Journal of Applied Polymer Science. 69, 1393-1402 (1998). DOI: 10.1002/(SICI)1097-4628(19980815)69:7<1393::AID-APP14>3.0.CO;2-V

29. Liew, K.W., Chia, S.Y., Kok, C.K., Low, K.O.: Evaluation on Tribological Design Coatings of Al2O3, Ni–P–PTFE and MoS2 on Aluminium Alloy 7075 Under Oil Lubrication. Materials and Design. 48, 77-84 (2013). DOI: 10.1016/j.matdes.2012.08.010

30. Shangguan, Q., Cheng, X.: On the Friction and Wear Behavior of PTFE Composite Filled with Rare Earths Treated Carbon Fibers Under Oil-Lubricated Condition. Wear. 260, 1243-1247 (2006). DOI: 10.1016/j.wear.2005.08.009

31. Ghosh, S.K., Perez, G., Goss, J.A., Beckford, S., & Zou, M.: Tribological properties of PDA+PTFE coating in oil-lubricated condition. Applied Surface Science. 534, 147627 (2020). DOI: 10.1016/j.apsusc.2020.147627Get

32. Hussain, A.R.J., Alahyari, A.A., Eastman, S.A., Thibaud-Erkey, C., Johnston, S., & Sobkowicz M.J.: Review of polymers for heat exchanger applications: Factors concerning thermal conductivity. Applied Thermal Engineering. 113, 1118-1127 (2017). DOI: 10.1016/j.applthermaleng.2016.11.041

33. The engineering toolbox: Resources, Tools and basic information for engineering and design of technical application (https://www.engineeringtoolbox.com/thermal-conductivity-d_429.html), Accessed September (2020)

Chapter 6

Conclusions and Future Work

6.1 Conclusions

The effect of the PTFE coating thickness on the tribological behavior of thick PDA/PTFE coating under 10 N normal load was studied. The PDA underlayer helps to improve the durability of the PTFE coating in every thickness studied, ranging from 3 μm to 42 μm. The PDA underlayer enhances the adhesion between the PTFE top coating and SS substrate, which resulted in the better durability of the PDA/PTFE coatings compared to the PTFE coatings. More importantly, the PDA/PTFE coating showed a pronounced increase in durability when the coating thickness was 34 μm or higher, proving our earlier hypotheses that there is an optimum thickness for a pronounced increase in coating durability. In addition to the better adhesion to the substrate and better load carrying capacity, the drop in contact pressure in the thicker coating was responsible for the pronounced increase in durability of coatings thicker than 34 μm. The 42 μm-thick PDA/PTFE coating is 4.1 times more durable than the PTFE coating of similar thickness. For the rest of the study, the coating thickness was maintained between 40-45 μm.

The effects of adding PDA in the PTFE matrix were studied using spray-coated coatings with coating thickness of 43±3 μm. The addition of hydrophilic PDA decreased the hydrophobicity of the PTFE coating from 142° to 121°. The non-compacted PDA+PTFE coatings were 11 times more durable in dry conditions than the PTFE coatings. They were much more durable due to the better adhesion of the coatings to the SS substrates, the enhanced transfer film formation, and the better load-carrying capacity of the coatings compared to the PTFE coatings. The non-compacted PDA+PTFE coating showed a porous structure. Hot compaction decreased the roughness and porosity of the coatings by 41 and 63 times, respectively. Furthermore, compacted PDA+PTFE

coating showed 22% lower COF and 2.60 times higher durability than those of the non-compacted PDA+PTFE coating, respectively, which confirms the earlier hypothesis that reducing the porosity of the PDA+PTFE coatings will have a beneficial effect on the tribological performance of the PDA+PTFE coatings. In addition to better adhesion to the SS substrate and better load-carrying capacity, reduction of porosity and roughness due to the hot-compaction prevented the local and global deformation of the compacted PDA+PTFE coatings during wear tests, which in turn improved the durability of the coating.

The tribological properties of compacted PTFE and PDA+PTFE coatings deposited by spray coating were studied and correlated to their mechanical properties. Both coatings were tested in boundary oil-lubricated conditions where a Mobil DTE-32 was used as the oil. Both coatings showed similar COF that is 62.5% lower than in dry conditions. The PDA+PTFE coatings were five times more durable than the PTFE coatings in boundary oil-lubricated conditions. The addition of PDA helped increase the Young's modulus of the coatings from 0.61 GPa to 0.97 GPa. The adhesion of the PDA+PTFE coating surface measured by an AFM tip was slightly higher than that of the PTFE coating surface. The better nanomechanical properties of the PDA+PTFE coatings and the cross-linking between the PDA and PTFE contributed to the better durability of the PDA+PTFE coatings than the PTFE coatings in oil-lubricated condition. The cross-linking of the PDA and PTFE occurred during the high-temperature annealing process. The delamination of the coating dominated the wear mechanism of the PDA+PTFE coatings after the wear depth reached a critical thickness.

Cu NPs of 0.125, 0.25, and 0.50 wt% were added to the PDA+PTFE coatings to study the wear mechanisms and the effects of NPs on the wear properties of PDA+PTFE coatings in oil-lubricated conditions. The addition of Cu NPs increased the Young’s modulus and decreased the

adhesion force and COF of the PDA+PTFE coatings. Additionally, the addition of 0.25 and 0.50 wt% Cu NPs enhanced the durability of the PDA+PTFE coatings by 52% and 33%, respectively. The improved tribological performance of the PDA+PTFE+0.25 wt% Cu NP and PDA+PTFE+0.50 wt% Cu NP coatings were attributed to the lower adhesion force to the counterface, the enhanced cross-linking between the PTFE and PDA in the presence of Cu NPs, the better adherence to the substrate, and the better load-carrying capacity of these coatings. In addition to the improved tribological performance, the addition of 0.25 wt% Cu NPs increased the thermal conductivity of the PDA+PTFE coating by 12%.

In summary, the tribology of thick PTFE coating enhanced by PDA in dry and oil-lubricated conditions has been studied in this dissertation. The PDA as an underlayer or constituent of PTFE coatings can improve the durability of the coating in dry conditions. The increase in durability can be attributed to the increase in adhesion between the substrate and the coating and the elimination of the global delamination and detachment from the substrate under frictional load. The durability of the PTFE and PDA/PTFE coatings showed a drastic increase when the coating thickness is 34 μm or higher under 10 N normal load due to the sudden decrease in contact pressure. Hot compaction helped to reduce the roughness and porosity of the coatings, which prevented global delamination of the coating and increased the load-carrying capacity of the PDA+PTFE coating, and hence enhanced the durability of the coatings over non-compacted PDA+PTFE and PTFE coatings. Similar to at the dry conditions, the PDA+PTFE coating is five times more durable than the PTFE coating in oil-lubricated conditions. The increase in durability can be attributed to the better nanomechanical properties, better load carrying capacity, and cross-linking between PDA and PTFE. However, the wear mechanism of the PDA+PTFE coating in oil-lubricated conditions is dominated by the delamination of the coating after wear depth reached a

critical thickness. The addition of 0.25 wt% Cu NPs delayed the delamination process and improved the durability of the PDA+PTFE coating by 52%. In addition to the better nanomechanical properties, the improved adhesion due to the addition of Cu NPs and further cross-linking of the PDA and PTFE in the presence of Cu NPs were responsible for the increase in durability of the PDA+PTFE+0.25 wt% Cu coating.

3.2 Future Work

Thick PTFE coatings have a wide range of applications. Even though the Tribological performance of the thick PTFE coatings have been extensively studied in this dissertation, there is still much to research in the future.

The PDA/PTFE thick coating was studied with only one PDA underlayer thickness. The effect of the thickness of the PDA underlayer of the PDA/PTFE coating could be studied. In addition, it will also be interesting to see the impact of having multilayered PTFE bonded together with PDA layers.

Even though adding PDA and Cu NPs helped improve the durability of the PTFE coating in oil-lubricated condition, PDA+PTFE and PDA+PTFE+Cu NP coatings still showed gross delamination after worn through 10-12 μm of the coating thickness. The porous structure and the not fully annealed coating at the cast iron-coating interface were responsible for the aggressive delamination. Better compaction and heat treatment process can be investigated to prevent the coating delamination.

The coating will be much more durable and applicable if the delamination is prevented. In a real-world setup, the oil usually gets contaminated by water during operations of the bearings. The next phase of this research includes studying the performance of PDA+PTFE coating in water

contaminated oil-lubricated conditions.

The PDA+PTFE coatings have the potential to be used to replace Tin-based Babbitt material in journal bearing application. The future direction of this work includes the actual bearing tests with PDA+PTFE coated cast iron and Tin-based Babbitt and compare the results.